



3 1176 00134 5801

NASA CR-159,523  
V.2

NASA CONTRACTOR REPORT

NASA CR-159523

NASA-CR-159523-VOL-2  
19790013164

FINAL REPORT  
LASER POWER CONVERSION  
SYSTEM ANALYSIS  
VOL. II

LIBRARY COPY

MAY 9 1979

LANGLEY RESEARCH CENTER  
LIBRARY, NASA  
HAMPTON, VIRGINIA

PREPARED UNDER CONTRACT NO NAS3-21137  
BY  
LOCKHEED MISSILES & SPACE COMPANY, INC.  
LOCKHEED PALO ALTO RESEARCH LABORATORY  
PALO ALTO, CALIFORNIA 94304  
FOR  
NASA-LEWIS RESEARCH CENTER  
CLEVELAND, OHIO  
SEPTEMBER 1978



1. Report No. NASA CR 159523		2. Government Accession No.		3. Recipient's Catalog No.	
4. Title and Subtitle  LASER POWER CONVERSION SYSTEM ANALYSIS Vols. I and II				5. Report Date March 15, 1979	
				6. Performing Organization Code	
7. Author(s) W. S. Jones, L. L. Morgan, J. B. Forsyth, J. P. Skratz				8. Performing Organization Report No. LMSC-D673466	
9. Performing Organization Name and Address  LOCKHEED MISSILES & SPACE COMPANY, INC. Lockheed Palo Alto Research Laboratory 3251 Hanover Street Palo Alto, CA 94304				10. Work Unit No.	
				11. Contract or Grant No. NAS 3-21137	
12. Sponsoring Agency Name and Address NASA-LEWIS RESEARCH CENTER 21000 Brookpark Road Cleveland, OH 44135				13. Type of Report and Period Covered Final 9/26/77 to 9/26/78	
				14. Sponsoring Agency Code 6344	
15. Supplementary Notes					
16. Abstract <p>The Laser Power Conversion System Analysis is reported in two volumes. Volume I describes the analysis for orbit-to-orbit laser energy transfer and conversion to electrical energy for spacecraft use. Volume II describes the analysis for orbit-to-ground laser energy transfer and conversion to electrical energy for consumer use on earth.</p> <p>The orbit-to-orbit laser energy conversion system analysis established a mission model of satellites with various orbital parameters and average electrical power requirements ranging from 1 to 300 kW. The system analysis evaluated various conversion techniques, power system deployment parameters, power system electrical supplies and other critical subsystems relative to various combinations of the mission model. The analysis showed that the laser power system would not be competitive with current satellite power systems from weight, cost and development risk standpoints.</p> <p>The orbit-to-ground laser power conversion system analysis investigated the feasibility and cost effectiveness of converting solar energy into laser energy in space and transmitting the laser energy to earth for conversion to electrical energy. The analysis included Space Laser Power Systems with electrical outputs on the ground ranging from 100 to 10,000 MW. The Space Laser Power System was shown to be feasible and a viable alternate to the microwave Solar Power Satellite. The narrow laser beam provides many options and alternatives not attainable with a microwave beam.</p>					
17. Key Words (Suggested by Author(s)) Energy conversion, energy transfer, laser, laser beam, laser power, laser relay, laser system, power system, space laser power, solar energy				18. Distribution Statement See distribution list  N79-21335#	
19. Security Classif. (of this report) Unclassified		20. Security Classif. (of this page) Unclassified		21. No. of Pages	
				22. Price*	

\* For sale by the National Technical Information Service, Springfield, Virginia 22161



## CONTENTS

Section		Page
1	SUMMARY	1
	1.1 Objectives	1
	1.2 Study Scope	1
	1.3 Study Results	1
	1.4 Conclusions	2
2	INTRODUCTION	3
	2.1 Background	3
	2.2 Study Description	3
	2.3 Study Results	8
	2.4 Conclusions	11
	2.5 Recommendations	11
3	TECHNICAL DISCUSSION	12
	3.1 Selected Space Laser Power System	12
	3.2 Proof-of-Concept	25
	3.3 Concept Evaluation and Cost	28
	3.3.1 SLPS Pilot Program Costs	28
	3.3.2 Full-Scale SLPS Costs	31
	3.3.3 SLPS Investment Cost Analysis	34
	3.3.4 Equal Installed Power Cost Comparison	38
	3.3.5 Mills/kW-Hr Cost Comparison	40
	3.3.6 Cost Sensitivities	42
	3.3.7 Cost Evaluation Summary	42
	3.4 Subsystem Evaluation	42
	3.4.1 Electric Power Generation From Solar Energy	43
	3.4.2 Laser Subsystems for Power Transmission	51

Section	Page
3.4.3 Phasing Array	62
3.4.4 Conversion of Laser Power to Electrical Power (Ground)	65
3.5 Parametric Systems Analysis	65
3.5.1 Laser Power Satellite and Relay Deployment	66
3.5.2 Ground Station Locations	68
3.5.3 System Concepts	75
3.5.4 Parametric Evaluations	77
3.6 System Safety	80
3.7 Beam Propagation and Environmental Effects	89
3.7.1 Diffraction and Turbulence	90
3.7.2 Attenuation	93
3.7.3 Thermal Blooming	93
3.7.4 Propagation at $\lambda < 1 \mu\text{m}$ : Ozone Destruction	100
3.8 Discussion of Results	102
4 REFERENCES	103

## ILLUSTRATIONS

Figure		Page
1	System deployment overview	1
2	System block diagram	6
3	Overall binary-cycle/CO <sub>2</sub> EDL system	13
4	Laser power station concept	15
5	Selected subsystem for electrical power generation	18
6	Ground site concept	21
7	Ground energy exchanger with binary cycle	23
8	500 MW <sub>e</sub> space laser power system	24
9	Space Laser Power System proof-of-concept overview	26
10	Orbit ground tracks	27
11	Proof-of-concept configuration	30
12	Dollars/kW cost comparison (77\$)	39
13	Mills/kW-hr cost comparison (77\$)	41
14	Energy exchanger/binary cycle	45
15	Energy exchanger parameters	47
16	Solar collector/concentrator construction concept	48
17	Structural beam construction	49
18	Reflector geometry	50
19	Effects of suns apparent angle	52
20	Secondary concentrator	53
21	CO <sub>2</sub> EDL subsystem: internal refrigeration	55
22	CO <sub>2</sub> EDL subsystem - external refrigeration	56
23	Electrical efficiency of CO <sub>2</sub> EDL subsystem with internal refrigeration	57
24	Electrical efficiency of CO <sub>2</sub> EDL subsystem with external refrigeration	58

Figure		Page
25	Carbon dioxide EDL electrical efficiency	59
26	CO EDL subsystem	60
27	Carbon monoxide EDL electrical efficiency	61
28	CO <sub>2</sub> solar-pumped subsystem	63
29	Phasing array	64
30	Earth coverage with 60° zenith angle	67
31	Absentee ratio of laser power satellites from earth occultations of relay units	69
32	LEO relay requirements, 0° inclined circular orbits	70
33	LEO relay requirements, 30° inclined circular orbits	71
34	LEO relay requirements, 90° inclined circular orbits	72
35	Effect of nodal location and inclination on LEO relay requirements	73
36	Ground elevations and normal percentage of cloudiness in the United States	74
37	Radiator evaluations	81
38	Permissible exposure level (4-1.4 μm)	85
39	Permissible exposure level (10.6 μm)	86
40	Protection radius extremes	87
41	Beam profile for selected configuration	88
42	Hufnagel model for the altitude dependence $C_n^2$ , modified below 1.6 km to represent moderate low-altitude turbulence ( $10^{-3} \text{ m}^{2/3}$ at $h = 0$ )	91
43	Time-average turbulent beam spread for a beam propagating from space to ground level, based on Hufnagel's turbulence model at high altitudes plus moderate low-altitude turbulence	92
44	Vertical atmosphere transmittance as a function of wavelength, due to ozone, Rayleigh scattering, and aerosol attenuation	94
45	Transmittance for a vertical line-of-sight through the entire atmosphere; dashed curve: Rayleigh scattering; solid curves, aerosol	95
46	Effective transverse wind-speed, $v_{av}$ , as a function of ground-level wind, $v_o$ , vertical gradient, $v'$ , and absorption scale height, $H$	97



Figure		Page
47	Slew rate at the receiver as the transmitter passes the local zenith	98
48	Limiting values of windspeed $v_{av}$ and low-altitude absorption $\alpha_0 H$ : for $(v_{av}/\alpha_0 H) \rightarrow (v_{av}/\alpha_0 H)_1$ , thermal blooming is significant	99

## TABLES

Table		Page
I	Candidate Subsystems	7
II	Systems Concepts Evaluated	9
III	Preliminary System Analysis Results	10
IV	Laser Power Station Specification	14
V	Laser Subsystem Specifications	19
VI	Ground Site Specifications	19
VII	Pilot Program Specifications	28
VIII	Pilot Vehicle Weight Statement (kg)	29
IX	SLPS Pilot Program Costs	32
X	SLPS Incremental Development Cost	33
XI	SLPS – Theoretical First-Unit Hardware Cost (77 \$M)	35
XII	Prorated Construction Base Cost and Mass	37
XIII	HLLV Transportation Cost and Mass (Base and Power Satellite)	37
XIV	Personnel Shuttle Transportation Cost	38
XV	Total SLPS Investment Cost for the Theoretical First Unit (77 \$M)	38
XVI	Systems Concepts Evaluated	75
XVII	Laser Power Satellites Efficiencies	78
XVIII	Space/Ground System Efficiencies	79
XIX	Orbital System Weight Breakdown: 1000 MW	82
XX	Component Dimensions	83
XXI	System Summary Results	84

## Section 1

### SUMMARY

Volume II of the Laser Power Conversion Systems Analysis, Contract NAS 3-21132, covers the evaluation of a Space Laser Power System relative to its capability to transfer energy from space to earth. This task was added to the original contract.

#### 1.1 OBJECTIVES

The objectives of the Space Laser Power System Analysis task are to develop a conceptual space-based system to convert solar energy, either directly or indirectly, to laser energy for transmission to ground sites, then convert the laser energy to electrical energy for consumption on earth; to establish the feasibility and technology requirements; and to evaluate the system for competitiveness with the microwave Solar Power Satellite.

#### 1.2 STUDY SCOPE

The primary emphasis of the study was the systems aspect of subsystem interactions and interfaces, particularly addressing power conversion techniques for both the space vehicle and ground site. Lesser emphasis was placed on the laser subsystems, optical subsystems, and pointing and tracking subsystems. The optical subsystems and pointing and tracking subsystems evaluated under Contract NAS 3-20372, Laser Rocket System Analysis, had similar requirements and alleviated the need for detailed analysis. The system concepts ranged from 100 to 10,000 MW of electrical power on the ground. A 500-MW system was conceptually designed in more detail.

#### 1.3 STUDY RESULTS

The study results showed Space Laser Power Systems are feasible with reasonable technology advances and are competitive economically with the microwave Solar Power Satellite. Specific advantages include major operation in low earth orbit (much easier access), reduction of land requirements by more than three orders of magnitude (85,000 to < 80 acres), and relatively low cost for proof-of-concept prior to major development and procurement expenditures.

#### 1.4 CONCLUSIONS

- The Space Laser Power System is a viable alternate to the microwave Solar Power Satellite
- System optimization and use of technology that will be available in the 1995 to 2000 time period will further enhance the Space Laser Power System
- The pilot program for proof-of-concept is reasonable with respect to the system costs and benefits
- More indepth studies and experiments should be initiated to further validate the results of this study and evaluate the Space Laser Power System with the microwave Solar Power Satellite.

## Section 2

### INTRODUCTION

#### 2.1 BACKGROUND

The use of lasers to transmit energy over long distances has been of interest since laser devices with significant power outputs appeared to be feasible. Kantrowitz (Ref. 1) examined the use of ground-based lasers to transmit energy to launch space vehicles to orbit. Orbit-to-orbit rockets supplying energy from remote lasers have been investigated as well as laser-powered airplanes. Other recent studies have investigated techniques for converting solar and laser energy into electrical energy. These studies and experimental programs have made significant advances in critical technologies such as lasers, large adaptive optics, pointing and tracking, beam propagation through the atmosphere, and energy conversion devices. With these recent advancements, it has become more evident that laser transmission of energy has many potential applications and may provide significant improvements and capabilities not otherwise attainable. The microwave technique has several characteristics that are disadvantageous such as the long wavelength (10 to 12 cm), interaction action with the ionosphere at very low flux levels and the possible interference with communications in nearby frequencies. A laser energy transfer system can definitely provide shorter wavelengths by 4 orders of magnitude ( $1.0 \times 10^{-1}$  to  $1.06 \times 10^{-5}$ ), which will reduce the size of transmitters and receivers, and while the data currently available are very limited, the ionosphere interaction and the possible interference with existing communications may be minimized or eliminated.

The Space Laser Power System can also be made to be more adaptable to current electrical power systems within the United States and elsewhere. The systems can be tailored to specific requirements for individual locals and, in fact, be used to provide energy to existing power generating facilities.

#### 2.2 STUDY DESCRIPTION

This Space Laser Power System study has been very timely and can apply additional stimuli to the ultimate goal of utilizing the unlimited solar energy resource to provide forever growing energy needs on earth. Laser energy transfer provides a competitive system to assure maximum cost effectiveness and an alternate to the microwave system should an insurmountable obstacle be encountered. The Space Laser Power System study described herein should be viewed as an effort to enhance the probability of Solar Power Satellites. In addition to an alternate method of energy transfer, this study provides an alternate energy conversion concept with significant potential for several applications.

The Space Laser Power System investigated in this study is by no means an optimum system. For example, the deployment of relays was established to provide the minimum number of relays and not necessarily the most efficient or economical system. Figure 1 shows a system deployment overview in which the laser power satellites are deployed in a low-earth, sun-synchronous orbit. Relay units are deployed in both geosynchronous equatorial orbit (GEO) and low-earth orbit (LEO). The GEO relays are stationary over the receiver sites, which in this illustration are on the far side of the earth. One GEO relay is deployed for each laser power satellite. As depicted in the illustrations, the relay units cover about  $45^\circ$  of earth longitude and will be obscured from a direct line-of-sight to the laser power satellite servicing it about 30% of the time. For the case depicted in Figure 1, a second set of relays are required in LEO at  $28.5^\circ$  inclination. These satellites are used when the laser power satellite is obscured from its GEO relay, at which time a double relay is used. That is, the laser power satellite will transfer energy to the LEO relay and the LEO relay will transmit the energy to the GEO relay, which in turn transmits to the ground sight. As the system increases in earth coverage, the need for LEO relays decrease until earth coverage reaches about  $135^\circ$ , at which time no LEO relays are required and the ratio of laser power satellites to relay units to ground sites equals 1:1:1. The deployment scheme is not necessarily optimum; it only minimizes the number of relays. Deployment schemes in which all relays are in LEO have not been analyzed. The LEO deployment schemes will require a larger number of relays but will operate at shorter ranges and thereby reduce the size of all optics in the system and/or reduce pointing requirements and will eliminate cost of transporting any weight to GEO.

Figure 2 shows the system block diagram which illustrates that three or four independent and remote elements must be coordinated with one another to function as a single system. The solar power satellite and relay unit(s) operate in space and the ground site could be located anywhere on earth. The system will convert solar energy, either directly or indirectly, to laser energy and transmit the energy to earth with the use of relays where the laser energy will be converted to electrical energy for consumer use.

Table I shows the candidate subsystems analyzed for possible use in system synthesis. The primary emphasis of the study centered around the subsystems for conversion of solar energy to electrical energy, the laser subsystems, and the conversion of laser energy to electrical energy on the ground. The analyses showed that an energy exchanger in combination with a turbine and a bottoming Rankine cycle would provide the maximum efficiency for converting solar energy into electrical energy. As the laser power satellite would possibly operate in LEO and be subjected to the Van Allen Belt throughout its life, photovoltaic devices would not be a suitable choice because of their degradation in this environment. The lasers considered were limited to the carbon-dioxide electrical discharge laser ( $\text{CO}_2$  EDL), the carbon monoxide electrical discharge laser (CO EDL), and the relatively new concept of a solar-pumped laser. The  $\text{CO}_2$  EDL and the solar-pumped laser operate at  $10.6\text{-}\mu\text{m}$  wavelength and the CO EDL operates at  $5.0\text{ }\mu\text{m}$ . The subsystems analyzed for conversion of laser energy to electrical energy included photovoltaics, thermal electronic (TELEC), Brayton cycle, and an energy exchanger with a binary cycle. The photovoltaic devices were eliminated

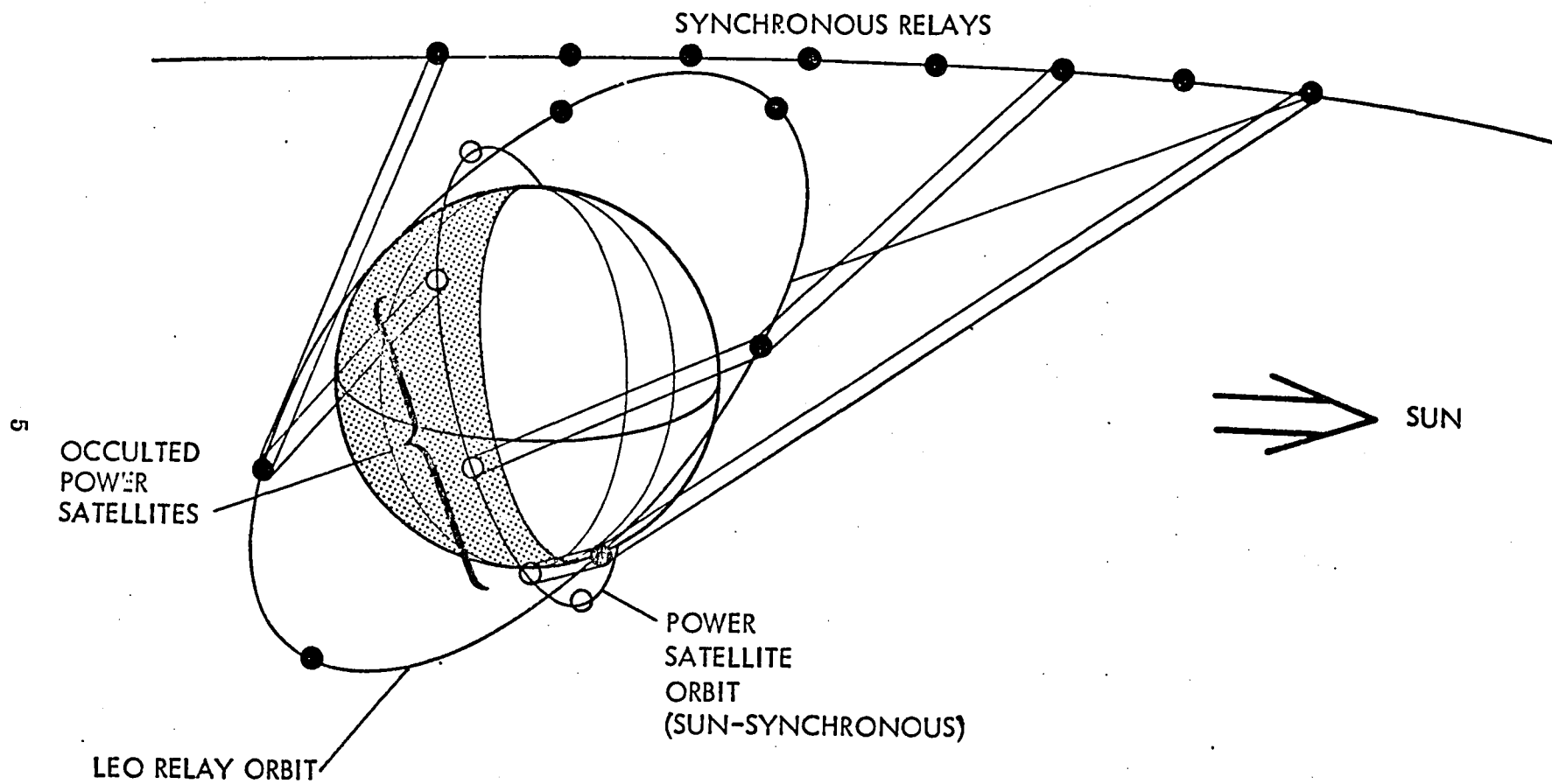


Figure 1. System deployment overview

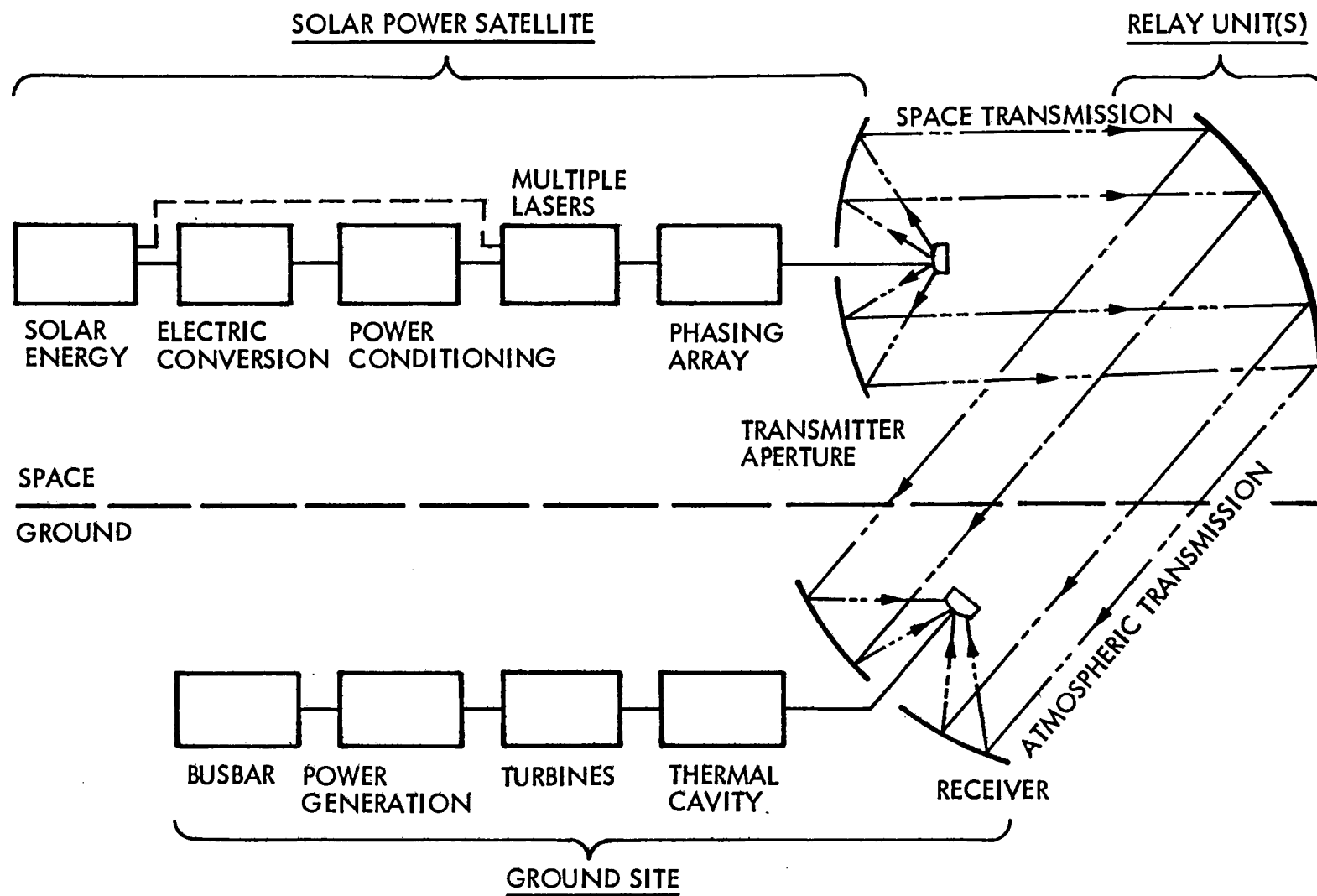


Figure 2. System block diagram



TABLE I. CANDIDATE SUBSYSTEMS

SUBSYSTEM/FUNCTION	CANDIDATES	TYPICAL EFFICIENCY (%)	REMARKS
ELECTRICAL POWER GENERATION IN SPACE	SILICON SOLAR CELLS	10.4 (7.3)	DEGRADATION IN LEO
	GALLIUM ARSENIDE CELLS	22 (12.5)	DEGRADATION IN LEO
	BRAYTON CYCLE	< 40%	—
	ENERGY EXCHANGER WITH TURBINE	58 <sup>+</sup>	—
	ENERGY EXCHANGER WITH BINARY CYCLE	73	MAXIMUM EFFICIENCY
LASER SUBSYSTEM FOR POWER TRANSMISSION	CO <sub>2</sub> EDL	20.2	EXCELLENT DATA BASE
	CO EDL	24.8	GOOD DATA BASE
	SOLAR PUMPED	(19.9)	LIMITED DATA BASE
CONVERSION OF LASER POWER TO ELECTRICAL POWER ON THE GROUND	PHOTOVOLTAIC	< 40	—
	THERMAL ELECTRONIC (TELEC)	45	—
	BRAYTON CYCLE	40	—
	ENERGY EXCHANGER WITH BINARY CYCLE	73	HIGHEST EFFICIENCY

early because of the laser wavelengths being considered. Again, the energy exchanger with binary cycle showed to be the most efficient and was selected as the primary candidate for system synthesis.

Preliminary system synthesis was performed on five different systems as shown in Table II. System III, with the solar-pumped laser, requires a significant amount of electrical power even though the laser is directly pumped. Therefore, an energy exchanger with binary cycle was also included. An energy exchanger with binary cycle for conversion of laser energy to electrical energy on the ground was selected for all five systems.

### 2.3 STUDY RESULTS

The results of the preliminary systems analysis is shown in Table III. The CO<sub>2</sub> EDL/binary, CO EDL/binary, and the solar-pumped laser systems all showed overall efficiencies about those attained in the Solar Power Satellite, and the total orbital weights were not significantly different from one another. On the other hand, the solar cell systems showed a low overall efficiency and considerably higher weights. One factor primarily contributed to the low-efficiency high-weight solar cell systems. The low efficiency of solar to electrical conversion caused the efficiency to be much lower (12.5% end of life versus 73%) and the weight much higher because of the increased area required to intercept the much higher solar energy required.

As a result of the system analyses, the CO<sub>2</sub> EDL/binary system was selected for more detailed analysis and conceptual design of a 500 MW<sub>e</sub> (output on the ground) system. The selection was based on the following:

- The existing data base for CO<sub>2</sub> EDL lasers is excellent and will provide confidence of feasibility with large growth potential with development of new, more efficient, lasers.
- The overall efficiency is lowest of the systems using binary energy conversion but is still in the range of the microwave SPS.
- The CO<sub>2</sub> wavelength (10.6  $\mu$ m) has good transmission and is most suitable for phasing multiple lasers to achieve any power level.
- The weight differences are close enough not to be a factor in the selection.

The selection was made to provide more confidence in the feasibility due to the nearer term technology requirements. In fact, laser manufacturers are confident that CO<sub>2</sub> lasers can be developed now to provide any power level desired.

The selected system was analyzed in more depth with some optimization of the solar collector, solar cavity, and the energy exchanger with binary cycle which resulted in an increase to about 6% end-to-end efficiency.

Cost analyses have shown that a 500-MW<sub>e</sub> Space Laser Power System will cost more per installed kilowatt when compared to the 5000 MW<sub>e</sub> and 10,000 MW Solar Power Satellites; however, by comparisons based on equal electrical output on the earth and

TABLE II. SYSTEMS CONCEPTS EVALUATED


SYSTEM	SOLAR ENERGY COLLECTOR	ELECTRICAL POWER CONVERSION	LASER SUBSYSTEM	GROUND POWER CONVERSION
I	REFLECTOR/CAVITY	ENERGY EXCHANGER AND BINARY CYCLE	CO <sub>2</sub> EDL	ENERGY EXCHANGER AND BINARY CYCLE
II	REFLECTOR/CAVITY	ENERGY EXCHANGER AND BINARY CYCLE	CO EDL	
III	REFLECTOR/CAVITY	ENERGY EXCHANGER AND BINARY CYCLE	SOLAR PUMPED LASER	
	REFLECTOR/SOLAR LASER CAVITY			
IV	REFLECTOR/SOLAR CELL ARRAY	SOLAR CELLS	CO <sub>2</sub> EDL	
V	REFLECTOR/SOLAR CELL ARRAY	SOLAR CELLS	CO EDL	

TABLE III. PRELIMINARY SYSTEM ANALYSIS RESULTS

SYSTEM NO.	TYPE	POWER ON GROUND (MW)	SOLAR POWER RECEIVED (MW)	OVERALL EFFICIENCY (%)	ORBITAL SYSTEM WEIGHT (kg)
I	CO <sub>2</sub> EDL/ E.E. BINARY	100 500 1000	2,017.3 10,086.6 20,173.2	} 4.96	1,469,000 6,926,000 14,774,000
II	CO EDL/ E.E. BINARY	100 500 1000	1,890.2 9,450.9 18,901.9	} 5.29	1,468,100 7,126,500 14,241,600
III	SOLAR PUMPED CO <sub>2</sub>	100 500 1000	1,573 7,865.9 15,732	} 6.32	1,926,000 7,107,000 14,353,000
IV	CO <sub>2</sub> EDL/ SOLAR CELLS	1000	95,524	} 1.04	22,840,000
V	CO EDL/ SOLAR CELLS	1000	89,500	} 1.17	21,840,000

by applying learning curves to all systems, the Space Laser Power System costs fall between the 5,000- and 10,000-MW<sub>e</sub> systems.

## 2.4 CONCLUSIONS

- The use of lasers to transmit energy from space to ground is a viable alternate to the microwave Solar Power Satellite.
- As the Space Laser Power System operates primarily in low earth orbit, development of large orbital transfer vehicles will not be required.
- The land use requirements for the Space Laser Power System is more than three orders of magnitude less than required by a microwave system. (This provides a safety factor three orders of magnitude less than current standards for corneal exposure to radiation between 1.4 and 10<sup>3</sup> μm wavelengths.)
- The cost for subscale proof-of-concept program will be significantly less for a laser system and can be completed prior to major funding commitments for developing the full system.
- The social, environmental, and political problems associated with the laser system will be on the same order as the microwave system.

## 2.5 RECOMMENDATIONS

- Analytical studies, technology development, and experimental programs should be continued for the microwave Solar Power Satellite and initiated for the laser alternate to fully establish the advantages and disadvantages of each.
- Specific Space Laser Power System programs recommended to be initiated include:
  - (1) Ecological and biological effects of laser beams
  - (2) Space Laser Power System Optimization to include all potential laser devices and low earth deployment schemes
  - (3) Space Laser Power System Space Construction Requirements
  - (4) Space Laser Power System Operational Requirements
  - (5) Space Laser Power System Transportation Requirements

### Section 3

## TECHNICAL DISCUSSION

The Space Laser Power System (SLPS) Analysis task of the Laser Power Conversion Systems Analysis investigated the use of lasers to transmit laser energy from space to ground for conversion to electrical energy. Other investigations (Refs. 2, 3) of laser systems have shown advantages of operating the lasers in LEO and using relay mirrors to transmit the energy to its final destination. The basic assumption at the beginning of the study was that the SLPS would not be imposed with the specific use of any subsystems or operating procedures of the Solar Power Satellite (SPS) but would be synthesized toward the subsystems and parameters best suited for the overall system. Because of the tight schedule and funding, true system optimization could not be accomplished. Many tradeoffs were not accomplished or only superficially investigated. For example, space construction was not investigated; however, significant advantages are known to exist because of the specific design concept of the collector/concentrator.

The approach to accomplishing this task was to evaluate several relay deployment schemes which would permit transferring the laser energy to ground sites, evaluate subsystems for energy conversion in space, energy conversion on earth, and a limited number of laser subsystems. From this matrix of subsystems, several systems would be synthesized and evaluated relative to one another. The preliminary system evaluation led to the selection of a single system which was analyzed in more detail and a conceptual design prepared. Cost analysis and evaluation was performed on the selected configuration.

The order of discussion in this section will be first to discuss the selected configuration and the proof-of-concept program that would lead to development of the full-scale system. The subsystem evaluation analysis will then be discussed, followed by the parametric system analyses.

### 3.1 SELECTED SPACE LASER POWER SYSTEM

The selected configuration for conceptual design is an SLPS using multiple CO<sub>2</sub> EDLs, multiple energy exchangers with binary cycles for energy conversion in space, and an energy exchanger with binary cycle for energy conversion on the ground. The configuration has a 500-MW<sub>e</sub> electrical output on the ground, and has three primary elements (systems within themselves) which are remotely located from one another, but must interface and interact as a single system. Figure 3 shows the Laser Power Satellite, relay unit, and ground station as the primary elements of the system and further shows the primary subsystems for the Laser Power Satellite and the ground station. The relay unit primary subsystems are a receiving aperture, a transmitting aperture, an optical train between the two, and a spacecraft.

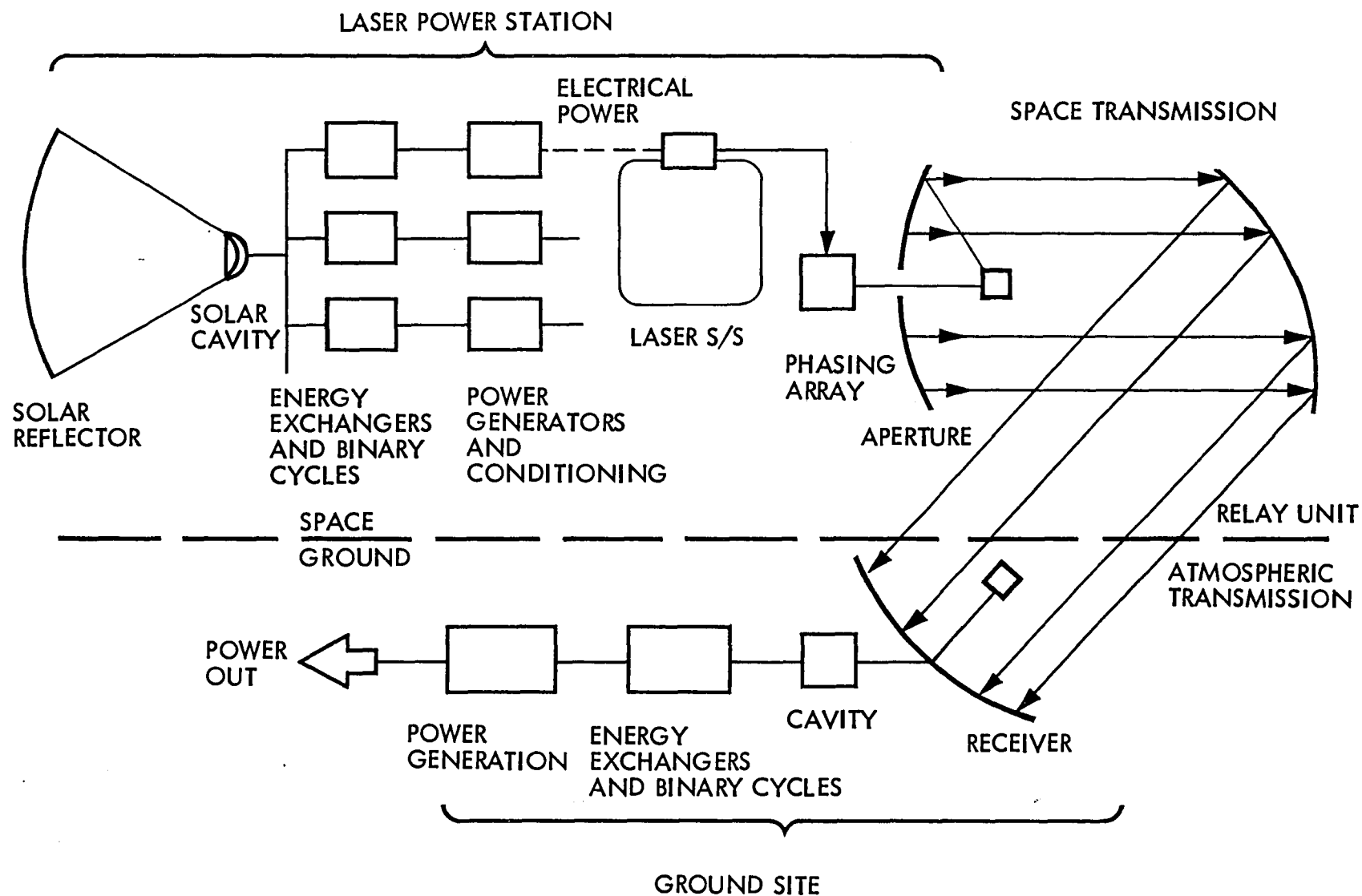


Figure 3. Overall binary-cycle/ $\text{CO}_2$  EDL system

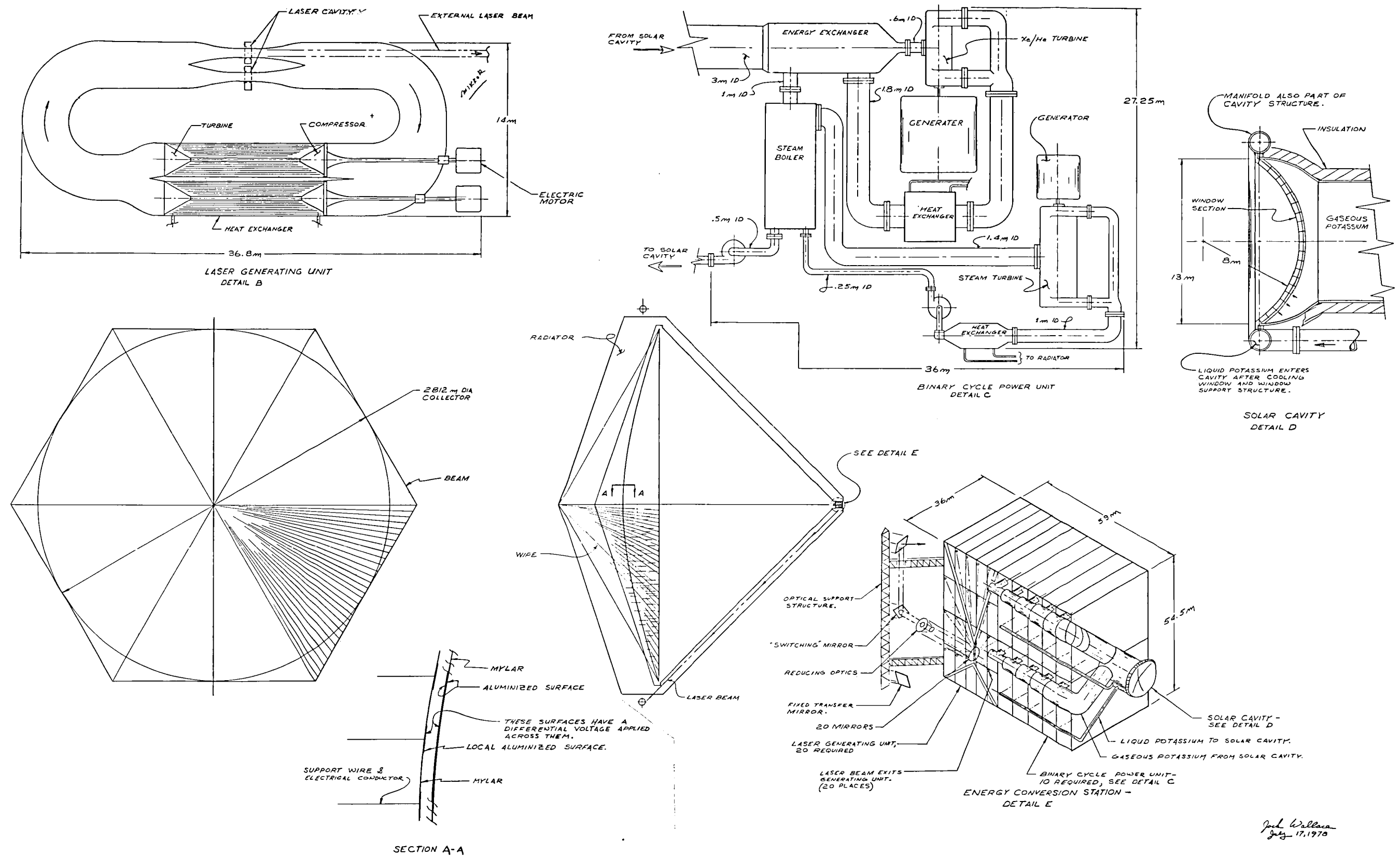
Table IV shows the specifications of the Laser Power Satellite. The solar collector is 2.7 km in diameter to collect 7.9 GW of solar energy. The laser power output is from 20 lasers at 45.5 MW each for a total output of 910 MW. The 31.5-m-diameter transmitter has an average flux density of about 10 W/cm<sup>2</sup> and with 99.85% reflectivity must reject 0.0015 W/cm<sup>2</sup> which does not require active cooling. The 3.0-m-diameter secondary has a flux density of about 12.5 kW/cm<sup>2</sup> and does require active cooling. The optics operate at 200°C to match the rejected heat from the laser and binary cycles requiring a total of 2,657-m<sup>2</sup> radiator area. Figure 4 is the conceptual design of the Laser Power Satellite, including detail and packaging layouts for the radiator, laser units, and energy exchangers and binary cycle units. The Laser Power Satellite will orbit the earth with the radiator surface normal to the flight path. This will afford a greater cross-sectional area relative to the drag component, but at altitudes greater than 900 km, the increased drag affect is more than offset by radiating from both sides of the radiator to black space. The reflector/condenser is a Mylar, Kapton, or other aluminized membrane structure of parabolic shape. Behind this reflecting membrane is another aluminized membrane held in position with an annulus structure constructed with plies of aluminum foil and a membrane. Pressurization of the annulus beyond the tensile yield strength of the aluminum foil will "set" the annulus and pressure can be released. In addition, support to the back membrane is provided by a series of tension wires. Static electrical positive and negative charges applied to the two membranes will hold the reflecting membrane in the proper shape. In fact, a grid on the back membrane in which the static charge can be varied will provide reflective surface shaping and better control of the reflected solar energy. The center view on Figure 4 shows the location on top and bottom of two 31.5-m-diameter transmitter apertures. The two apertures will provide 4 $\pi$  sr of beam pointing and fast switching of the beamed energy when it is necessary. The switching mirror is shown in the packaging layout of detail E on the figure.

TABLE IV. LASER POWER STATION SPECIFICATION

Solar Power Collected (MW)	7,913.0
Collector Diameter (m)	2,710.0
Electrical Power to Laser (MW)	3,958.0
Laser Power Output (MW)	910.0
(20 Lasers at 45.5 MW each)	
Transmitter Aperture Diameter (m)	31.5
Secondary Mirror Diameter (m)	3.0
Transfer Mirror Size (m)	3.0 $\times$ 4.2
Mirror Reflectivity (%)	99.85
Optics Heat Rejection (MW)	11.8
Radiator Area (m <sup>2</sup> )	2,656.7
Mirror Operating Temperature (°C)	200.0

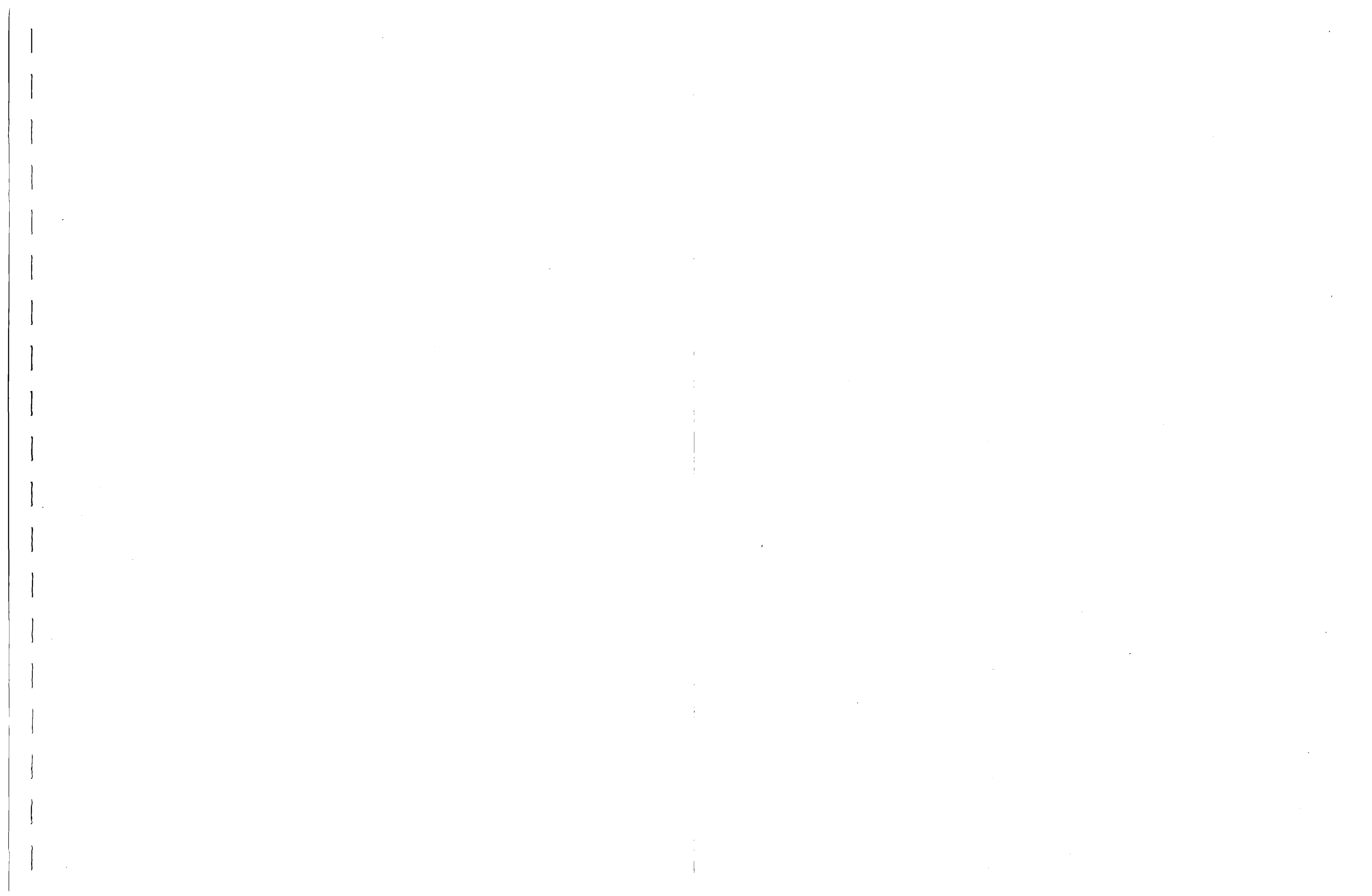
The orbital electrical power generation/subsystem for the selected configuration is the energy exchanger with the binary cycle. The sizes of the components and the general schematics are shown in Figure 4. Each of the subsystems were reexamined after the parametric studies and the design produced in greater detail. The solar collector/concentrator and secondary concentrator reduces the solar energy spot to enter the





Jack Williams  
 July 17, 1970

Figure 4. Laser power station concept



13-m-diameter solar cavity window (Figure 4, Detail D). The concave solar cavity window design is based on a material with properties similar to sapphire (tensile strength of 15,000 psi at 1000 K). The window is segmented and cooled by the incoming potassium with technology similar to cooling rocket engines with internal temperatures far exceeding the material capability. The incoming solar energy is absorbed directly by the potassium which is heated to 3400 K average temperature. The outlet pressure from the cavity will be 177 psi. The shell design was based on tungsten alloy, which is regeneratively cooled with potassium. The yield strength of the cavity materials were considered to be 10,000 psi, which is within the cooling capabilities. The insulation on the outside consists of radiation shields of refractory metals.

The principal subsystem of the electric power generation system is the integrated energy exchanger, turbine cycle (modified Brayton), and a Rankine cycle. The selected thermodynamic cycle is shown in Figure 5. The objectives of the design were to reduce the solar cavity pressure and raise the radiator temperatures to reduce weight. Tradeoff studies were performed to accomplish these objectives; however, the subsystem is not optimized and represents a compromise between parameters. The Rankine cycle resulted in a high pressure steam system, based upon the interrelationship of the thermodynamic cycle parameters.

Reviewing the required total electrical output ( $\sim 4.3$  GW), ten energy exchangers with binary cycles were selected for the configuration. This resulted in reasonably sized subsystems with 425.1 MW of power output each which would supply two lasers and provide reliability of maintaining a majority of the power in case of a malfunction. The physical dimensions of the subsystem are shown (unpacked and packaged) in Figure 4. The total radiator area required for all ten units is 329,000 m<sup>2</sup>. The overall thermodynamic efficiency was 73.5%.

Two electrical power generators are operated by each binary cycle, resulting in 20 electrical generators. The generators will produce alternating current, and the voltages will likely be less than 50,000 V. To produce the 7400 Vdc and the 150,000 Vdc required for the CO<sub>2</sub> electrical discharge lasers, it will be necessary to provide transformers, rectifiers, and filters.

Twenty laser subsystems are used in the power transmission subsystem to assure that the required laser powers would be well within the extrapolated projections for the CO<sub>2</sub> electric discharge lasers. The laser subsystem is shown with dimensions in Figure 4, Detail B. Each subsystem has two optically connected laser cavities. The recirculation loop involves a compressor which compresses the lasing gas with a pressure ratio of 1.5, which results in a temperature of 655 K. The gas is then cooled by a heat pipe radiator to 321 K, enters the turbine, and is expanded to a ratio of 1.26. The energy generated in this expansion is transmitted back to the compressor to reduce the power requirements. The laser device characteristics were obtained from examination of the data presented in Ref. 10, and from consideration of the system requirements shown in Table V.

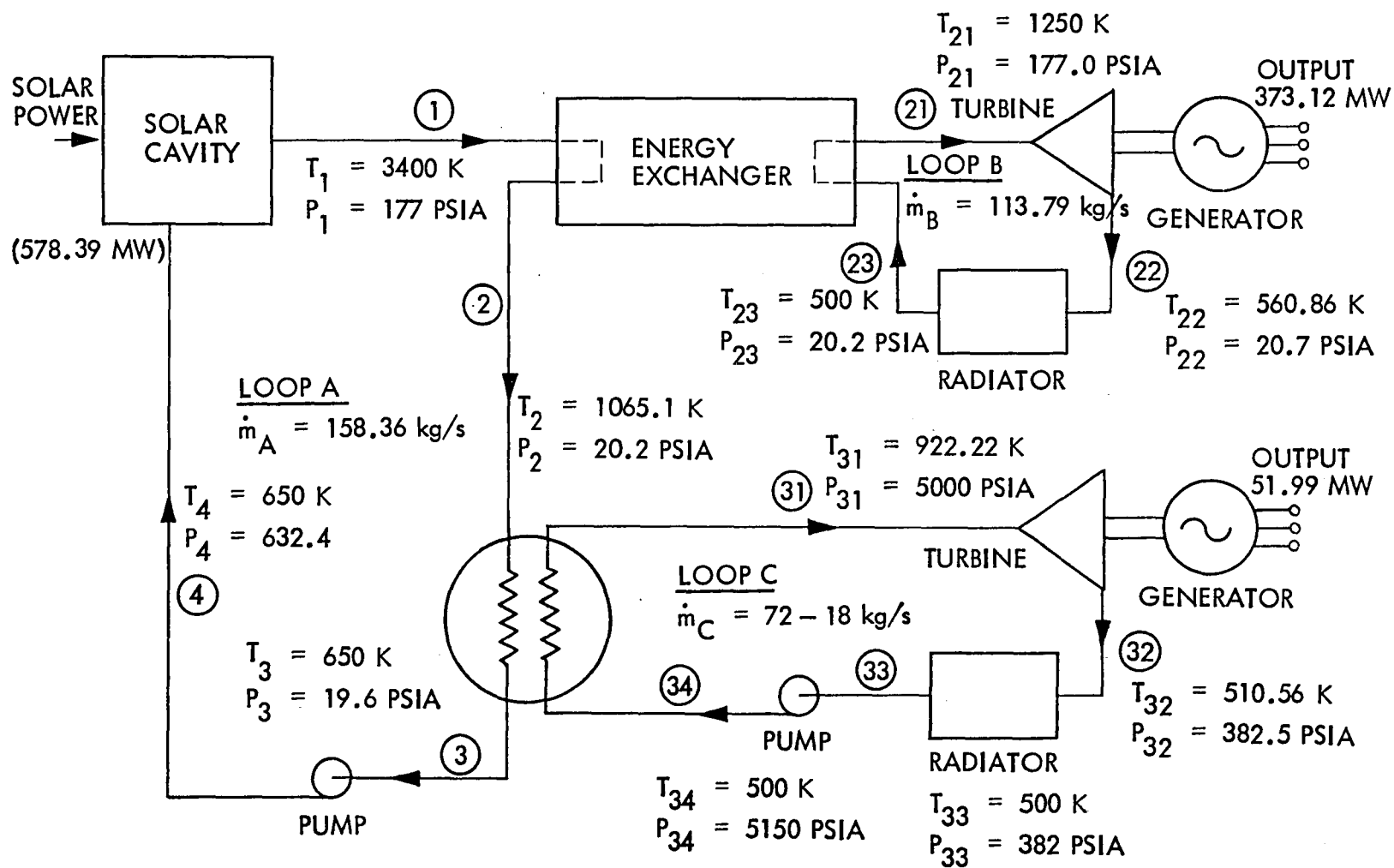


Figure 5. Selected subsystem for electrical power generation

TABLE V. LASER SUBSYSTEM SPECIFICATIONS

Laser Output Power (per Laser)	45,510 kW
Cavity Pressure	450 Torr
Cavity Temperature	300 K
Cavity Mach No.	0.4
Cavity Electrical Efficiency	28.3%
Cavity Specific Power	120 kJ/kg

The resulting overall electrical efficiency of this system is 23%, and the total radiator area for 20 lasers is 811,000 m<sup>2</sup>.

Space relay units are located in geosynchronous equatorial orbit located at the same or near longitudes as the ground stations. The function of the relay units are to receive the laser energy, correct wavefront aberrations, and refocus the energy on the ground station receiver. The relay units have a 31.5-m-diameter, off-axis, receiver aperture which reduces the beam diameter and transfers the energy to the 31.5-m-diameter transmitter aperture via an optical train. As the beam leaves the transmitter aperture, samples are taken and adjustments to the aperture are made to minimize wavefront errors and focus the beam on the ground receiver. Both the receiver and transmitting apertures have cooperative pointing and tracking systems to maintain accurate beam control throughout the transfer range. The transmitter aperture also has a ranger to assure focusing correctly. A spacecraft is an integral part of the relay unit and performs all the normal spacecraft functions such as guidance and navigation, communications and control, vehicle stability, and provides electrical power for all functions.

The function of the SLPS ground station is to receive the laser energy and convert this energy into electrical power for consumption on earth. The SLPS ground station basic specifications are shown in Table VI.

TABLE VI. GROUND SITE SPECIFICATIONS

Receiver Aperture Diameter	31.5 m
Electrical Power Output	500 MW
Location	< 53° Latitude
Land Requirements	62 acres

The receiver aperture is sized to receive the beam from a 31.5-m-diameter transmitter located in GEO. The beam intensity on the receiver is Gaussian with a peak intensity at the center of 284 W/cm<sup>2</sup> with an intensity of  $1.2 \times 10^{-4}$  W/cm<sup>2</sup> at 200-m radius for a beam coming straight down through the atmosphere. At a zenith angle of 60°, the 200-m radius will increase by a factor of 2 in one direction. This ellipse contains 251,327 m<sup>2</sup> (62 acres) which will provide a safety factor 1000 times less than the current safety standard (0.1 W/cm ) for corneal exposure to 10.6-μm laser radiation. The location requirement assures that zenith angles to the relay will not exceed 60° when the relay is in GEO. The 60° zenith angle is about as large as can be tolerated

because of the increased distance through the atmosphere. The 500-MW<sub>e</sub> output on the ground was selected as a reasonable single power load to be applied to current electrical grids on earth, particularly when the relatively small land requirement will permit locating the ground stations near the consumer areas without the necessity of transfer over long distances on the ground. Figure 6 shows the ground station concept for this configuration. The receiver optics are 31.5-m-diameter, but are not required to have near diffraction-limited performance and, therefore, adaptive optics are not required. Diffraction-limited performance relates to the beam spread, and in the case of the 31.5-m-diameter aperture and 10.6-μm wavelength, the diffraction limit is about 0.4 μrad. Because the total range from the receiver aperture to the thermal cavity is less than 100 m, a beam spread of 100 μrad would only require the cavity window to be larger in radius by about 1 cm. The receiver, as shown in Figure 6, has limited gimbals in two axes. The gimbals are primarily to provide pointing capability related to the site latitude. The relay in GEO is essentially stationary relative to the receiver pointing requirements.

The laser energy is received on the receiver aperture, reduced, and transferred to the thermal cavity. The thermal cavity at the ground station is designed similar to the orbital cavity except the window can be much smaller (1- to 2-m diameter).

Only one energy exchanger with binary cycle is required for the generation of the 500 MW of electrical power on the ground. The rejection of heat from the subsystem on the ground is not dependent upon space radiators and, therefore, it is possible to lower the rejection temperature by employing water cooling. This consideration was included in analyses to increase the efficiency of the subsystem. Also, the weight of the cavity for heating the potassium is not an important consideration, and the pressure in this ground system cavity was raised. The resulting system is shown in the schematic in Figure 7, and the dimensions are presented in Figure 6. As may be seen, this subsystem is substantially different from the space subsystem. The heat from the subsystem is transferred to cooling water which is subsequently cooled in a cooling tower. The overall efficiency of this subsystem is 75.5%, which is an improvement over the space subsystem.

Two ground electrical power generators (441.2 MW and 69.2 MW) are used to produce the 500 MW of output. These are conventional alternating current generators that are within the operating range of existing powerplants.

One significant point about the ground stations is that current powerplants operating from heat engines driving generators could be operated with the SLPS providing the thermal energy instead of fossil fuels. Sizing of the system to meet specific requirements of an existing facility would present no significant penalties to the system other than operating at the efficiency of current facilities as opposed to the conceived ground station.

Figure 8 shows the system flow for the 500 MW<sub>e</sub> selected configuration including subsystem efficiencies, power requirements, and weights on orbit. The laser power station weighs 3,212 metric tons (MT) (~ 7,000,000 lb) and the relay unit weighs 105 MT (232,500 lb). The system collects 7,913 MW of solar energy and outputs 500 MW of electrical power for an overall systems efficiency of 6.3%.

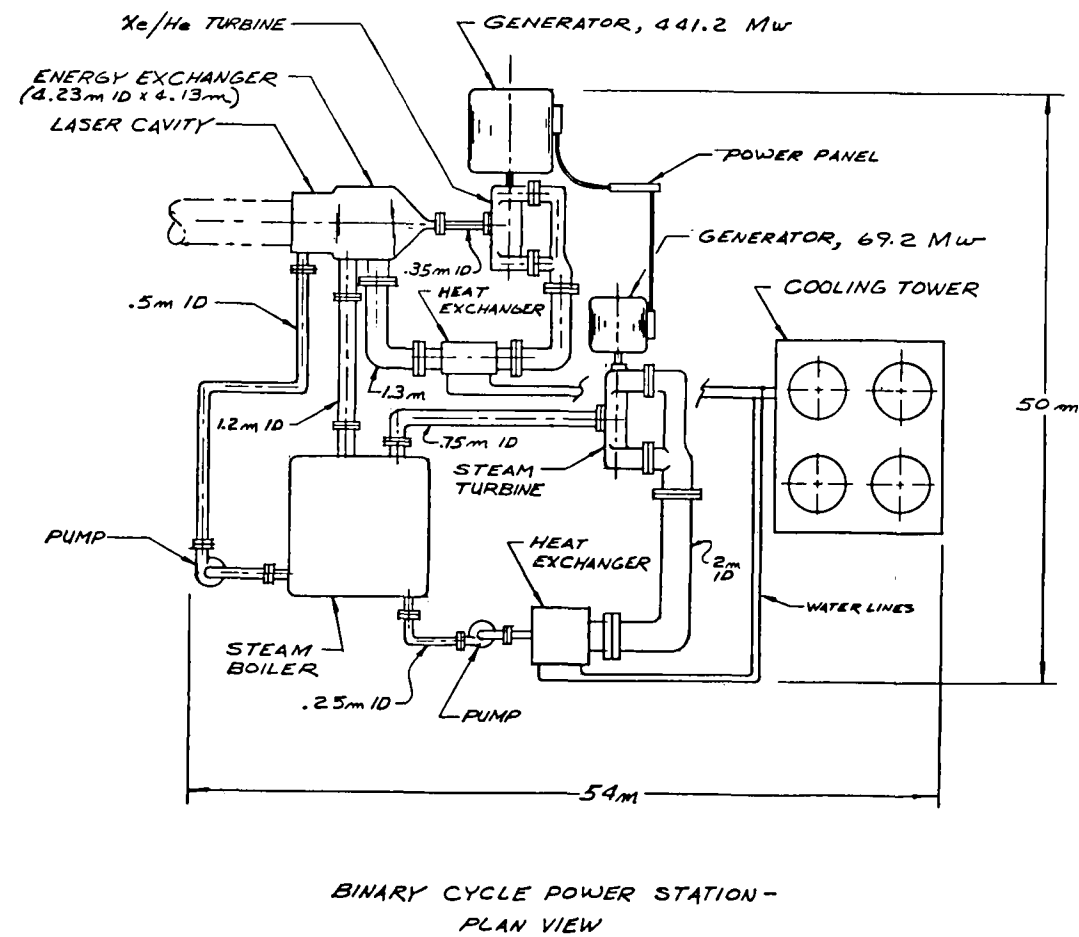
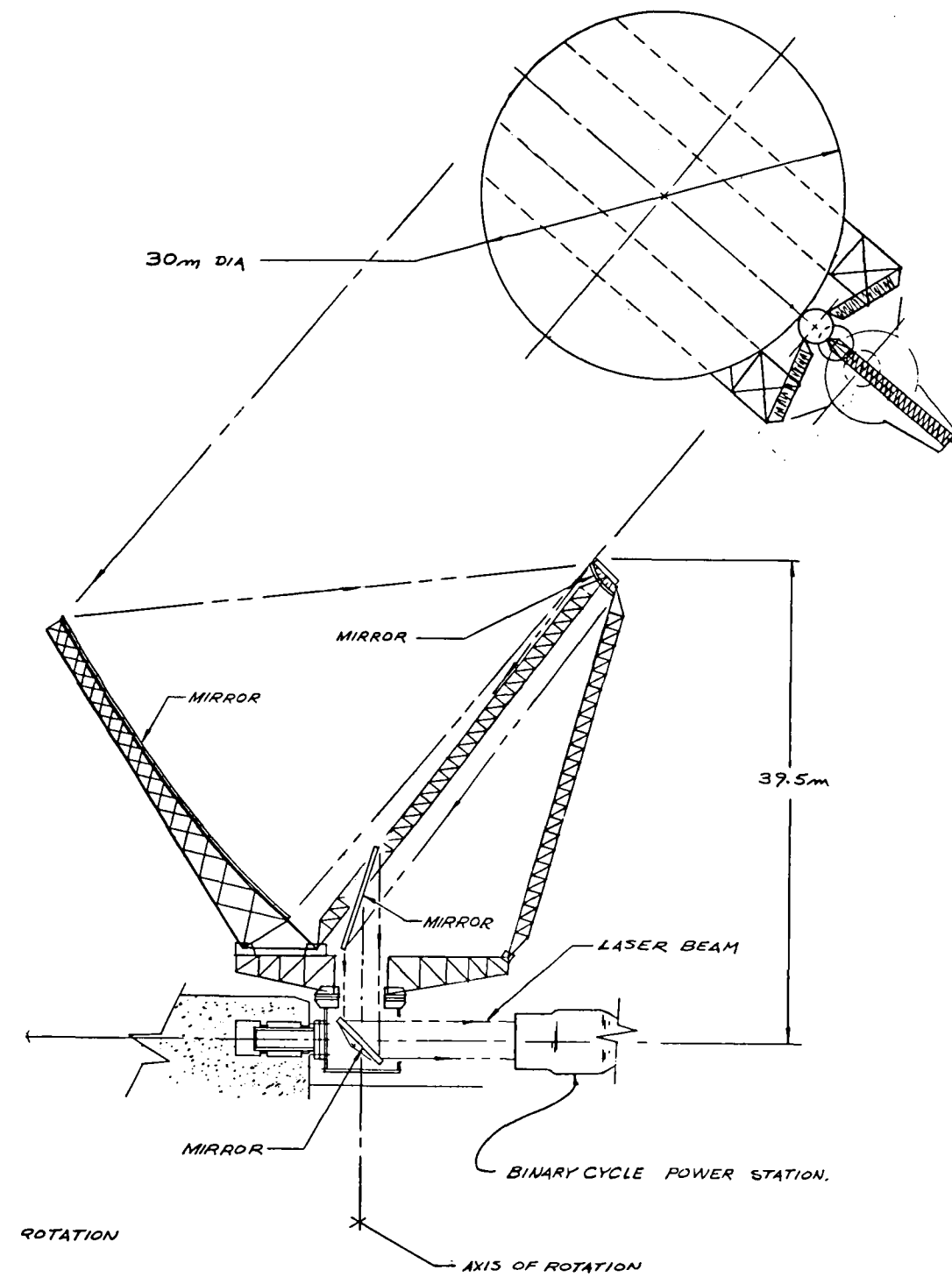


Figure 6 Ground site concept





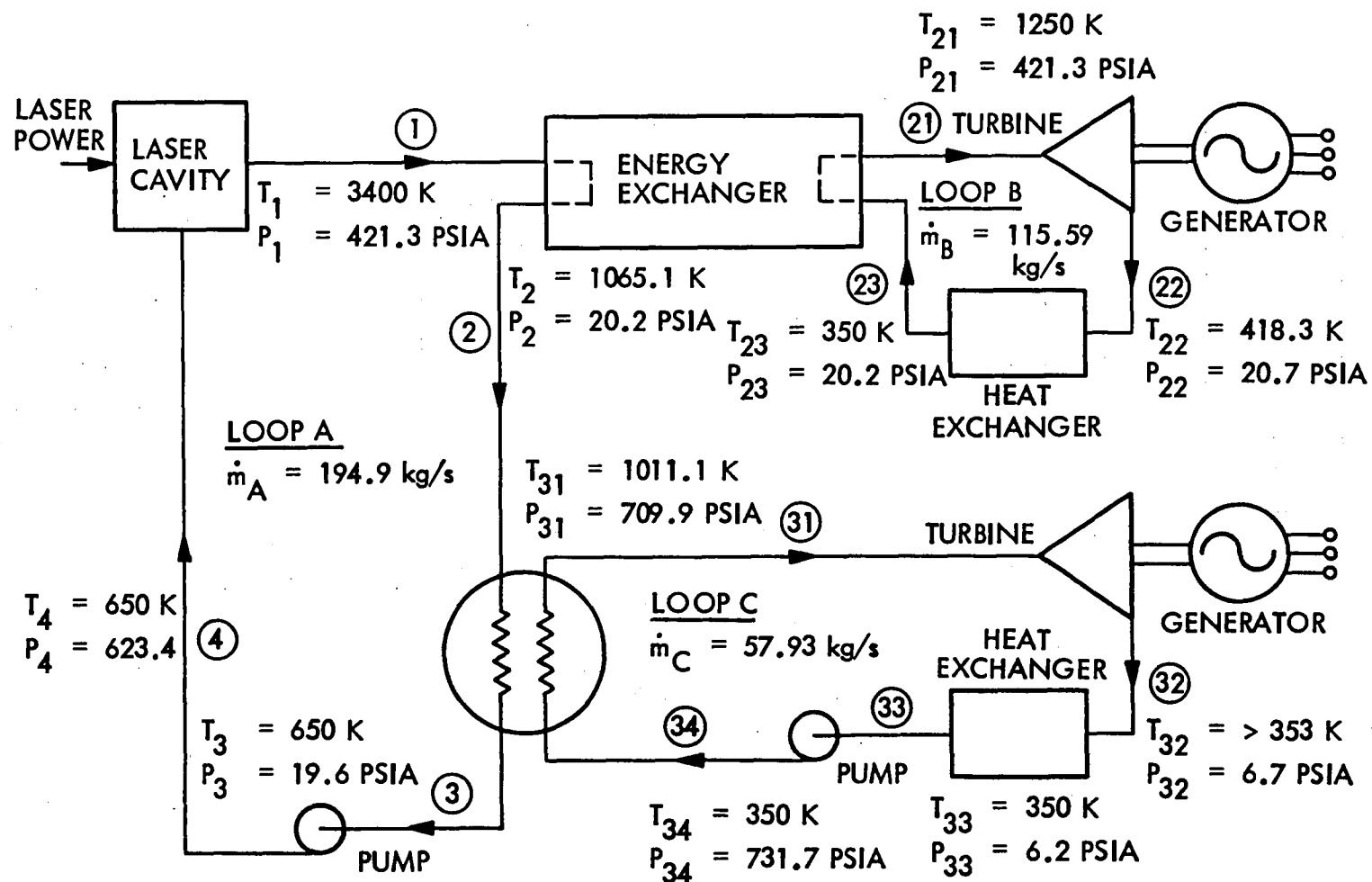


Figure 7. Ground energy exchanger with binary cycle

	Collector	Solar Cavity	EE/Binary Cycle	Power Generation and Conditioning	Laser	Spacecraft, Structure, Radiators, Etc.	Transmitter Aperture and Optical Train
Unit Efficiency (%)	85	86	73.5	93.1	23	—	98.7
System Efficiency (%)	85	73.1	53.7	50.0	11.5	—	11.4
Power In (MW)	7,913	6,726	5,784	4,251	3,958	—	910
Power Out (MW)	6,726	5,784	4,251	3,958	910	—	899
Orbital Weight (kg)	242,850	517,750	1,326,330	717,660	1,809,000	128,653	97,811
						Spacecraft 4,108	Telescope (2) 89,812
						Structure 94,433	Beam Reduction 5,379
						Radiators 6,032	Phasing Array 1,539
						Stabilization 24,080	Optical Train 1,181

	Space Transmission	Space Relay	Atmospheric Transmission	Ground Receiver	Thermal Cavity	Binary Cycle	Electrical Generation
Unit Efficiency (%)	95	99	85	96	98	75.5	98
System Efficiency (%)	10.8	10.7	9.1	8.7	8.5	6.5	6.3
Power In (MW)	899	854	845	718	690	676	510
Power Out (MW)	854	845	718	690	676	510	500
Orbital Weight (kg)	—	105,438	—	—	—	—	—
		Transmitter 44,703					
		Receiver 46,729					
		Optical Train 945					
		Spacecraft 5,900					
		Radiators 5,762					
		Structure 1,023					
		Miscellaneous 376					

Figure 8. 500 MW<sub>e</sub> space laser power system

### 3.2 PROOF-OF-CONCEPT

Should the Space Laser Power System prove to be feasible and a benefit to mankind, the funding commitment necessary would probably be the largest single commitment in history. Before such a commitment will ever be made, solid proof of the concept must be established beyond doubt. The configuration and tests discussed in this section are one concept to establish the proof of feasibility prior to major funding commitments for full-scale development of:

- The system itself
- Construction facilities in space
- Supporting transportation systems
- Supporting operational requirements

The proof-of-concept configuration discussed here can be developed and tested very early with only the use of the shuttle required for transportation and without space construction facilities. This pilot system will demonstrate at a subscale level all the subsystem and system interactions of a full-scale system.

The configuration selected has an electrical output on ground of 500 kW<sub>e</sub>. This size is large enough to show scalability and achieve the efficiencies, but small enough to be relatively economical. Figure 9 shows an overview of the proof-of-concept operation. The operation is based on the capability of the Space Shuttle of achieving an orbit of 185-km by 2000-km due east from the Eastern Test Range with a payload of 18,140 kg (40,000 lb). This orbit has a period of 107.27 min. Two Shuttle loads will place both the laser power station and the relay in orbit approximately 3000 km apart. The ground station could be located in the southwest United States at about 30° longitude. Figure 10 shows three consecutive ground tracks in which the laser power station and the relay each would be within a 3000-km range of the ground station for about 15 min. By directing the laser beam from the power station directly during its period in range and then via relay during its period in range, about 30 min of operating time can be achieved for about 4 or 5 consecutive orbits, then a waiting period would be required until the orbit regression proceeded enough for the laser power station to again be in phase with the ground station. Operational tests could be performed during the "in range" periods to prove all operating procedures required of a full-scale system. Many other scenarios are, of course, possible including full-time operation of the ground station electrical power generation. The specifications of such a pilot program are shown in Table VII. The laser power station would have a laser power output of 910 kW and a transmitter aperture diameter of 4.5 m (14.76 ft). Both the receiver and transmitter apertures of the relay would be 4.5-m diameter. The receiver aperture on the ground would be 18.75-m diameter. Table VIII is a detailed weight statement for the pilot laser power station and relay unit. The proof-of-concept system flow is shown in Figure 11.

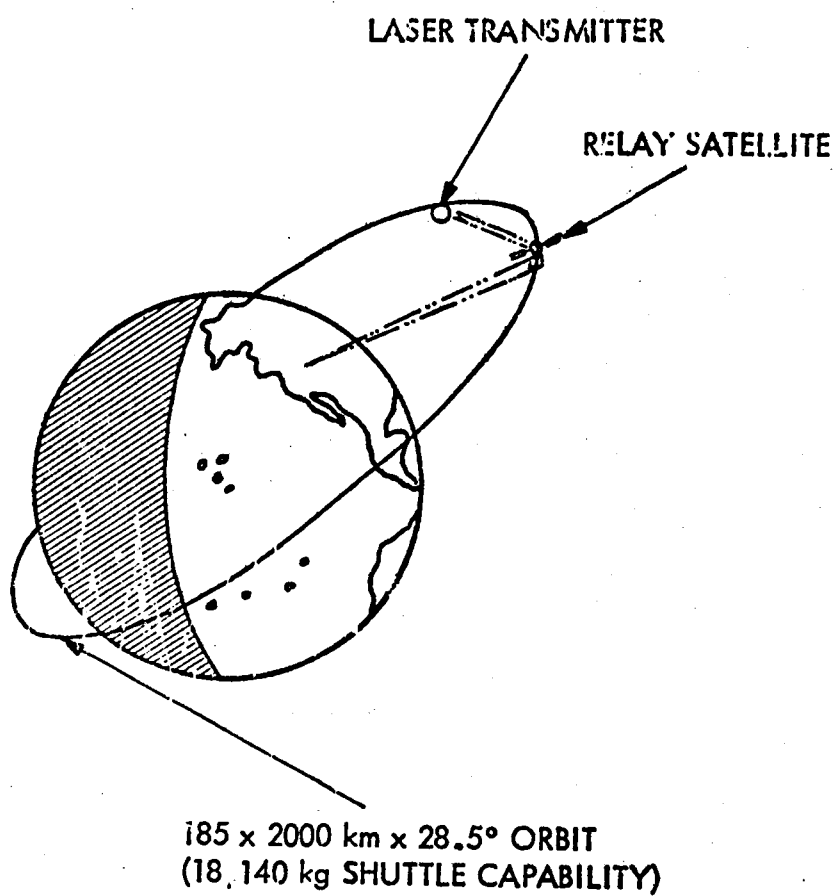


Figure 9. Space Laser Power System proof-of-concept overview

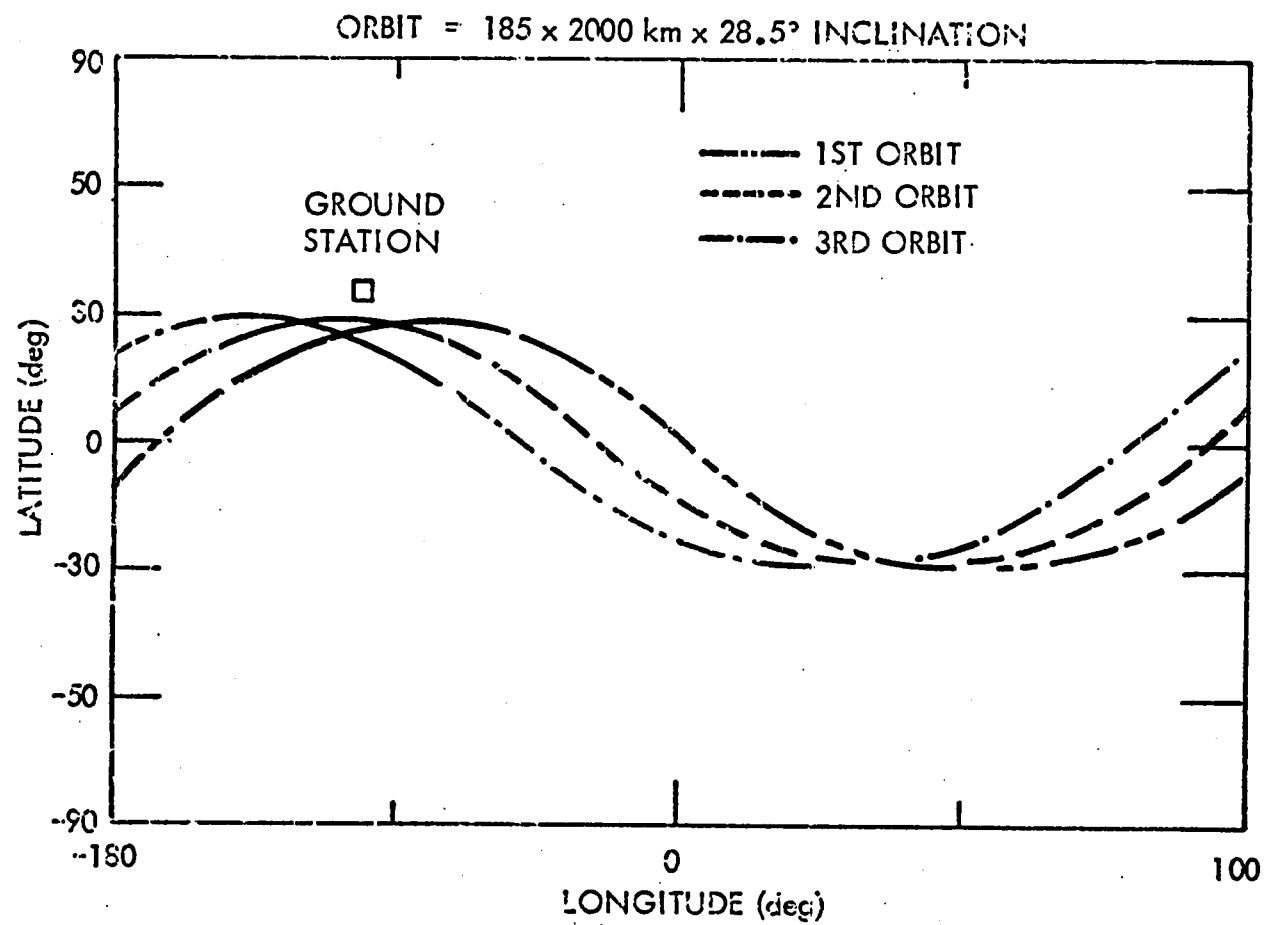


Figure 10. Orbit ground tracks

TABLE VII. PILOT PROGRAM SPECIFICATIONS

Laser Transmitter Satellite		
Electrical Power (kW)		3,958
Laser Power (kW)		910
Transmitter Aperture Diameter (m)		4.5
Relay Unit		
Transmitter Aperture Diameter (m)		4.5
Receiver Aperture Diameter (m)		4.5
Ground Station		
Receiver Aperture Diameter (m)		18.75
Electrical Power at Bus Bar (kW)		500

### 3.3 CONCEPT EVALUATION AND COST

The evaluation of Space Laser Power System (SLPS) economics and comparison of these to the Solar Power Satellite (SPS) system was performed jointly by LMSC and ECON, Inc. LMSC performed the detailed costing of the SLPS pilot program, incremental development cost estimating for the full-scale SLPS, the hardware cost derivation for SLPS production, and the annual operations and maintenance cost estimation excluding on-orbit personnel and transportation.

ECON, Inc., was primarily responsible for SLPS and SPS system cost and economics comparison, and cost sensitivity analyses. To perform a valid comparison, ECON, Inc., used their computerized SPS cost model which includes the latest SPS cost data, comparable transportation costs, construction base costs, on-orbit personnel costs, and uniform support factors for such activities as systems integration, program management, etc. Also, the use of the ECON model assured that for both the SLPS and the SPS comparable cost categories were included for direct relative \$/kW and mills/kW-hr comparison. The following subsections describe in more detail the cost and economic analysis performed in this study.

#### 3.3.1 SLPS Pilot Program Costs

LMSC estimated the pilot program costs for a subscale 500-kW system consisting of a single power satellite, a relay satellite, and a ground station. To accomplish the proof-of-concept flight demonstration, the Shuttle launch vehicle was used to deliver both the power satellite and the relay satellite to  $185 \times 2000$ -km orbit at  $28.5^\circ$  inclination. Two flights are required, since the Shuttle must use an OMS unit (orbit maneuvering system unit) to that orbit; however, there is no need for upper stages (i.e., OTV). The power satellite requires one on-orbit assembly operation to integrate the satellite delivered in two Shuttle flights. It was assumed that this can be performed with the OMS, and on-orbit construction base is not required for the pilot program.

TABLE VIII. PILOT VEHICLE WEIGHT STATEMENT (kg)

	Power Satellite	Relay Satellite
Transmitter	1,292	1,292
Primary Aperture	435	435
Secondary	130	130
Tracker	120	120
Ranger	31	31
Turret and CMGs	<u>576</u>	<u>576</u>
Receiver	—	956
Primary Aperture		440
Secondary		75
Tracker		120
Turret and CMGs		<u>321</u>
Acquisition Sensors	57	114
Optical Train	202	129
Spacecraft	1,238	626
Guidance and Navigation	45	45
C3	54	54
Computer	77	77
Thermal	40	40
El. Power	109	109
Stabilization and Control	680	68
Structure	<u>233</u>	<u>233</u>
Support Structure	620	308
Radiators	1,275	—
Heat Exchangers	—	27
Power Generation	27,596	—
Collector	235	
Solar Cavity	15,700	
Binary Cycle	8,780	
Power Generation	832	
Power Conditioning	240	
Laser	<u>1,809</u>	
Total (kg)	<u>32,280</u>	<u>3,452</u>

	Collector	Solar Cavity	Binary Cycle	Power Generation and Conditioning	Laser	Spacecraft, Structure, Radiators, Etc.	Transmitter Aperture and Optical Train
Unit Efficiency (%)	85	86	73.5	93.1	23	—	98.7
System Efficiency (%)	85	73.1	53.7	50.0	11.5	—	11.4
Power In (kW)	7,913	6,726	5,784	4,251	3,958	—	910
Power Out (kW)	6,726	5,784	4,251	3,958	910	—	899
Orbital Weight (kg)	235	15,700	8,780	1,072	1,809	3,190	1,494
				Generators 832		Spacecraft 1238	Primary 435
				Conditioning 240		Structure 620	Secondary 130
						Radiators 1275	Tracker 120
						Miscellaneous 57	Turret and CMGs 576
							Ranger 31
							Optical Train 202

	Space Transmission	Space Relay	Atmospheric Transmission	Ground Receiver	Thermal Cavity	Binary Cycle	Electrical Generation
Unit Efficiency (%)	95	99	85	96	98	75.5	98
System Efficiency (%)	10.8	10.7	9.1	8.7	8.5	6.5	6.3
Power In (kW)	899	854	845	718	690	676	510
Power Out (kW)	854	845	718	690	676	510	500
Orbital Weight (kg)	—	3,452	—	—	—	—	—
		Transmitter 1292					
		Receiver 956					
		Optical Train 129					
		Spacecraft 626					
		Structure 308					
		Miscellaneous 141					

Figure 11. Proof-of-concept configuration



Other assumptions applied to the pilot vehicle were the use of a single telescope and single laser on the laser power satellite. The use of the same sensors on both the relay and the power satellite permitted sharing of the single development cost on common items. The common equipment philosophy was carried throughout the SLPS design and cost estimating to reduce both development and unit costs. The costs of technology development prior to the pilot program were not estimated.

The costing methodology applied primarily parametric estimators such as \$/kW, \$/lb, and various cost estimating relationships (CERs) to arrive at the hardware unit costs by subsystem. The unit costs were scaled to derive the development, engineering model, and flight prototype hardware. In scaling, assumptions were made with respect to each subsystem as to whether a complete engineering model is to be developed and whether a flight prototype is required. For spacecraft and structures costing, historical CERs were used. For optics, lasers, and sensors, CERs based primarily on study data were applied. The power generation costs were derived via estimators and projections of \$/kW, \$/m<sup>2</sup> and \$/lb for analogous equipment. The ground station power equipment was costed using current commercial power station \$/kW on-line cost.

Table IX presents the estimated SLPS Pilot Program costs. These costs have been estimated in 1977 year dollars. The 500-kW pilot program of \$857 million includes two Shuttle flights at \$24 million each (this covers the OMS kits also) and \$5 million each for Shuttle integration and mission planning.

### 3.3.2 Full-Scale SLPS Costs

#### 3.3.2.1 Development Cost

It is assumed that after the pilot program and the proof-of-concept demonstration is completed, full-scale SLPS development will be started. The SLPS development costs represent incremental development based on the assumption that engineering models of various subsystems will be built and ground tested. The modular design of the power satellite permits the construction of an engineering model which uses one of the ten power generation modules and a subscale collector system. Similarly for ground testing, 20 laser cavities are not needed, since 2 lasers are fed by one power generation module.

The optics and sensor development costs, which are common to both the power and relay satellites, were shared by these two systems; however, separate spacecraft development costs were estimated for each satellite due to the significantly different payload requirements of each and the different orbits.

Table X shows the \$1.5 billion additional (after the pilot program) development cost for the full-scale SLPS. This estimate is in 1977 dollars and does not include development of an HLLV, OTV, and the construction base. Also, it was assumed that no full-scale flight test will be performed since it is reasonable to expect that once the first SLPS unit is built and deployed that it will be tested on-orbit prior to proceeding with the rest of the production.

TABLE IX. SLPS PILOT PROGRAM COSTS  
(1977 \$ MILLIONS)

Subsystems	Power Satellite	Relay Satellite	Ground Station	Total
Optics and Sensors:	\$100.4	\$ 94.0	\$84.1	\$278.5
Telescopes	\$ 35.3	\$43.4	\$71.7	
Turrets	5.0	4.2	5.8	
Optical Train and Control	28.3	27.8	3.4	
Trackers	11.9	7.0	3.2	
Rangers	3.9	1.5	—	
Acquisition Sensors	<u>16.0</u>	<u>10.1</u>	<u>—</u>	
Power Generation:	250.1	—	4.7	254.8
Collector	5.4	—	—	
Solar Cavity	} 170.0	—	} 0.7	
Binary Cycle				
Power Generation	23.0	—	—	
Power Conditioning	7.8	—	—	
Laser	43.9	—	—	
Interface Equipment	—	—	1.0	
Communications Equipment	—	—	3.0	
Spacecraft & Structures:	24.2	19.2	—	43.4
Spacecraft	17.3	17.3	—	
Stabilization and Control	3.8	1.0	—	
Radiators & Heat Exchangers	2.0	0.2	—	
Support Structure	<u>1.1</u>	<u>0.7</u>	—	
Subsystem Total	<u>\$374.7</u>	<u>\$113.2</u>	<u>\$88.8</u>	\$576.7 M
System Costs:				
Facilities				18.0
C3 Modification				10.0
Ground Support Equip				9.8
Sys Engrg & Integr.				86.5
System Grd Test				23.1
Launch & Flt Oper				15.0
Shuttle Integr. & Mission Plan				10.0
Shuttle Flight Fees				48.0
Data				21.9
Program Mgm't				<u>37.6</u>
Pilot Program Total*				<u>\$856.6 M</u>

\*Excludes technology development.

TABLE X. SLPS INCREMENTAL DEVELOPMENT COST  
(1977 \$ MILLIONS)

Subsystems	Power Satellite	Relay Satellite	Ground Station	Total
Optics and Sensors:	\$340.5	\$338.7	\$ 5.0	\$ 684.2
Telescopes	\$121.8	\$191.7		
Turrets	49.0	70.0	} \$ 5.0	
Optical Train and Control	61.3	47.2		
Beam Reduction Telescope	54.3	—		
Phasing Subsystem	24.7	—		
Trackers	12.5	12.5		
Rangers	2.4	1.6		
Acquisition Sensors	<u>14.5</u>	<u>15.7</u>		
Power Generation:	252.9	—	45.0	297.9
Collector	22.7		—	
Solar Cavity	44.5		—	
Binary Cycle	101.9		40.0	
Power Generation	25.0		—	
Power Conditioning	12.5		—	
Lasers	46.3		—	
Interface Equipment	—		3.0	
Communication Equip	<u>—</u>		<u>2.0</u>	
Spacecraft & Structures:	97.0	47.6	—	144.6
Spacecraft	32.3	37.1		
Stabilization and Control	4.7	1.9		
Radiators and Heat Exchangers	} 60.0	} 8.6		
Support Structure				
Subsystem Total	\$690.4	\$386.3	\$50.0	\$1126.7
System Costs:				
Facilities				17.5
C3 Modification				30.0
Grd Support Equip				21.5
Sys Engrg & Integr				161.6
System Grd Test				43.1
Data				39.6
Program Mgm't				<u>68.0</u>
Incremental Development Total*				<u>\$1508.0 M</u>

\*Excludes: transportation, construction base, flight test, and technology development costs.

The total SLPS program peculiar development cost, as shown in Tables IX and X, results in costs of about \$2.4 billion to which the selected HLLV, OTV, personnel Shuttles, and construction base development costs must be added. Costs of \$12 to 20 billion have been estimated for these items in NASA sponsored SPS studies and these were not analyzed in this study.

### 3.3.2.2 SLPS Hardware Cost

The SLPS unit hardware investment costs were estimated by LMSC as shown in Table XI. These costs represent the theoretical first unit hardware cost for the laser power satellite, the relay satellite, and the ground station. They were derived by applying a 90% learning curve to an average unit cost for a given subsystem. Also shown in Table XI is the average unit cost over a buy of 120 systems.

Assuming SLPS concept requirements of one-on-one-on-one (power/relay/ground station), the average SLPS unit hardware costs \$1.4 billion in 1977 \$. This hardware cost excludes the support costs, transportation costs and on-orbit assembly costs, which were incorporated into total investment dollars by ECON, Inc. The investment cost analysis is discussed in section 3.3.3.

### 3.3.2.3 Operations and Maintenance

LMSC estimated the annual operations and maintenance costs excluding transportation to orbit and on-orbit personnel costs. These estimates were based on the review of satellite components and the required replacement heights including station keeping propellants. The ground station was assumed to be manned around the clock by a 2-man operations crew which would communicate with the satellites and monitor the equipment. Maintenance and repair operations would be performed by roaming crews serving all the system ground stations. The resulting LMSC operations and maintenance cost estimates were:

Power Satellite	\$13.2 million/yr/satellite
Relay Satellite	7.2 million/yr/satellite
Ground Station	5.5 million/yr/ground station

These estimates became inputs to the mills/kW-hr analysis performed by ECON, which incorporated on-orbit transportation and personnel requirements over a 30-yr time span. This analysis is discussed in section 3.3.5.

### 3.3.3 SLPS Investment Cost Analysis

The following section outlines the results from ECON's equivalent theoretical first unit (TFU) cost comparison of the Lockheed SLPS with the current Boeing and Rockwell SPS configurations. The Lockheed SLPS is sized at 0.5 GW, the Boeing SPS at 10 GW, and the Rockwell SPS at 5 GW; all sizing represents unit power at the busbar.

TABLE XI. SLPS - THEORETICAL FIRST-UNIT HARDWARE COST\* (77 \$M)

	Power Satellite	Relay Satellite	Ground Station
Telescopes	\$ 210.7 M	\$210.7 M	\$ 75.6 M
Optical Train	48.6	41.6	8.1
Beam Reduction Telescope	36.1	-	-
Phasing S/S	25.2	-	-
Trackers	8.3	8.3	5.1
Rangers	2.4	1.4	-
Acquisition Sensors	10.4	10.4	-
Subtotal	<u>\$ 379.6 M</u>	<u>\$210.3 M</u>	<u>\$ 91.4 M</u>
Spacecraft	\$ 20.5	\$ 21.0	
Radiators	100.0	1.7	
Heat Exchangers	2.5	2.7	
Support Structure	17.7	1.3	
Stabilization and Control	9.1	2.1	
Subtotal	<u>\$ 149.8 M</u>	<u>\$ 28.8 M</u>	
Collector	\$ 90.6	-	-
Cavity	222.6	-	-
Binary Cycle	602.1	-	
Power Generation	148.1	-	\$106.5
Power Conditioning	83.3	-	-
Lasers	269.2	-	-
Communication Equipment	-	-	3.0
Interface Equipment	-	-	1.0
Storage (Flywheel)	-	-	0.6
Subtotal	<u>\$1415.9 M</u>		<u>\$111.1 M</u>
Total First-Unit Hardware	<u>\$1945.3 M</u>	<u>\$339.1 M</u>	<u>\$202.5 M</u>
Average Unit Cost* (120 Units on 90% L.C.)	<u>\$1101.0 M</u>	<u>\$191.9 M</u>	<u>\$114.6 M</u>

\*Excludes: system engineering and integration, program management, ground and space assembly, and transportation.

### 3.3.3.1 Analysis Groundrules and Assumptions

The following groundrules were observed in making this comparison. All hardware costs were considered to be on a "first-unit" basis; that is, no learning was applied except in the case where a high production run for a given element within a single satellite occurred (such as would be the case for amplifiers within a microwave configuration). A uniform 5.55% was applied to the hardware cost of the satellite, the ground station, and the space construction base to represent the cost of program management and systems engineering and integration.

The concept of a construction base for a solar thermal satellite developed by Boeing Co. (as reported in Boeing D180-22876-5, Vol. V, System Definition Study, Part II) was used to generate mass and cost estimates for a facility to construct the Lockheed SLPS. Whereas the modules of the Boeing Solar thermal satellite are almost exactly the same dimensions as the Lockheed satellite, the Boeing construction base is far more elaborate than that which would be necessary to construct a Lockheed SLPS as it is presently envisioned. (A major difference, of course, is Lockheed's inflatable reflector structure.) The cost estimate resulting from this approach is conservative with respect to the Lockheed system.

The costs and masses of the assembly equipment and the space transportation systems are amortized over the number of satellites that can be produced with this equipment. How rapidly this amortization occurs (hence, how high a cost is assigned to each satellite) depends on the design life of the equipment and the rate at which the satellites are being constructed. Construction rates of 8, 16, and 32 satellites per year were considered.

The transportation capabilities and costs used were the latest data extracted from the NASA SPS studies. The characteristics of the Heavy Lift Launch Vehicle are similar to those developed by Boeing, as follows: payload to LEO = 391,000 kg; unit procurement cost = \$1 billion (1977); average cost per flight = \$8.8 million. The orbit transfer vehicle (OTV) used to place the relay satellite in geosynchronous orbit was assumed to be the common stage OTV, having the following characteristics: payload per transfer = 400,000 kg; unit mass = 890,000 kg; unit cost = \$82 million; average cost per flight = \$2.26 million. Finally, the personnel shuttle vehicle used for crew rotation is assumed to be a shuttle derivative with the following characteristics: 75 passengers per flight; unit cost of \$220 million; average cost per flight = \$12.6 million. An HLLV load factor of 90% was assumed. A crew rotation rate of one complete crew rotation every 90 days was assumed.

The SLPS relay satellite was assumed to be launched to orbit ready to be deployed. Consequently, an OTV unit is launched to LEO by two HLLV flights, and an additional half flight is assumed to be necessary to orbit the relay satellite itself. (Fractional HLLV flights are used throughout because it is assumed that other material is launched as well to bring the flight to full payload capacity.)

The cost and mass of the space construction base are as follows: \$7.935 billion and 8560 MT, with 100 MT of consumables being necessary every 22 days. The design life of the entire facility is assumed to be 25 years. The base is designed to be manned by a crew of 760.

The entire investment cost is discounted from time of procurement to time of initial operation at the rate of 7.5% per annum. The investment costs are assumed to follow a cash flow profile characterized by a beta distribution beginning 4 years before initial operation and peaking 6 months before operation.

### 3.3.3.2 Investment Costs

Total SLPS investment costs for the TFU were generated applying the above ground-rules. The SLPS hardware costs from Table XI were increased by a 5.55% support factor to arrive at the following TFU costs:

Power Satellite	\$2053.26 M
Relay Satellite	357.92
Ground Station	213.74

The construction base, HLLV transportation and construction base personnel shuttle transportation costs were derived and prorated per unit SLPS as shown in Tables XII, XIII, and XIV, respectively. The costs were kept parametric with respect to annual construction rate. The relay satellite transportation costs were estimated at \$24.26 M each:

$$(2-1/2 \text{ HLLV flights}) \times (\$8.8 \text{ M/HLLV flight}) + (\$2.26 \text{ M/OTV flight})$$

Table XV shows the summarized investment (hardware, construction base, and transportation) costs for the first SLPS unit. At the construction rate of 16 units per year, the discounted cost per kW installed is \$6100. The latest estimates that ECON has indicated that comparable TFU cost per kW installed for the considerably larger Boeing and Rockwell SPSs are \$4500 and \$3800, respectively.

TABLE XII. PRORATED CONSTRUCTION BASE COST AND MASS

Construction Rate/Year:	8	16	32
Costs/SLPS (77 \$M)	\$ 39.675	\$ 19.858	\$ 9,919
Mass (kg)	242,800	121,400	60,700

TABLE XIII. HLLV TRANSPORTATION COST AND MASS  
(BASE AND POWER SATELLITE)

Construction Rate/Year:	8	16	32
Cost/SLPS (77 \$M)	\$127.6	\$124.1	\$122.3
Mass to LEO (kg $\times 10^6$ )	5.083	4.961	4.901

TABLE XIV. PERSONNEL SHUTTLE TRANSPORTATION COST

Construction Rate/Year:	8	16	32
Cost/SLPS (77 \$M)	\$63.84	\$31.92	\$15.96

TABLE XV. TOTAL SLPS INVESTMENT COST FOR THE THEORETICAL FIRST UNIT (77 \$M)

	Construction Rate/Year		
	8	16	32
Power Satellite	\$2053.26 M	\$2053.26 M	\$2053.26 M
Relay Satellite	357.92	357.92	357.92
Ground Station	213.74	213.74	213.74
Prorated Space Base	39.68	19.84	9.92
HLLV Transportation	127.60	124.10	122.30
Relay Transportation	24.26	24.26	24.26
Personnel Shuttle	<u>63.84</u>	<u>31.92</u>	<u>15.96</u>
Undiscounted Total	\$2880.30 M	\$2825.04 M	\$2797.36 M
Discounting Factor	<u>× 1.08</u>	<u>× 1.08</u>	<u>× 1.08</u>
Discounted Total	<u>\$3110.72 M</u>	<u>\$3051.04 M</u>	<u>\$3021.15 M</u>
Discounted \$/kW Installed at First Unit:	\$6221	\$6102	\$6042

### 3.3.4 Equal Installed Power Cost Comparison

To perform equal capability cost comparison of the three systems of such differing point design capabilities (0.5 GW SLPS and 5 or 10 GW SPSs), LMSC normalized them in terms of number of units installed to provide the same amount of power at the busbar. The selected construction rate used was 16 units per year and a 90% learning curve was applied to the TFU SLPS and SPS hardware. The resulting cost comparison is shown in Figure 12.



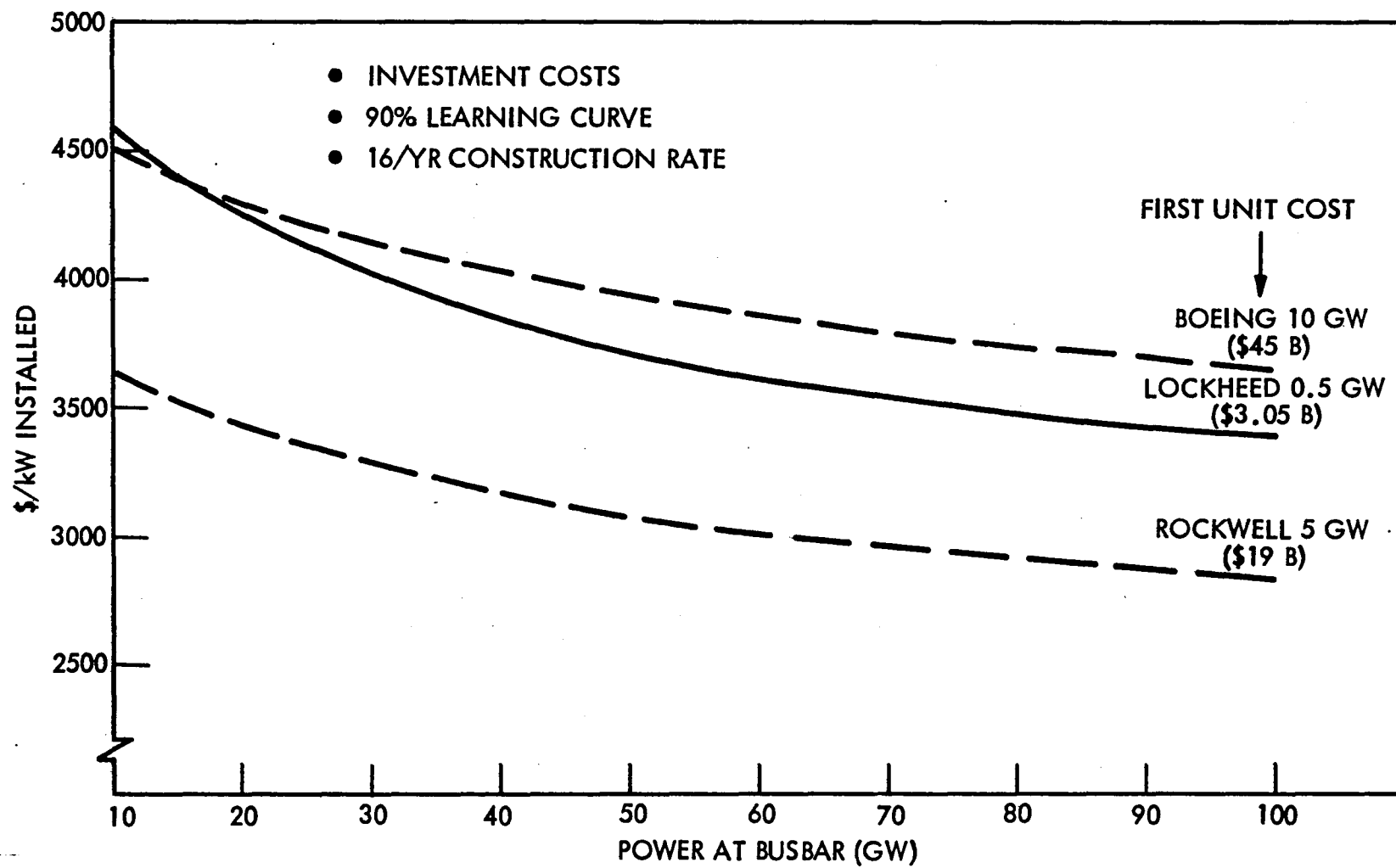


Figure 12. Dollars/kW cost comparison (77 \$)

For example, to deliver 50 GW at the busbar, 5 Boeing SPSs are required, 10 Rockwell SPSs, and 100 Lockheed SLPSs. The resulting respective investment costs per installed kW are \$3950, \$3090, and \$3730.

The application of production learning philosophy to Space production may be highly debatable, especially for a design concept which is to be produced in an orbital highly automated construction base, such as has been proposed for Boeing and Rockwell concepts. The Lockheed design concept is not envisioned to require any on-orbit production, only on-orbit assembly of about 15 segments of the power satellite and no assembly at all of the relay satellite. Therefore, the application of production learning curve to on-the-ground construction is felt to be highly justified, especially when the concept involves so many of the same modular and common components produced at high production rates.

The learning curve was applied in this case (Figure 12) to TFUs for all concepts in order not to bias the analysis. Also, for the sake of direct cost comparison, the same on-orbit construction base costs were prorated to the 0.5 GW Lockheed design as are used for the 10-GW Boeing design including the full staff of 760 people. It is felt that this allows for additional cost conservation, since this study scope did not include SLPS assembly base concept analysis and costing.

Not included in the installed \$/kW cost comparison in Figure 12 are the costs of power reserve on the ground. These costs are expected to be especially significant for the high power design concepts and to benefit the smaller scale SLPS.

### 3.3.5 Mills/kW-Hr Cost Comparison

ECON generated estimates of mills/kW-hr for the Lockheed, Boeing, and Rockwell concepts. These costs are based on 30-year operations period at 90% availability and include both investment and operations and maintenance costs. Also ECON discounted the costs at 7.5%. The resulting estimates of the theoretical first unit, which is used by ECON for all their analyses, is as follows:

0.5 GW Lockheed SLPS	73.4 mills/kW-hr
10.0 GW Boeing SPSs	53.1 mills/kW-hr
5.0 GN Rockwell SPSs	45.9 mills/kW-hr

LMSC carried the mills/kW-hr cost comparison further by performing the comparison at equal power and by extending ECON's estimates. The results of this comparison are shown in Figure 13. Using 50 GW at the busbar as an example, the following costs were estimated:

0.5 GW Lockheed SLPS	44.87 mills/kW-hr
10.0 GW Boeing SPS	46.57 mills/kW-hr
5.0 GW Rockwell SPS	37.34 mills/kW-hr

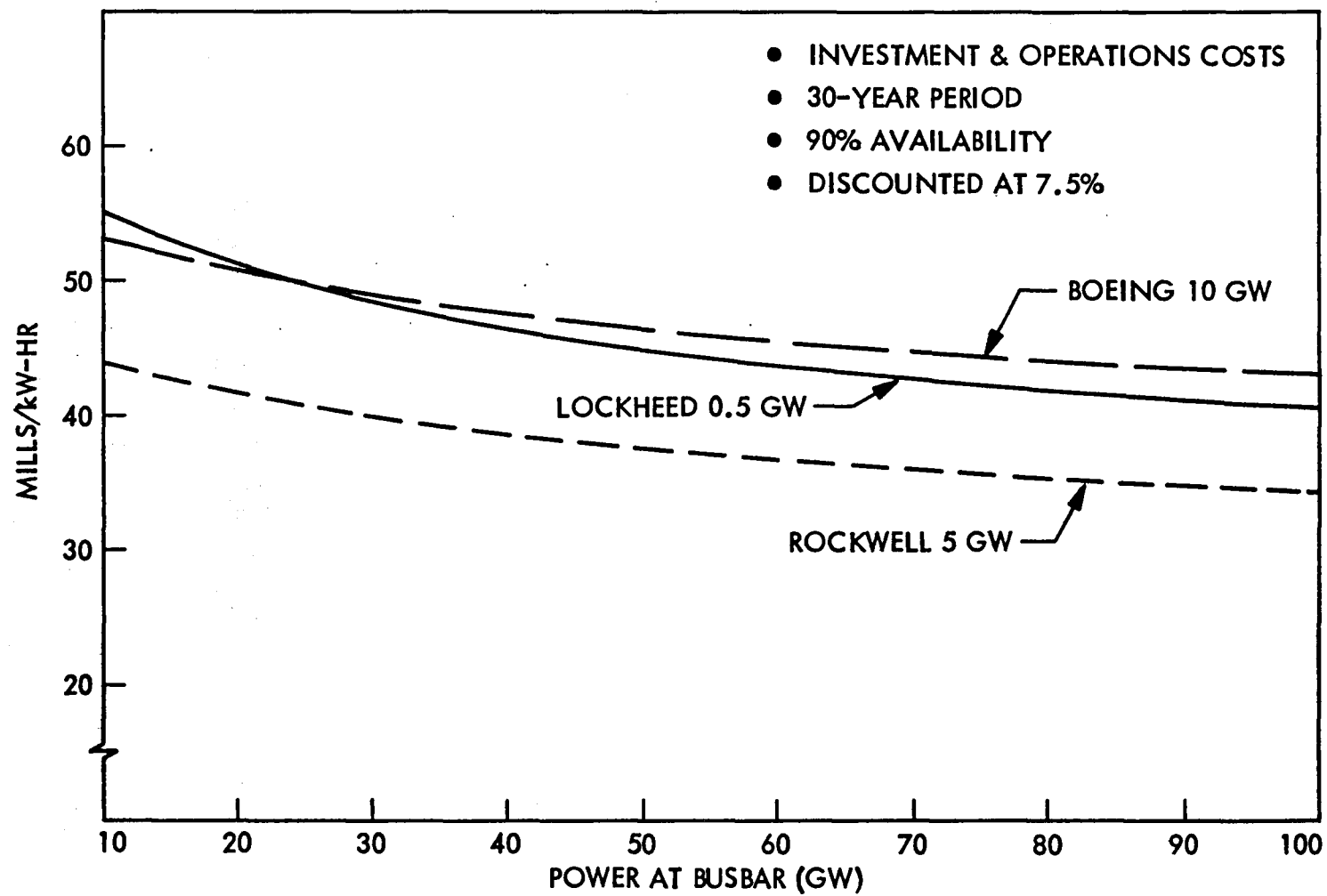


Figure 13. Mills/kW-hr cost comparison (77 \$)

### 3.3.6 Cost Sensitivities

ECON investigated several cost sensitivities of the SLPS system. SLPS mass on orbit and given SLPS configuration were investigated with the following results:

- Mass on orbit —  $\Delta$  \$0.0009/kW installed for each additional kilogram.
- 2 GEO Relay Satellites per SLPS unit —  $\Delta$  \$382/kW installed.
- 1 GEO and 1 LEO Relay Satellite per SLPS unit —  $\Delta$  \$360/kW installed.
- 2 ground stations per SLPS unit —  $\Delta$  \$214/kW installed.

These sensitivities were performed at the theoretical first-unit basis and for the nominal production rate of 16 units/year, which results in nominal SLPS TFU cost per installed kW of \$6102. (See Table X.) Therefore, if the SLPS mass on orbit grows by 10,000 kg, the cost per installed kW becomes \$6111. If the baseline SLPS configuration of one power satellite, one GEO relay, and one ground station is revised to two GEO relays, the TFU \$/installed kW become \$6484. Similarly, if for redundancy purposes two ground stations are required per SLPS unit, then the estimate is \$6316/kW.

### 3.3.7 Cost Evaluation Summary

As the foregoing analyses results have indicated, the Lockheed SLPS concept is quite competitive with the proposed considerably larger (10 to 20 times) SPS concepts. The proposed subscale 500 kW SLPS pilot program at less than \$1 billion (\$857 million) is considerably lower in cost than the proposed non-scalable pilots for the large SPS concepts.

The costs per installed kW are higher for the SLPS at the first unit, since it is a smaller system; however, at equal power levels at the busbar the SLPS is in the same \$3000 to \$4000 range with the large SPSs. (See Figure 12.) On the basis of mills/kW-hr, the SLPS is similarly competitive with the other concepts in the 35 to 45 range. At the projected 50 GW at the busbar the SLPS estimate of 45 mills/kW-hr (see Figure 13) compares directly with the current costs of power at 4.5¢/kW hr.

This cursory economic and cost analysis did not permit investigation of the SLPS on-orbit assembly base requirements in terms of size, machinery, and personnel. Also a closer look at the transportation costs is needed, especially the OTV and the Personnel Shuttle which were felt to be oversized for the SLPS needs. Also, further cost and economic analyses should consider the cost of the reserve on the ground, which has been a significant omission so far; especially, when such diverse (in power) concepts are compared. Another cost impact not considered in this study is the relative technology development for the SLPS and SPS concepts. The microwave/biological problem solution may drive the SPS technology development costs more than the size and complexity of the hardware.

## 3.4 SUBSYSTEM EVALUATION

The purpose of evaluating various methods and techniques to accomplish the various subsystem requirements and capabilities was to reduce the matrix of parametric

system analyses by eliminating subsystem candidates that would not provide the required capability, would not interact or interface acceptably with other subsystems, or would significantly decrease the overall system efficiency. Not all subsystems were evaluated in detail. For example, receiving and transmitting apertures for the laser power station and relay units were evaluated in the Laser Rocket System Analysis (Ref. 2) and are still being studied in current contracts; therefore, evaluation for this study was not necessary. Large adaptive optics were first shown to be feasible in a NASA Lewis Research Center study performed by ITEK (Ref. 4), and have been continually advancing since. Cooperative pointing and tracking was demonstrated in the laboratory several years ago for laser communications systems. Pointing and tracking is also continuing to advance in technology status and was not evaluated in this study. The primary emphasis of subsystem evaluation centered on energy conversion — solar to electric, solar to laser, electric to laser, and laser to electric.

#### 3.4.1 Electric Power Generation From Solar Energy

The electric power generation subsystem has a significant impact on the Space Laser Power System using lasers for power transmission. The operational modes selected for these systems result in exposure levels in the Van Allen belts which significantly affect the performance of photovoltaic cells. Also, maximum power generation efficiency is desired, even if this may result in somewhat higher weights. The operation of the SLPS with laser power transmission does not require the transfer of these resulting masses to geosynchronous orbit.

##### 3.4.1.1 Silicon Solar Cells

Silicon solar cells for use in the SLPS have been well documented in a number of studies (Refs. 5 and 6). Extrapolations of technology have been made to predict laboratory conversion efficiencies as high as 18%. Current laboratory efficiencies are on the order of 12%, but these do not usually exceed 10% in actual arrays. Since the desired operational mode for the SLPS is in low earth orbit, the resulting efficiency has been determined to be approximately 7% because of degradation from passing through the Van Allen Belt.

##### 3.4.1.2 Gallium Arsenide Solar Cells

Gallium arsenide solar cells are capable of higher efficiencies than silicon cells, and appear to have higher resistance to Van Allen belt radiation (Refs. 7 and 8). However, to achieve these higher efficiencies, the cells must operate at high concentration ratios, 100 to 1000, while maintaining low temperatures. LMSC has examined factors involved and the effects of the Van Allen belts, and has concluded that in this application the end of life efficiency would likely be on the order of 12%, even though the efficiencies could theoretically be as high as 22%.

##### 3.4.1.3 Brayton Cycle

The Brayton cycle systems have been discussed in Volume I of this report. The efficiencies of the cycle are directly relatable to the allowable turbine inlet temperature,

which is a material limitation. As pointed out in Volume I, the solar Brayton cycle has been extensively investigated. The cycle requires a solar concentrator to achieve the desired temperatures in a solar heated cavity, which in turn heats the working gas before it enters the turbine. The data indicate that the maximum achievable cycle efficiency is less than 40%.

#### 3.4.1.4 Energy Exchanger With Turbine Cycle

The efficiency of the Brayton cycle can be significantly increased by replacing the compressor and heater in the cycle with an energy exchanger. (The energy exchanger is discussed in Volume I.) The energy exchanger systems are presented in Refs. 9, 10, 11, 12.

As discussed in Ref. 9, a solar concentrator may be used to heat a working fluid in a cavity. The vaporization of liquid potassium and super-heating to 3400 K is a viable approach. Potassium vapor absorbs solar radiation within approximately 1 m of path length. The high temperature potassium is expanded in the energy exchanger where it compresses and consequently heats the gas employed in the turbine cycle. The working gas may be a helium-xenon mixture which is adjusted in molecular weight so as to have the same acoustic velocity at its temperature as the potassium vapor. The high temperature gas is expanded through the turbine to produce work. Since the cycle is not 100% efficient, the gas must subsequently be cooled in a radiator before entering the energy exchanger for recompression.

In this cycle, the potassium, which is a mixture of condensed vapor and gas, is completely liquified in a radiator, and the liquid is then pumped back into the solar cavity for vaporization.

Assuming that the potassium vapor has a temperature of 3400 K and the working gas enters the turbine at 1250 K, this cycle was found to have a thermodynamic efficiency of 58%.

#### 3.4.1.5 Energy Exchanger With Binary Cycle

The overall efficiency of the thermodynamic cycles of an energy exchanger with turbine can be increased by the addition of a bottoming Rankine cycle. This cycle is illustrated in Figure 14. As presented in the figure, Loop A is the heated potassium loop, Loop B is a helium-xenon gas loop, and Loop C is a steam loop. For the purpose of the comparisons of various systems, the radiator temperature were established at approximately 300 K. (These temperatures were increased in the conceptual design presented in section 3.1.) The system operating parameters are principally established by the selection of the turbine inlet temperature and the radiator temperature and the potassium maximum temperature. If the energy exchanger inlet pressure in Loop B is assumed, the other pressures are established from the temperature ratios. It was determined that for maximum efficiency, it was desirable to allow the potassium to condense in the energy exchanger. The quality of the gas-vapor mixture was established at 40%, which determines the outlet temperature of the potassium from the energy exchanger.

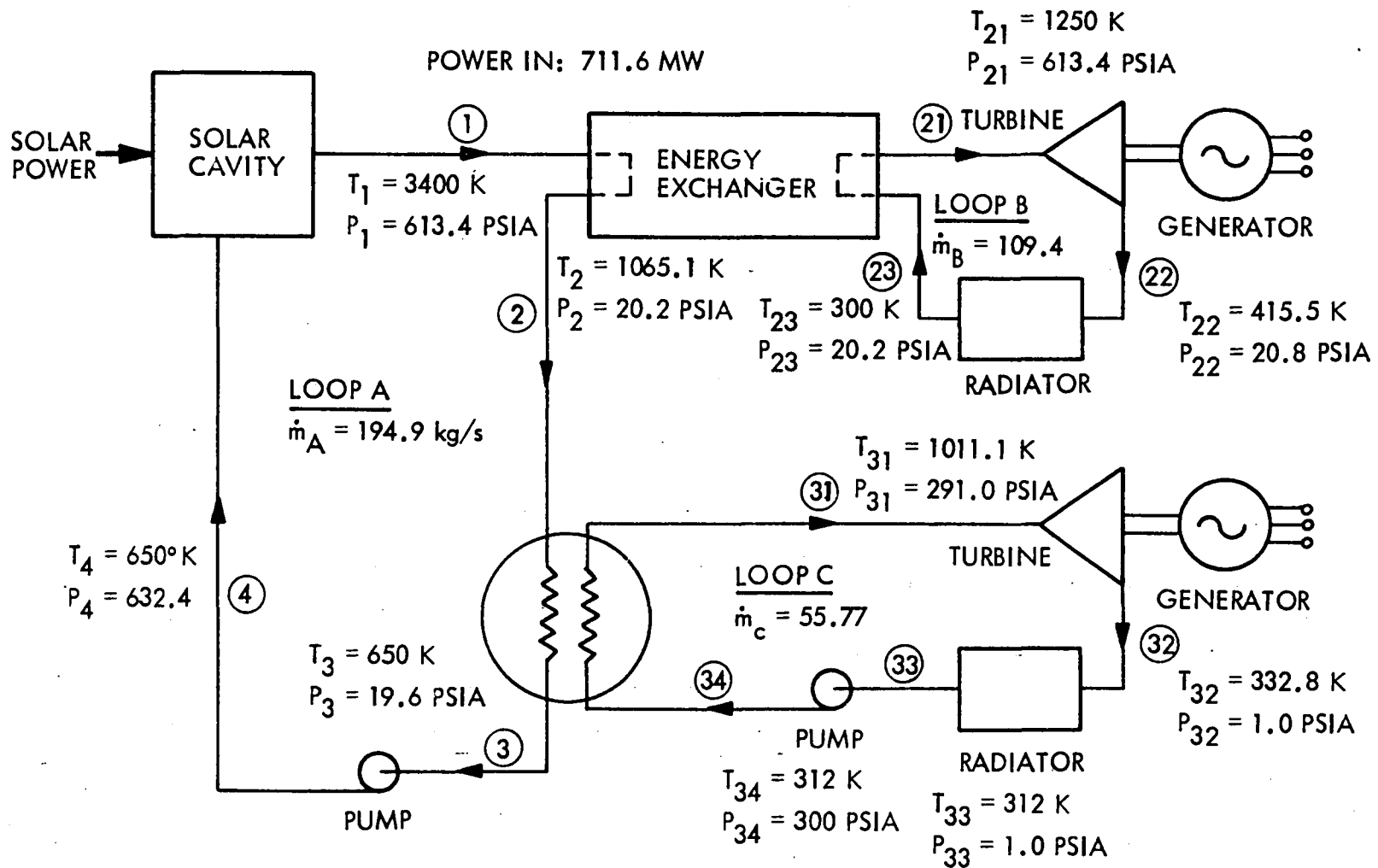


Figure 14. Energy exchanger/binary cycle

Computer programs were used in determining the sizes and weights of the energy exchangers. These were principally based upon the relationships presented in Ref. 13. The major factors influencing the design are: (1) tip velocity assumptions, (2) assumed number of cycles per channel per revolution, (3) assumed mach numbers, (4) state conditions of the fluids, and (5) flow-rates. Typical data for the energy exchanger requirements from Figure 14 are presented in Figure 15.

The overall efficiency of the energy exchanger/binary cycle illustrated in Figure 14 was determined to be 73%. The fraction of the power which is output from Loop B is 0.846. With the remaining fraction of 0.154 from Loop C. The resulting high efficiency is very dependent upon this ratio. Loop B is a very efficient cycle, and it is desirable to maximize the output from this loop.

#### 3.4.1.6 Solar Collector/Concentrator

A solar collector/concentrator is required for all solar energy conversion techniques evaluated in this study except for the silicon solar arrays. The gallium arsenide solar arrays were evaluated and a solar concentration of 500 suns was selected which governs the spot size on which the solar energy must be concentrated. The dynamic thermal cycles evaluated generally require the concentration to be in as small an area as possible, and a secondary concentrator was conceived to provide additional concentration above that attainable from the primary concentrator.

The basic concept selected for this application was developed on an in-house program, Starlet/Starlite, which was a three-stage rocket and spacecraft designed to explore the outer planets (Pluto in < 10 years). The purpose of the concentrator at that time was to concentrate the solar energy at 30 to 40 astronomical units (AU) to the level of unconcentrated solar energy at 1 AU. This concept was developed and a subscale model (10-ft diameter) built and tested for structural integrity. This concentrator concept was formed aluminized Mylar with annulus structural members made of plys of aluminum foil and Mylar which, when pressurized beyond the tensile yield strength and depressurized, would maintain its shape and provide the structural integrity required in the near zero "G" operating environment. The model tested maintained its structural requirements in a 1-G environment. In the same time period, a smaller model was constructed in which the membrane was held in shape by electrostatic charges. This model also worked well.

The solar collector/concentrator concept selected for this system is shown in Figure 16 and incorporates both previous concepts and is adapted to this particular application. For example, all systems requiring solar concentration will have excess heat to reject; therefore, the radiator is utilized as structure around the collector/concentrator. The outside perimeter is maintained both by an annulus-type beam and structural beams as shown in Figure 17. The transmitter units are mounted to this structural beam. The reflector geometry is simplified into a series of cone frustrums taking the general shape of a parabola as shown in Figure 18. In the figure,  $R_s$  is the spot radius,  $R_o$  is the radius of obscuration, and  $\alpha_s$  is 1/2 the apparent angle of the sun. The cone

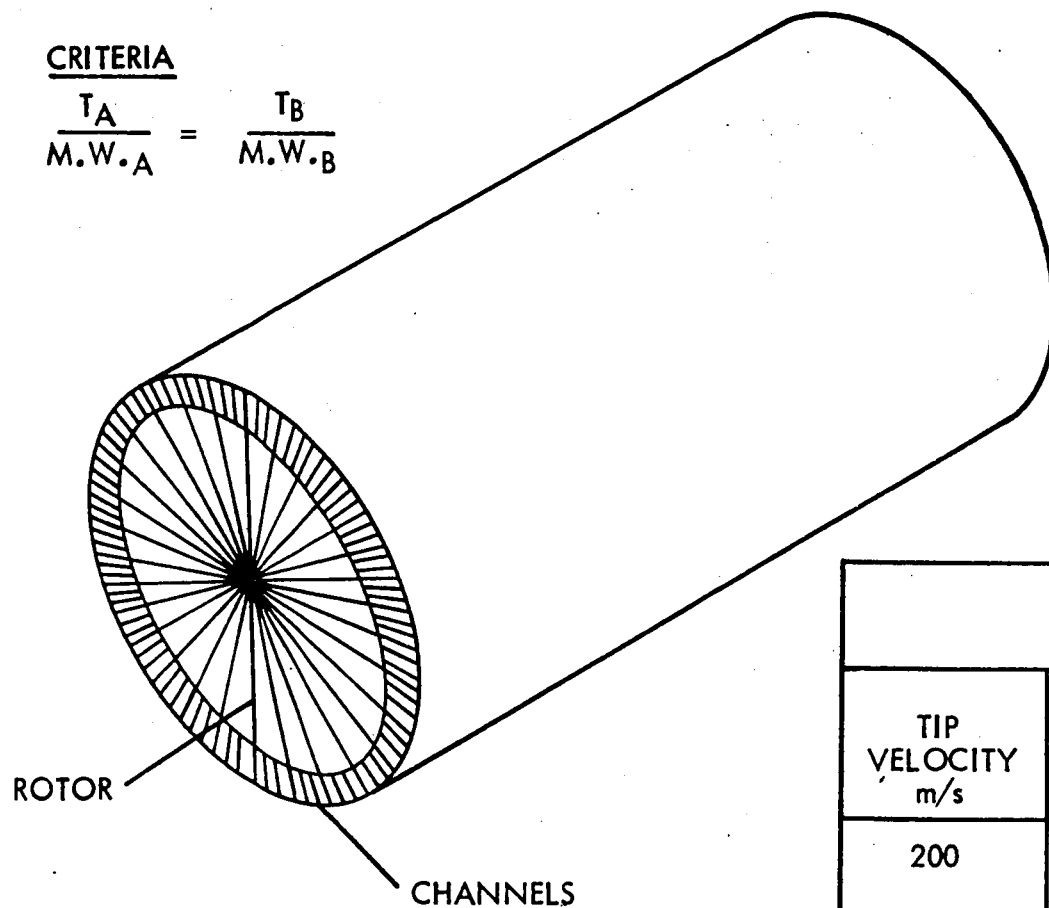


CRITERIA

$$\frac{T_A}{M.W._A} = \frac{T_B}{M.W._B}$$

PARAMETERS

- TIP VELOCITY
- CYCLES/CHANNEL/REV
- MACH NUMBERS
- STATE CONDITIONS



TYPICAL TWO CYCLE DATA						
$\dot{m} = 109.4 \text{ kg/sec}$						
TIP VELOCITY m/s	REV/ s	DIA (m)	L (m)	CHANNELS		
				NO.	H (cm)	W (cm)
200	6.3	3.07	5.98	130	18.6	7.6
700	11.8	5.74	3.2	450	10.	4

Figure 15. Energy exchanger parameters

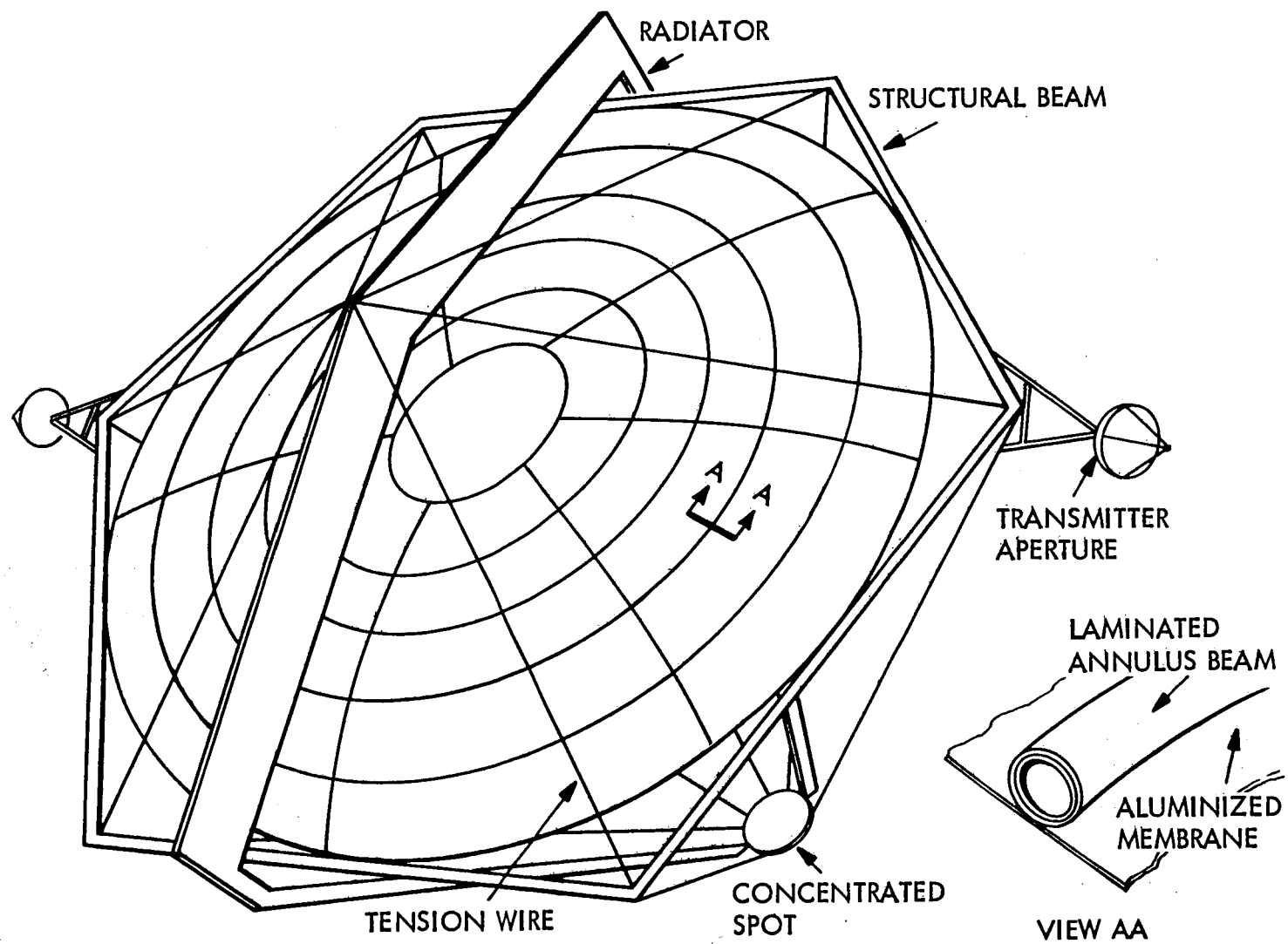


Figure 16. Solar collector/concentrator construction concept

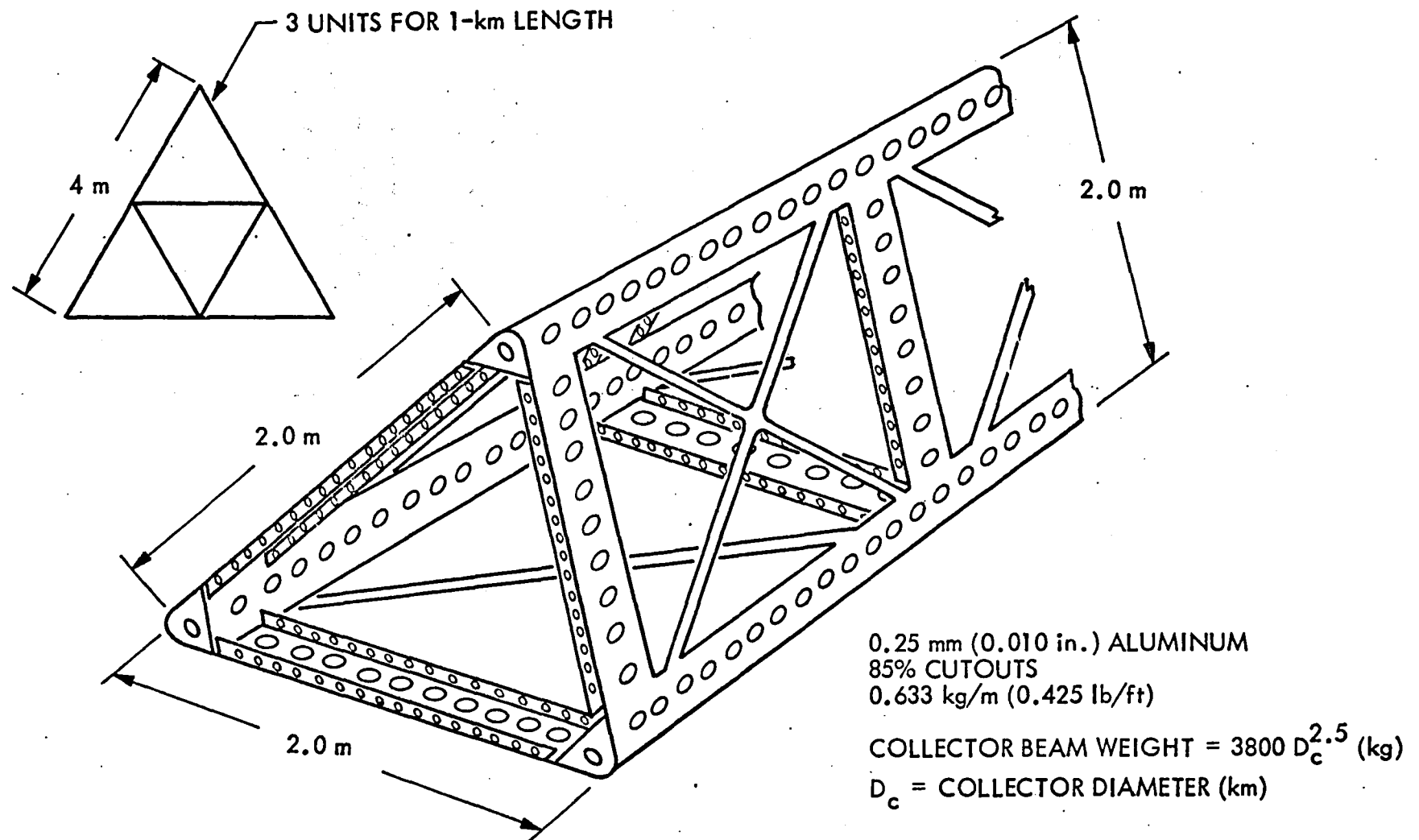


Figure 17. Structural beam construction

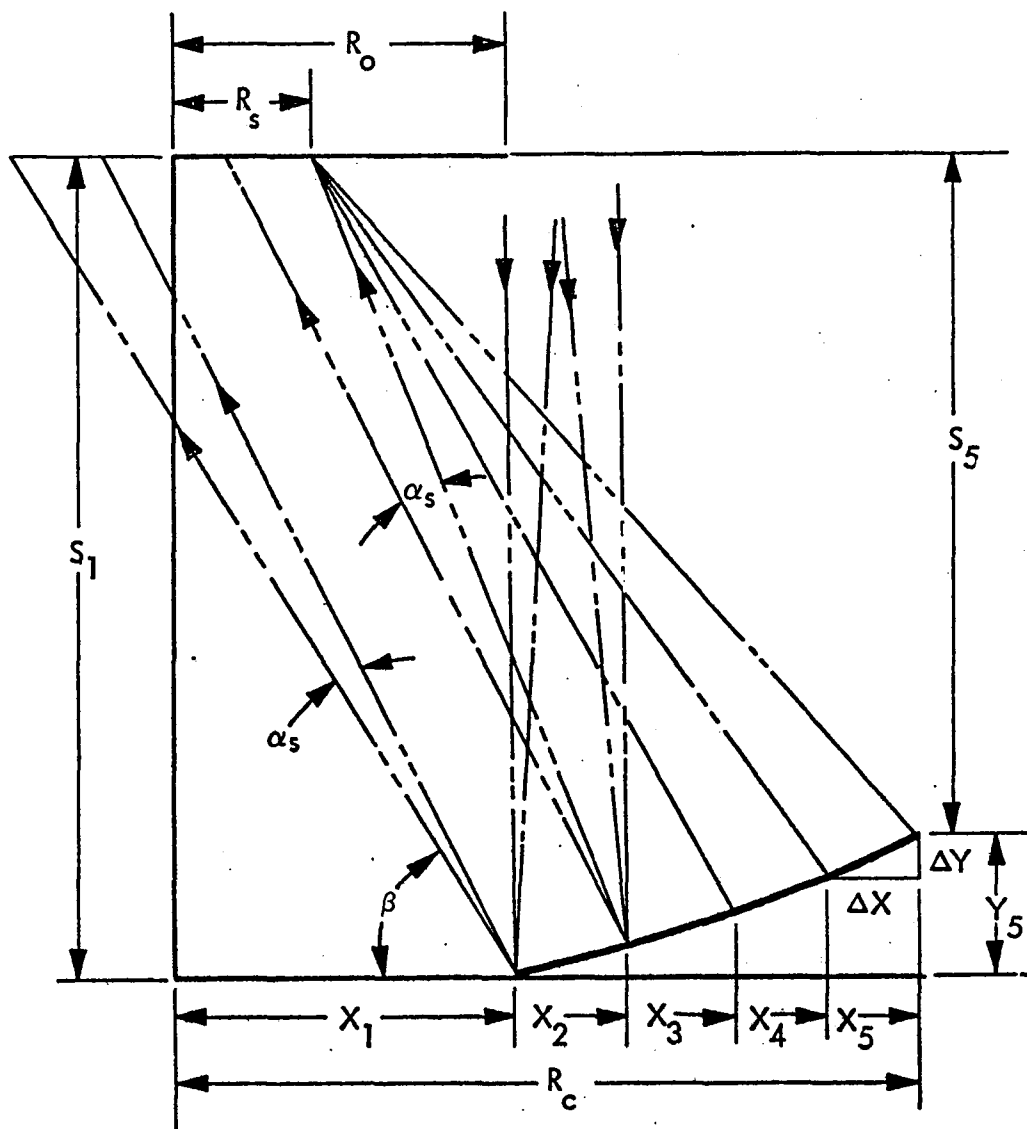


Figure 18. Reflector geometry

angles and size are computed so that the solar energy including that contained in the half angle will be reflected within the spot diameter. Annulus beams will be used at each cone frustrum intersection. In addition a back membrane supported from the tension wires will have a grid so that varying electrostatic charges can be applied and improve the efficiency of concentration and reduce losses of stray light because of manufacturing tolerances. For those systems requiring the solar energy to be deposited into a thermal cavity, the minimum spot size is desirable. This minimum spot size is a function of the apparent angle of the sun, the concentrator diameter, and the f number to which the concentrator is designed. Figure 19 shows that an f number of 0.6 is optimum regardless of the diameter of the concentrator; however, the spot size does increase with the concentrator diameter. The 0.6 f number results in a sun angle of  $45^\circ$  from the outside of the reflector to the spot. Figure 20 shows a secondary concentrator that provides an additional 29 percent reduction. With all of these features in the collector/concentrator, the construction is relatively simple and a conservative estimate of the efficiency is that 85% of the collected energy will be deposited on the concentrated spot.

#### 3.4.1.7 Solar Heated Cavities

The cavity for vaporizing and heating the potassium for the energy exchanger with binary cycle is an important weight item in the systems. The potassium must absorb the solar energy directly and potassium does this very effectively, as presented in Ref. 17. A solar window is required which has good transmission, heat transfer, and strength at temperature. The properties of sapphire are satisfactory. The window has been designed as a spherical segment, which is fitted in the cavity to form a concave surface. The windows are installed in panes with the potassium introduced through the supporting structure, forming a relatively cool vapor barrier between the window and superheated potassium. The cavity must be designed to be as small as possible to reduce the weight since it is operating at such temperature extremes and at relatively high pressures. Tungsten alloys appear to be satisfactory, but must be regeneratively cooled to produce sufficiently high yield strengths to produce acceptable weights. Graphite may be used as an insulating material to reduce the surface temperature. High temperature radiation shields are required on the outside of the cavity to reduce heat losses by radiation.

#### 3.4.2 Laser Subsystems for Power Transmission

The laser subsystems for power transmission are required to have the following characteristics:

- High electrical efficiency
- Relatively high-energy densities (specific power)
- Continuous operating capability, necessitating closed cycles

These requirements limited the candidates of the carbon dioxide and carbon monoxide electric discharge lasers, and possibly the solar pumped lasers. (The free-electron laser was considered as a candidate, but at that time, insufficient data were available

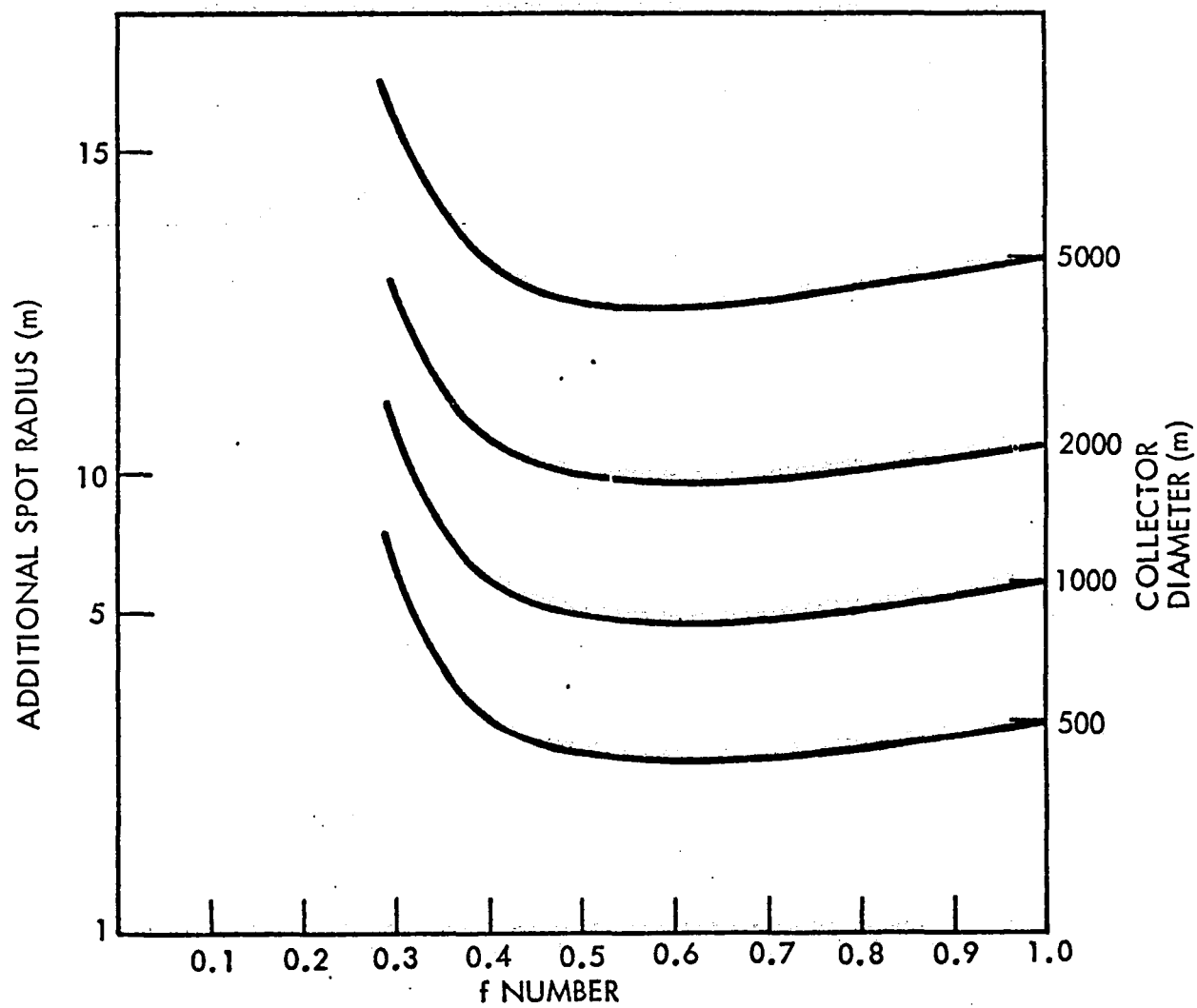


Figure 19. Effects of suns apparent angle

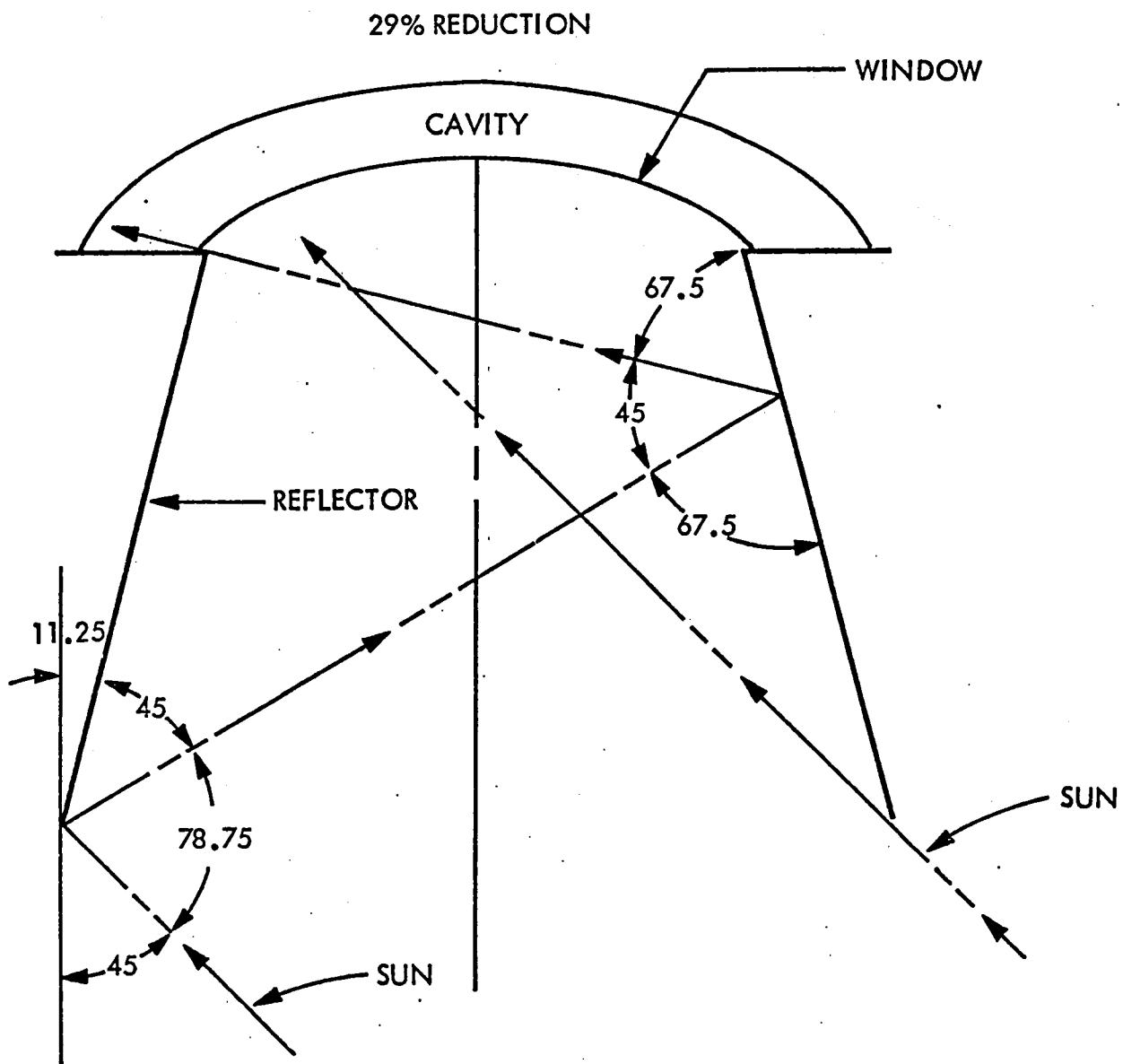


Figure 20. Secondary concentrator

for evaluations.) The performance parameters for the electrical discharge laser devices were selected from Ref. 14. The performance information for the solar pumped lasers was obtained from Ref. 15.

#### 3.4.2.1 Carbon Dioxide Electric Discharge Laser ( $\text{CO}_2$ EDL)

Two closed-cycle laser subsystems were considered for the  $\text{CO}_2$  EDL. These are shown in Figures 21 and 22. The closed-cycle system shown in Figure 21 has a heat removal system based upon "over-compressing" the lasing gases to raise the temperature, and then removing the heat in a heat pipe radiator and subsequently expanding the gas through a turbine which returns energy to the compressor. The alternate approach shown in Figure 22 uses a conventional refrigeration cycle to remove the heat. It was assumed in the analyses that this system utilized water vapor as the refrigerant. The heat was transferred to a heat-pipe radiator. These two closed-cycle laser subsystems were compared in a parametric study in which the laser output power, electrical efficiency, and laser specific power were varied over the likely range of values. It was found from this study that the system shown in Figure 22 was lighter in weight than that shown in Figure 21. However, the system shown in Figure 21 had a better overall electrical efficiency. A comparison of the electrical efficiencies is shown in Figures 23 and 24.

These parametric studies also indicated that the best overall compression ratio for the system shown in Figure 21 was approximately 2. (These results are consistent with those in Ref. 14.) The relationships between the subsystem parameters are shown in Figure 25. From these studies and the data in Ref. 14, the selected laser subsystem was the  $\text{CO}_2$  EDL with internal refrigeration whose parameters are:

Laser Electrical Efficiency	25%
Cavity Specific Power	120 kJ/kg
Overall Electrical Efficiency	20.2%

#### 3.4.2.2 Carbon Monoxide Electric Discharge Lasers

The carbon monoxide lasers were based upon supersonic, low-temperature laser cavities, as presented in Ref. 14. The closed-cycle laser subsystem is shown in Figure 26. A study was conducted to determine the effects of the subsystem parameters. The results are shown in Figure 27. Based on these data, and information from Ref. 14, the following subsystem parameters were selected:

Laser Electrical Efficiency	50%
Cavity Specific Power	400 kJ/kg
Overall Electrical Efficiency	24.8%

#### 3.4.2.3 Carbon Dioxide Solar-Pumped Laser

The solar-pumped laser definition studies were in the initial phases at the time these studies were conducted. The basic information employed was obtained directly from



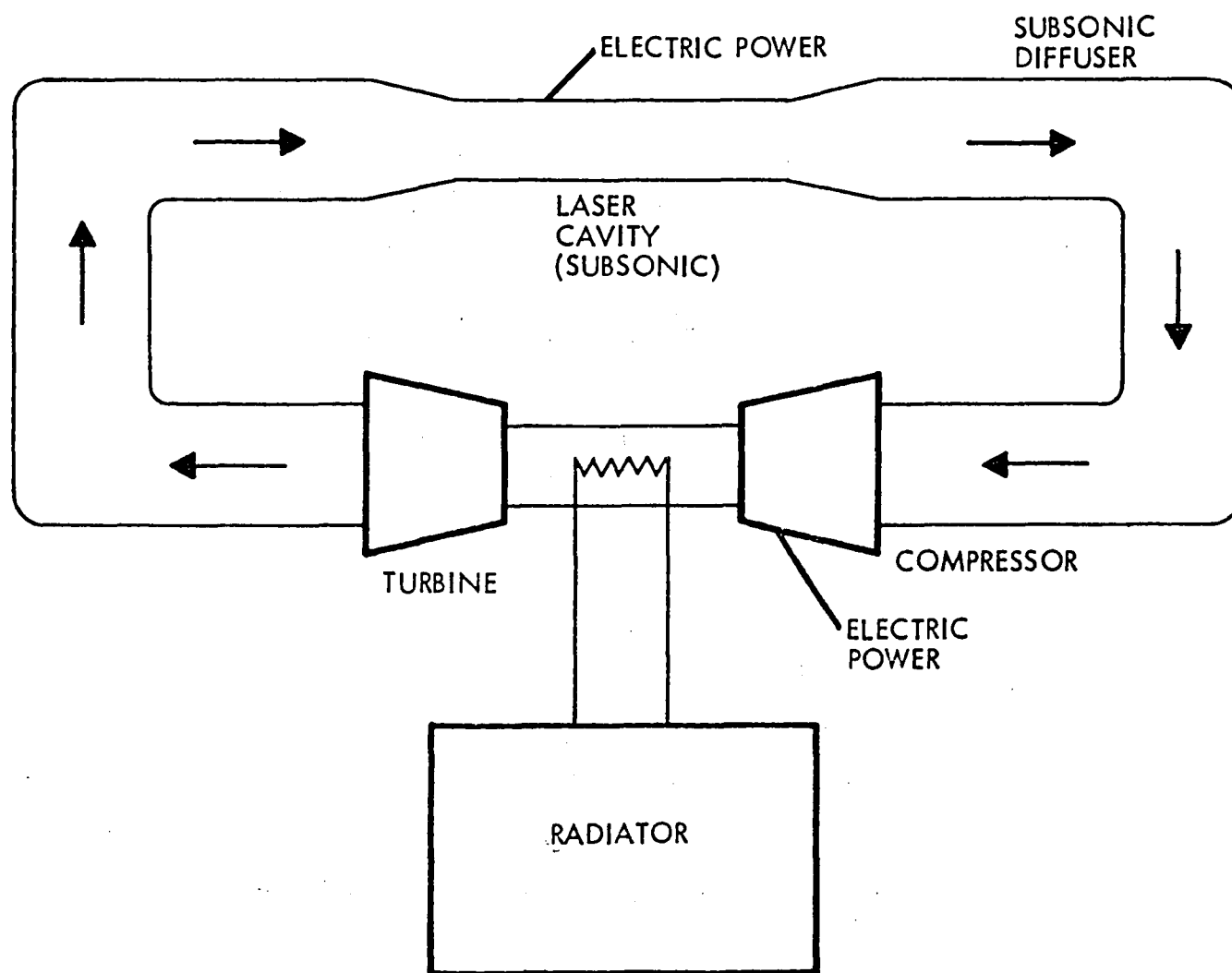


Figure 21. CO<sub>2</sub> EDL subsystem: internal refrigeration

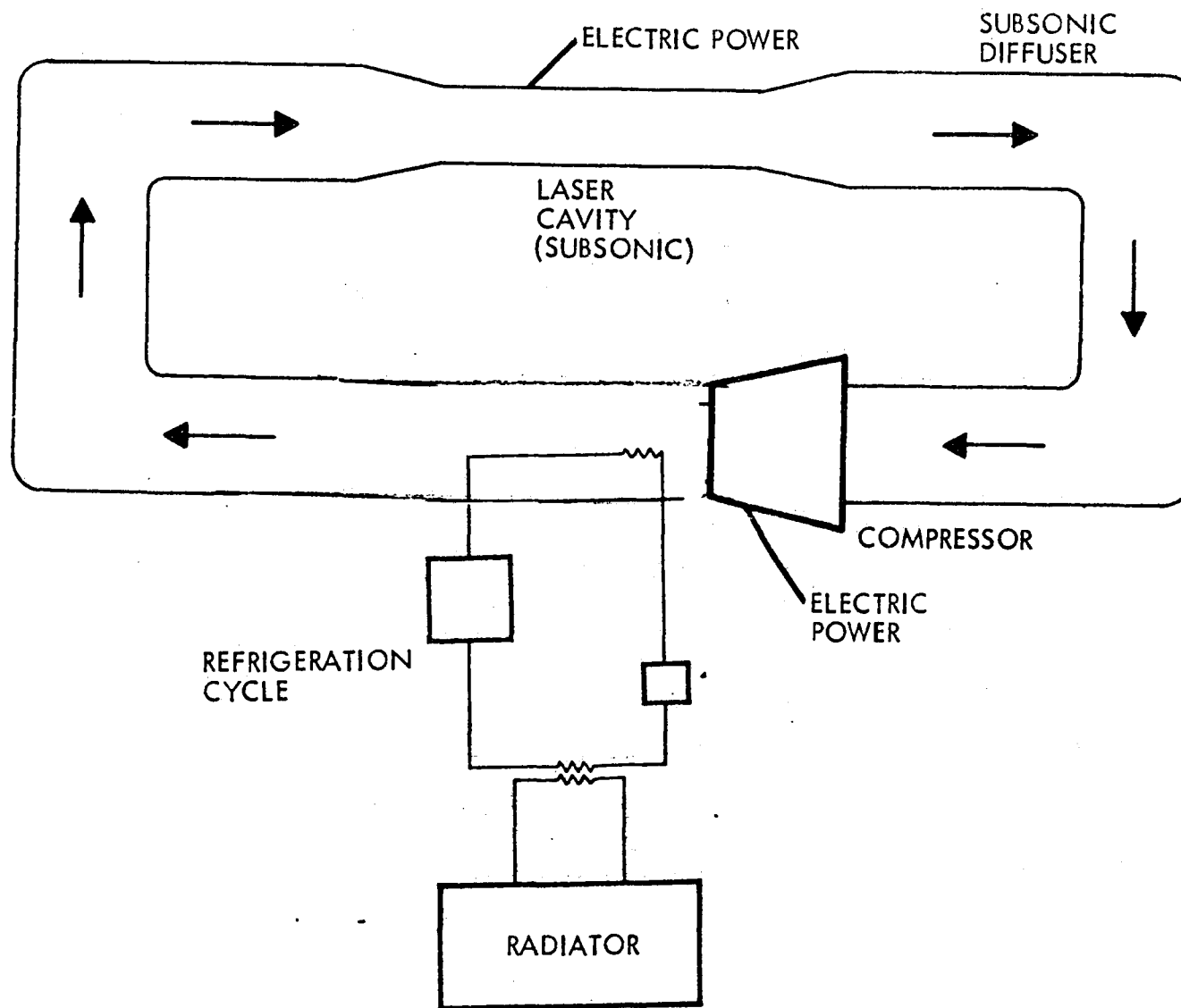


Figure 22. CO<sub>2</sub> EDL subsystem – external refrigeration

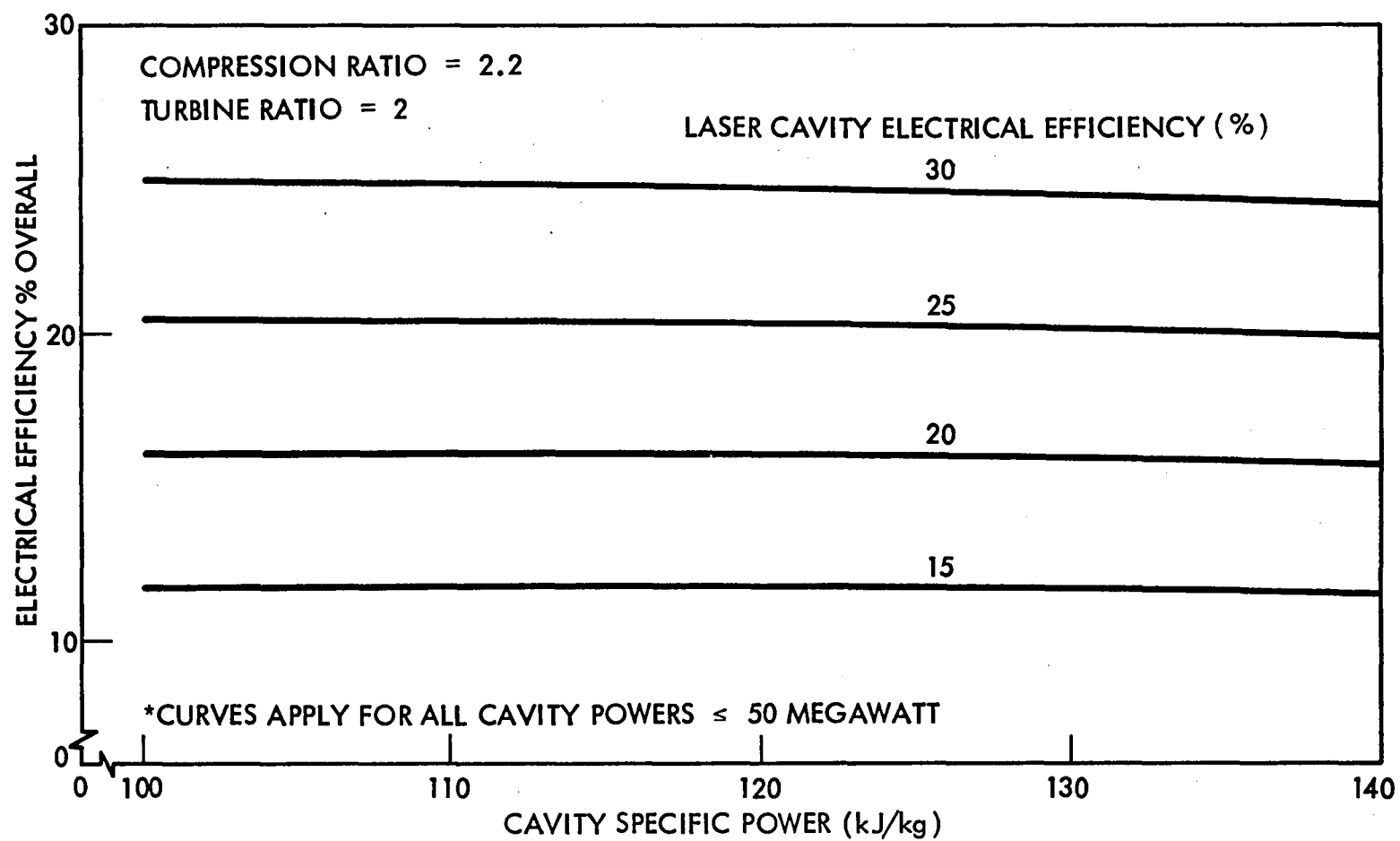


Figure 23. Electrical efficiency of CO<sub>2</sub> EDL subsystem with internal refrigeration

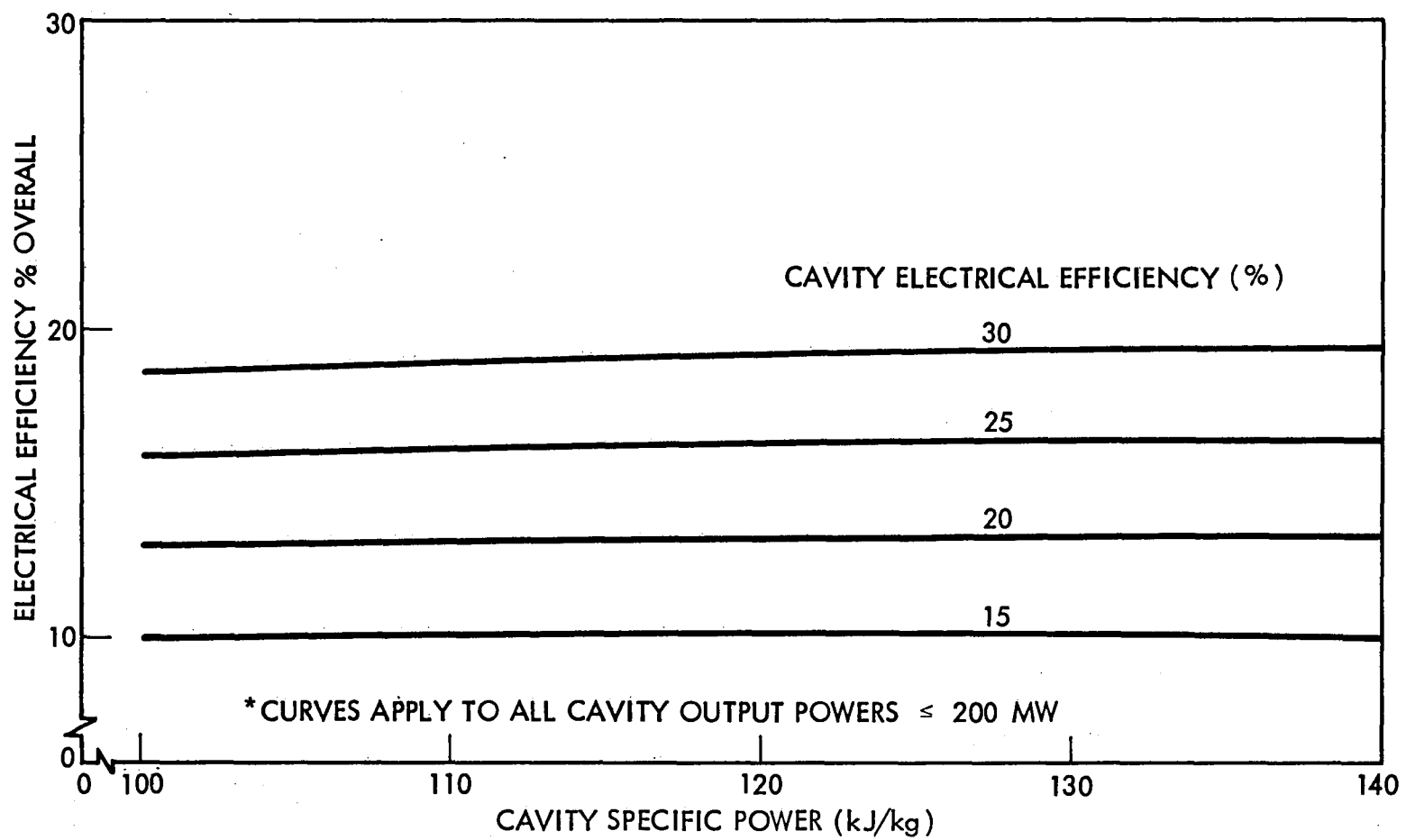


Figure 24. Electrical efficiency of CO<sub>2</sub> EDL subsystem with external refrigeration

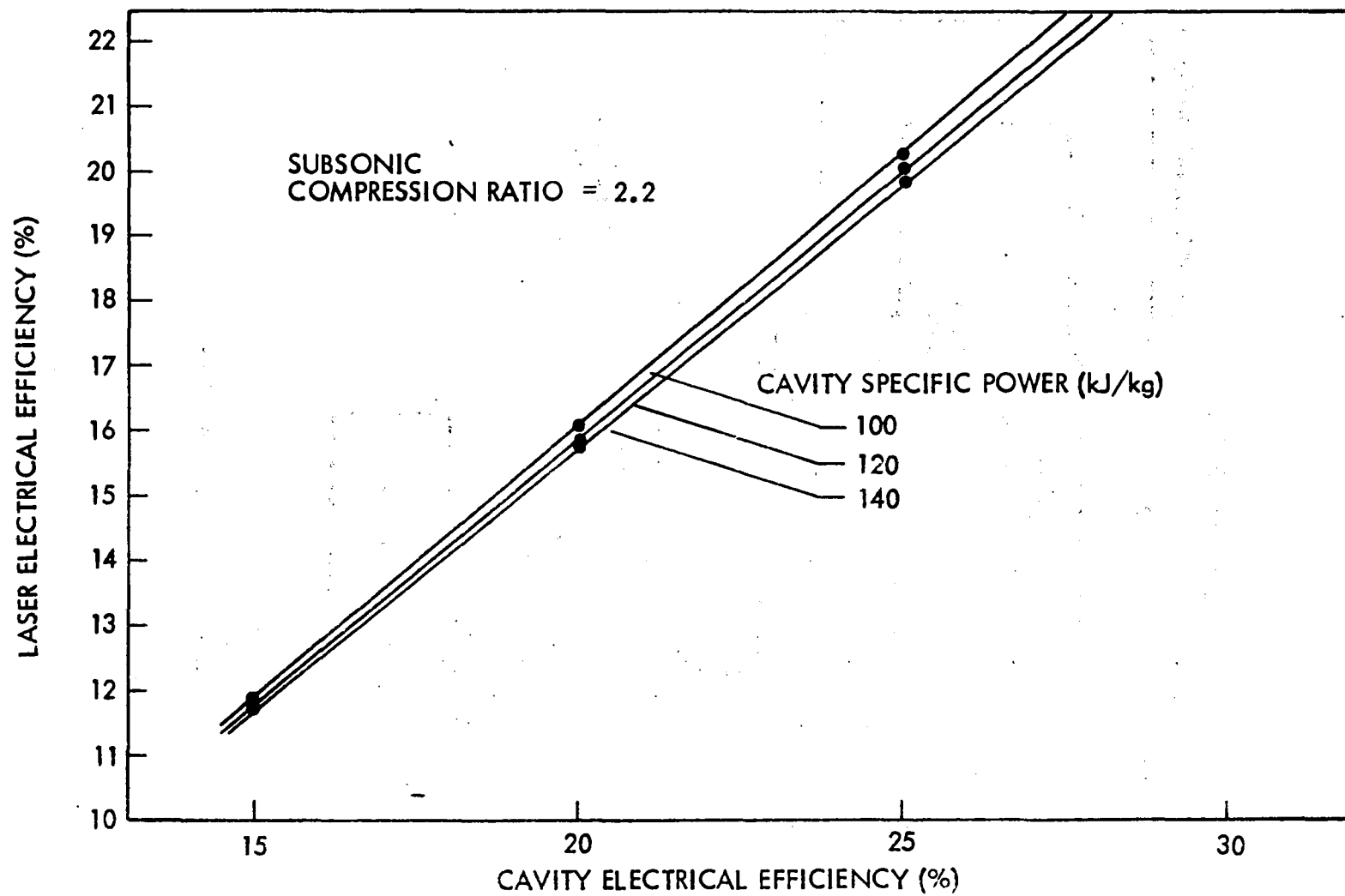


Figure 25. Carbon dioxide EDL electrical efficiency

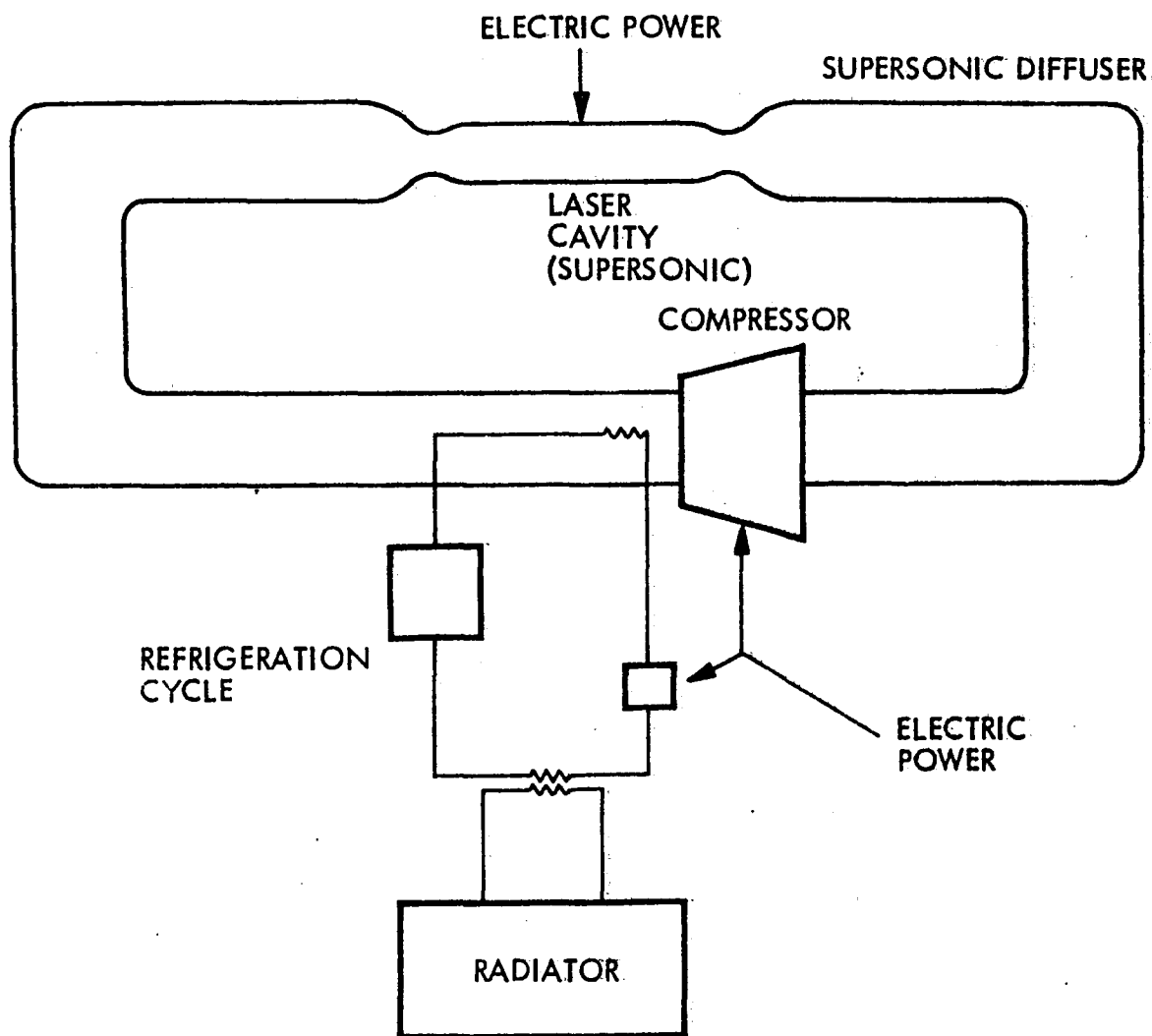


Figure 26. CO EDL subsystem

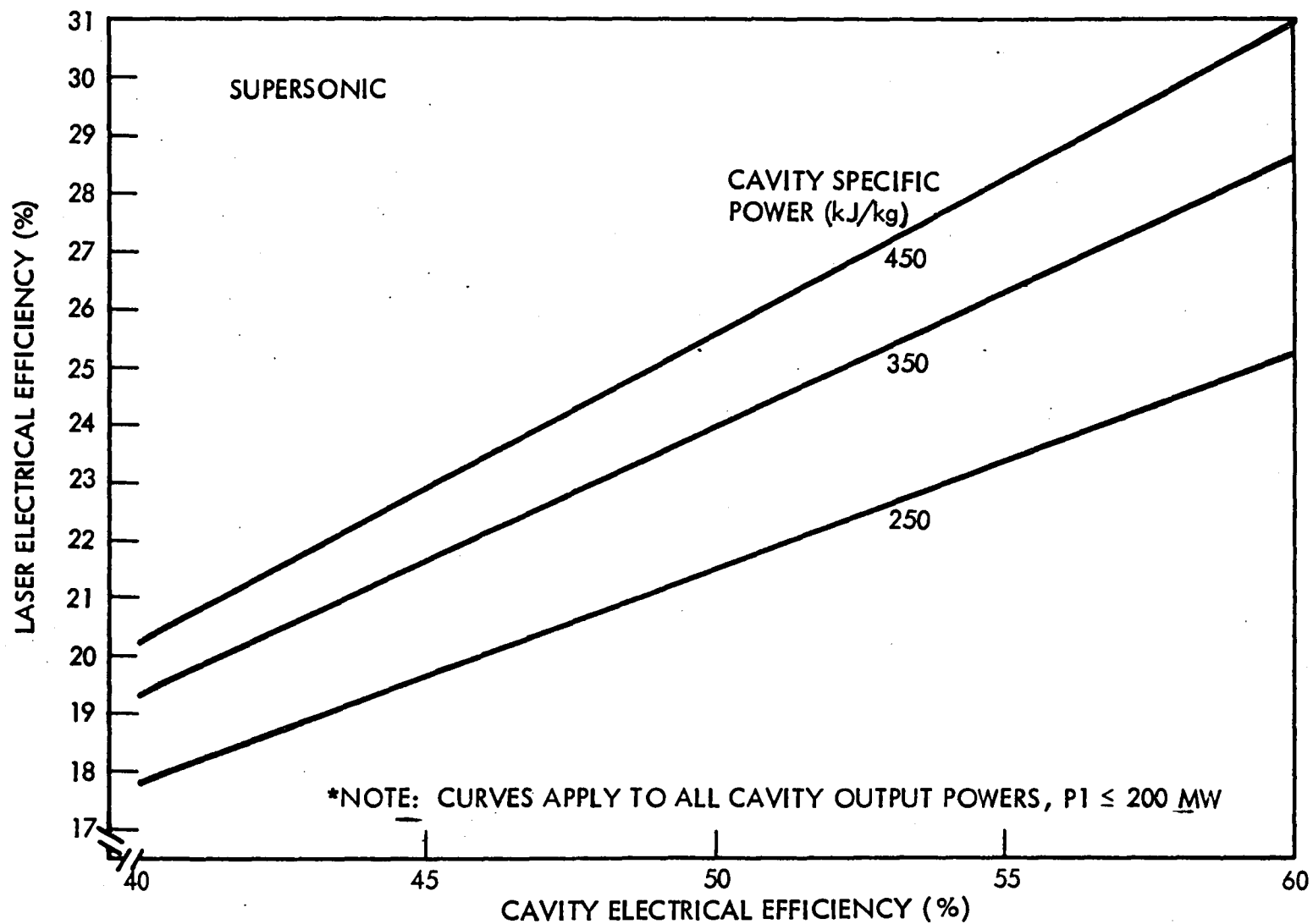


Figure 27. Carbon monoxide EDL electrical efficiency

Mathematical Sciences Northwest (Ref. 15). The laser was assumed to operate by pumping carbon monoxide in a blackbody cavity which is heated by solar radiation. The laser is a "transfer laser" in which the energy in the carbon monoxide is transferred to carbon dioxide so that the output is at the carbon dioxide wavelength (10.6  $\mu\text{m}$ ).

The closed-cycle subsystem which was assumed is presented in Figure 28. After the carbon monoxide and the carbon dioxide mix in the laser, the mixture is cooled by a heat-pipe radiator to approximately 300 K. The gas then passes through a recuperator where it is cooled and is then refrigerated to approximately 125 K and the carbon dioxide is separated. The cold carbon monoxide then passes through the recuperator and is compressed prior to entering the laser. Likewise, the carbon dioxide must be compressed and conditioned.

Electrical power is required to operate the refrigeration system and to provide the recirculation. A laser model was prepared based upon information from Mathematical Sciences Northwest inputs. The overall electrical efficiency was determined. The performance parameters selected were:

Laser Solar Efficiency	35%
Laser Specific Power	80 kJ/kg
Overall Electrical Efficiency	46%
Combined Solar and Electrical Efficiency (not directly relatable to power)	19.9%

### 3.4.3 Phasing Array

In the analysis of laser subsystems, it was determined that a single laser of the power levels required in the SLPS would not be practical and multiple lasers would be required. To maintain a near-diffraction-limited beam spread in transferring the energy of long distances, the individual laser beam wavefronts will have to be matched to one another or phased locked. Wavefront interferences will cause the beam to spread significantly more than the diffraction effects. Two techniques have been investigated for phasing multiple laser beams. One is accomplished in the lasers themselves and the other is accomplished outside of the laser with a phasing array. If the laser manufacturers cannot provide phase locking of multiple lasers, then a phasing array similar to the concept shown in Figure 29 will be used. This concept shows a bank of 20 lasers beams going to individual transfer optics which relocates the beam to a desired pattern of a second set of transfer optics. The second set of transfer optics directs the beams into reducing optics out of which a director mirror directs the beam to either of two transmitter telescopes. The transmitter expands the beams and focuses on the target to which the energy is to be transferred. From the lasers to the outgoing beams on the transmitting telescope, each beam is still a separate identity. They do not begin to merge until they are in the far field. However, phase locking must be accomplished before the beams leave the transmitter aperture. At the transmitter aperture the beams have been expanded to the lowest flux density that will be accomplished. This is the easiest place to sample the wavefronts of all the beams to assure phase locking. Also,



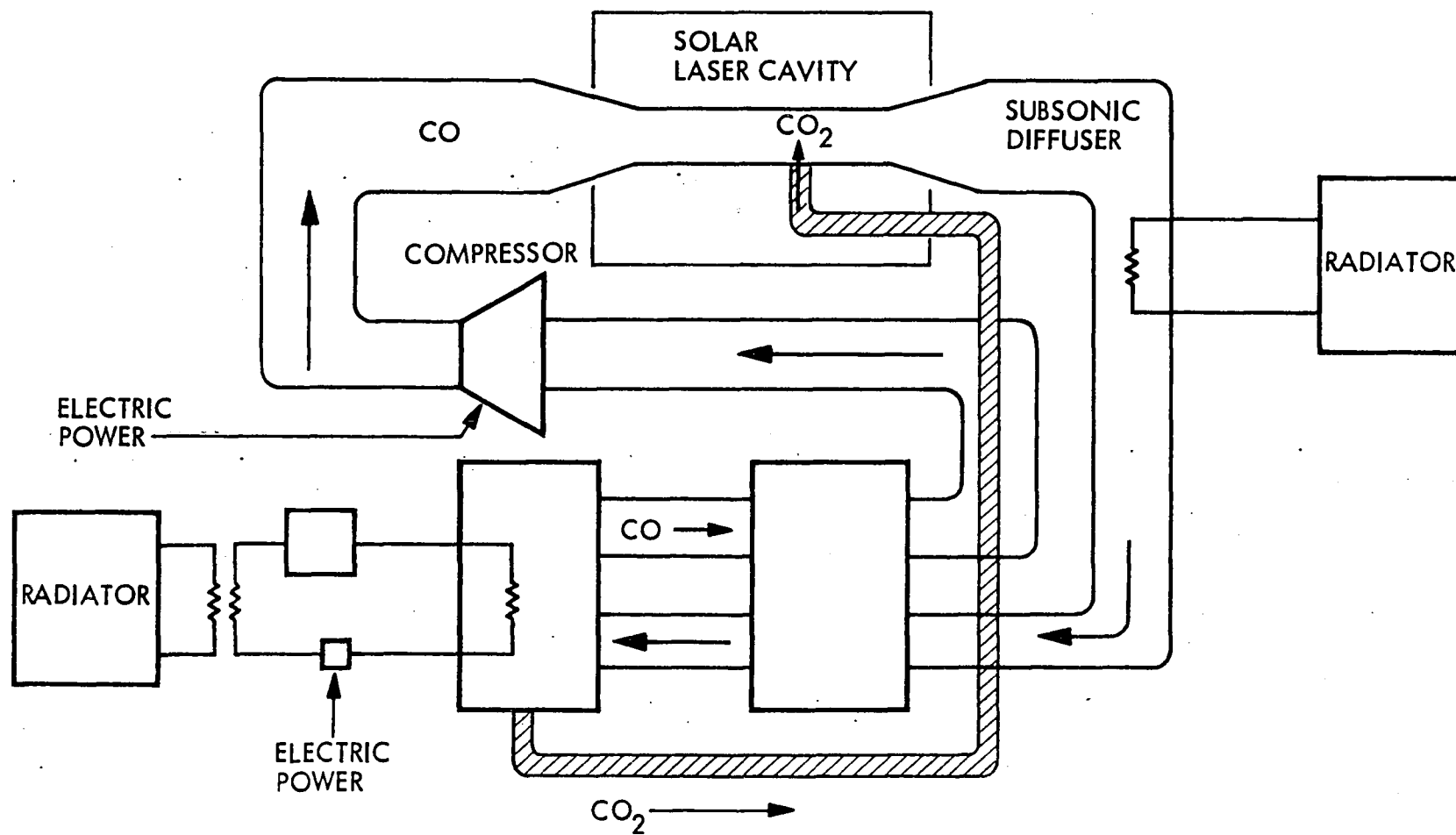


Figure 28. CO<sub>2</sub> solar-pumped subsystem

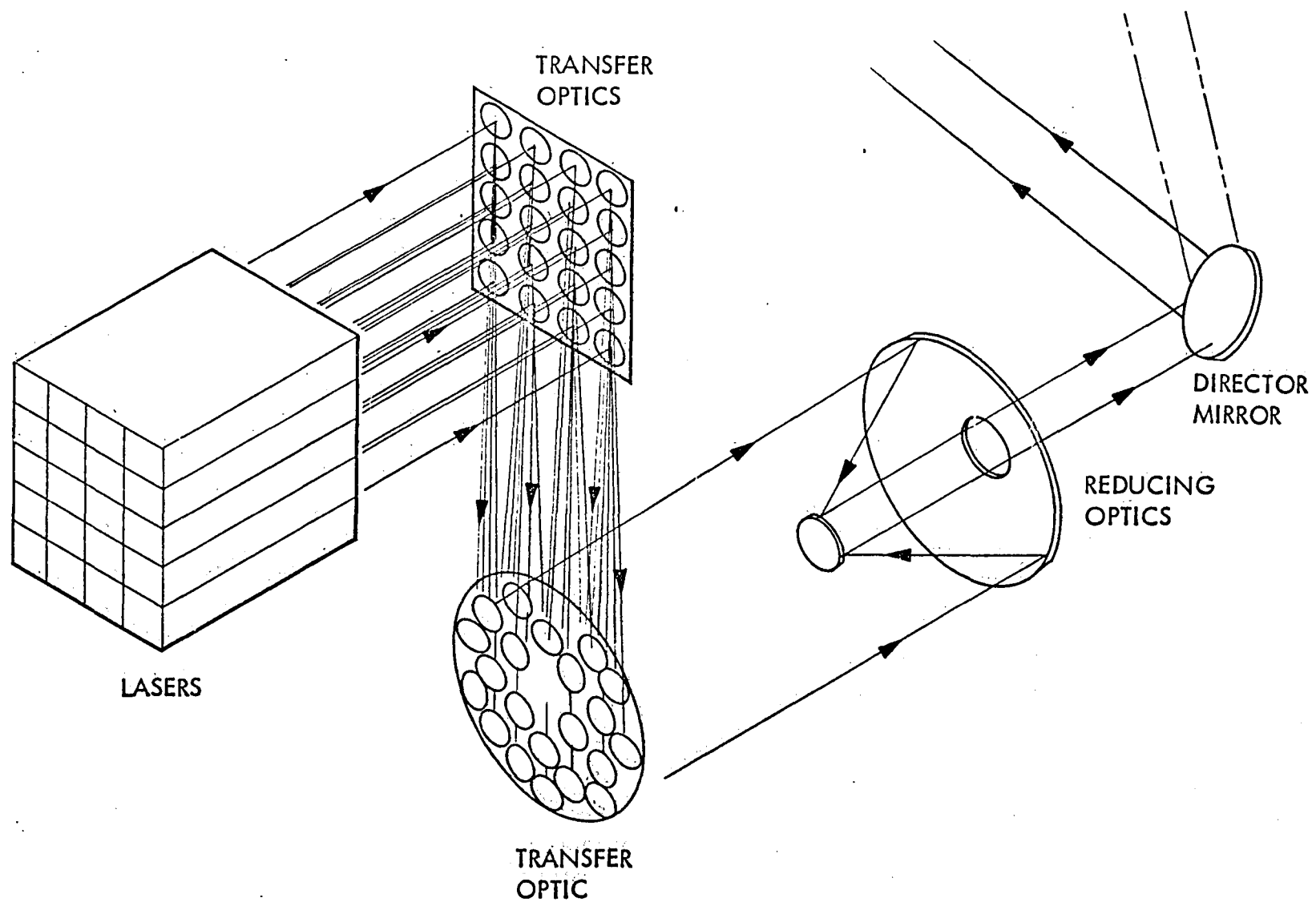


Figure 29. Phasing array

at this point the wavefront aberrations caused by transfer optics can be cleaned up. The worst condition of wavefront phasing is one-half wave; therefore, the maximum required movement of either set of transfer mirrors would be one-half wavelength. By adjusting the position of the transfer optics, phasing can be accomplished. While the illustration shows 20 lasers, any number can be handled in the same manner.

#### 3.4.4 Conversion of Laser Power to Electrical Power (Ground)

The laser energy beamed to the ground must be converted to electrical power in an efficient system. Several candidate systems were examined.

- Photovoltaic

The photovoltaic conversion system has been discussed in Volume I. In a ground installation, the approach could be to either an array approximately 32 m in diameter for direct illumination or to use a telescope to heat a blackbody cavity which will re-radiate the energy to an enclosed photovoltaic array. In either case, the efficiency of conversion should be approximately 40%; however, the direct illumination would require a laser wavelength of  $\sim 0.9 \mu\text{m}$ .

- Thermoelectronic (TELEC)

The operation of the TELEC device is presented in Volume I. A telescope would be required on the ground which is approximately 32 m in diameter which will concentrate the beam for the TELEC device. The efficiency of the TELEC device would be approximately 45%.

- Brayton Cycle

The Brayton cycle would use a telescope to concentrate the beam for heating the working gas in a heat exchanger. The temperature limitations discussed in Volume I would limit the efficiency to less than 40%.

- Energy Exchanger With Binary Cycle

The energy exchanger with binary cycle is discussed in section 3.4.1. A telescope will be used to concentrate the beam into a cavity where the beam is absorbed in potassium vapor (liquid potassium being converted to gas and superheated). The cycle utilized is that presented in Figure 14. This system is exceptionally well suited for ground applications. The radiators would be replaced by water heat exchangers with the water subsequently cooled in towers. Without changing the temperatures, this system would have an efficiency of 73%. (In the selected conceptual design in section 3.1, the efficiency has been improved by modifying the cycle.)

### 3.5 PARAMETRIC SYSTEMS ANALYSIS

The purpose of this parametric systems analysis is to evaluate system capabilities and sensitivities synthesized from various subsystems discussed in section 3.4, then

compare the various systems to select a single system for more detailed analysis and preparation of a conceptual design to a level that would permit estimating costs and evaluating the system competitiveness with other systems conceived to perform the same function.

The approach to accomplishing the systems analysis was to evaluate the various subsystems to eliminate those that would not contribute to the overall efficiency. Since the schedule and funding would not support detailed optimization of the overall system, system efficiency was chosen as the objective to which optimization would be aimed with the constraints that the laser power satellite would operate in low earth orbit (LEO) and relay units would be used to transfer the energy to the ground stations. This operational mode was selected to minimize the orbital weight necessary to be transported to geosynchronous equatorial orbit (GEO). The use of relays will reduce the overall system efficiency by about 0.1%. With these assumptions, analyses were performed to determine deployment parameters for the laser power satellite, relay units and ground stations. Systems were then synthesized and evaluated.

### 3.5.1 Laser Power Satellite and Relay Deployment

Orbital deployment of the Laser Power Satellite and relay units must be coordinated so that laser energy transfer can be continuous to any selected location on earth. The Laser Power Satellite must also be in view of the sun which provides the original energy source. The time that the Laser Power Satellite is in the earth's shadow and cannot function is dependent upon its orbit parameters and can range from 0 to about 30%. The zero time in shadow can be accomplished by sun-synchronous orbits which range in inclination from about 96 to 99° depending upon the orbit altitude which is limited to about 6,000 km (3,240 nmi) maximum. Geosynchronous equatorial orbits are in shadow about 5% of the time, and low earth orbits in the same plane as the sun are in shadow about 30% of the time. The use of relays can provide some distinct advantages. The Laser Power Satellite can be deployed in low-earth, sun-synchronous orbit which provides solar energy 100% of the time and avoids the costs associated with deployment of the large, heavy satellite in GEO. Also, transmission ranges can be shortened which relax optics and pointing requirements; however, the tradeoffs necessary to realize the shortened ranges was not performed in this study. A relay unit was assumed to be in GEO at the same longitude as the Ground Station and the penalty of the longer range accepted. The deployment of the relay unit in GEO also limits the location of ground stations between 53° north and south latitudes as shown in Figure 30. This limitation is due to the zenith angle of the incoming laser beam at the ground station. Zenith angles above 60° cause the distance through the atmosphere to increase sharply which deteriorates energy transmission. If the transfer of energy is considered for the United States only, then only Alaska will not be able to receive the benefits. World-wide use of solar power satellites, which may be the only political solution to deployment of such a system, would eliminate a large sector of population in the Northern Hemisphere. The Southern Hemisphere population are mostly within the 53° latitude limit that can be covered by a GEO relay unit.

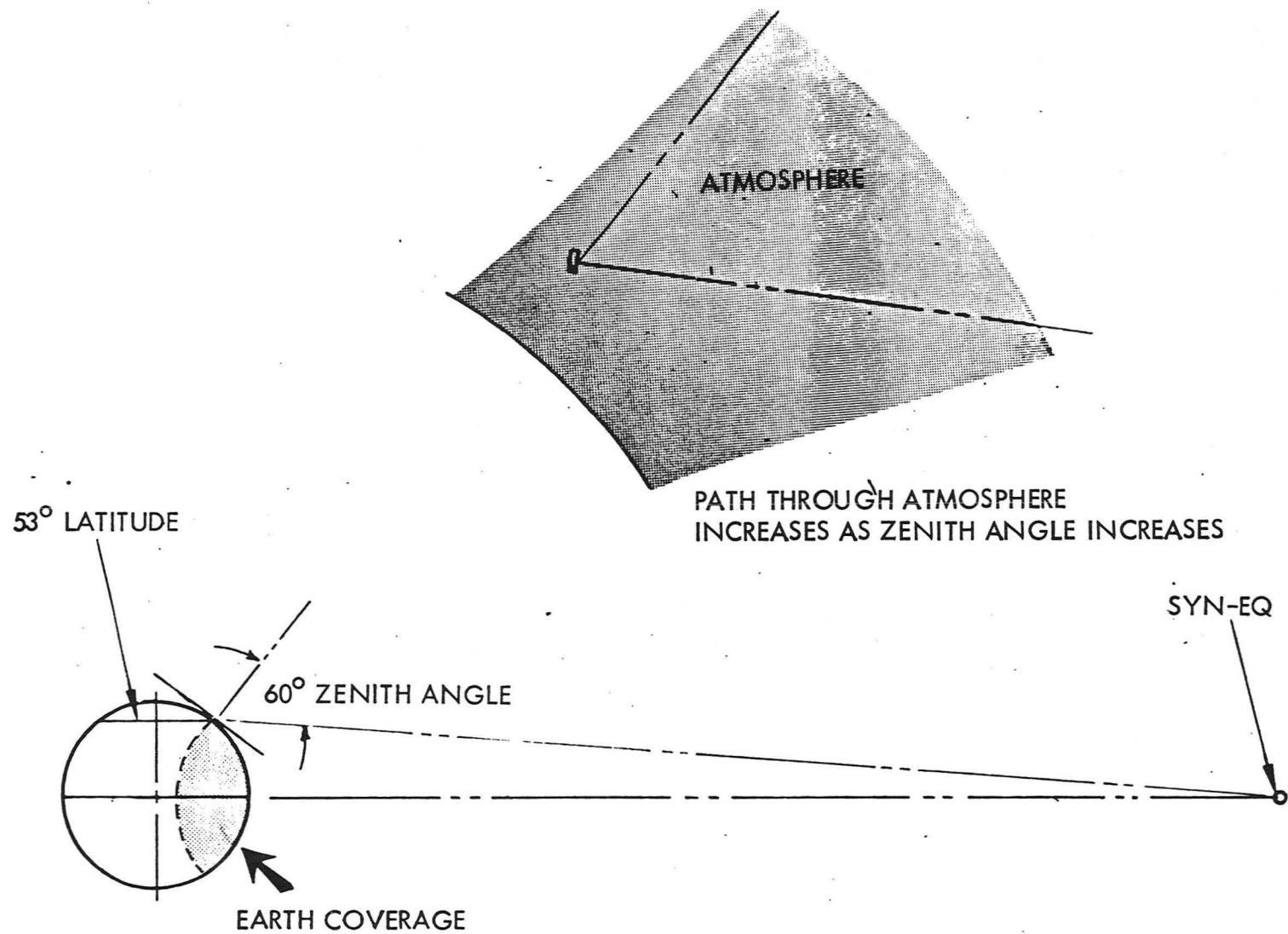


Figure 30. Earth coverage with 60° zenith angle

With the assumptions that the Laser Power Satellite would be in sun-synchronous orbit and a relay unit located in GEO at the same longitude as the ground station, an analysis was made of absentee ratios of the Laser Power Satellites from earth occultations of the relay units. Figure 31 illustrates that the coverage of the earth required and the altitude of the Laser Power Satellite influence the absentee ratio. For the purpose of drag considerations, the Laser Power Satellite must be at about 900-km (486 nmi) altitude or greater. Therefore, about 30% of the Laser Power Satellites will be obscured from the relay units for a coverage of the continental United States. Larger coverages of the earth result in smaller absentee ratios until at about 135° of coverage the absentee ratio reaches zero. To avoid Laser Power Satellites being in positions in which they are obscured and cannot transmit energy, LEO relays can be deployed so that the obscured Laser Power Satellites can transfer energy to the LEO relay which in turn relays the energy to the GEO relay. Several orbital parameters were investigated as indicated by Figures 32, 33, and 34 for LEO relays in circular orbits at various altitudes for Laser Power Satellites in sun-synchronous orbits at 573- and 900-km altitude. Zero degrees inclination (Figure 32) showed to be the worst case with 30 and 90° inclinations (Figures 33 and 34, respectively) being about equal in number of LEO relays required per Laser Power Satellite. Because of orbit regression, the nodal location of the LEO relays in respect to the Laser Power Satellite orbits will vary between  $\pm 90^\circ$ . Figure 35 shows the effect of the nodal variation for LEO relays at 0, 30, and 90° inclinations at 7500-km (4050-nmi) altitude with the Laser Power Satellite at 900-km (486-nmi) altitude for 45° spread of the GEO relay units and ground stations. The 0° inclination effect is constant and the number of LEO relays required would be about 62% of the number of Laser Power Satellites. The 90° inclination orbit requires the least number of LEO relays at all nodal differences except zero at which point the requirement is equal to that of the 30° inclined orbit. Since the 90 and 30° inclinations have the same worst-case requirement and the design must be based on worst case, the 30° inclination was selected because it is a much easier orbit to attain.

### 3.5.2 Ground Station Locations

The location of the ground station is important from the standpoints of weather, elevation, and location of the consumer. Cloudy weather deters the efficiency of transferring laser energy and, if sufficiently heavy, can block transmission completely. While a study has not been made, the possibility of "burning" a hole through clouds for energy transfer does exist. The elevation of the ground station is important because the atmospheric effect to laser beam transmission decreases as the elevation increases. This results from the decreased density of the atmosphere. Location of the ground stations near the consumers will reduce the cost of transmitting the energy over long ground distances. The control of electrical power output and the cost of distribution will be the same as if a current system were used. Figure 36 shows that probably more than 90% of the population of the 48 continental United States live in areas that are cloudy less than 50% of the time with vast areas less than 40%. The figure also shows that elevations greater than 1 km (3,281 ft) exist in most states except along the Mississippi Valley and Florida. With these data, two scenarios are obvious. With additional ground stations, a continuous supply of power can be maintained by switching

- POWER SATELLITES IN SUN-SYNCHRONOUS ORBIT
- OCCULTED POWER SATS REQUIRE LEO RELAYS

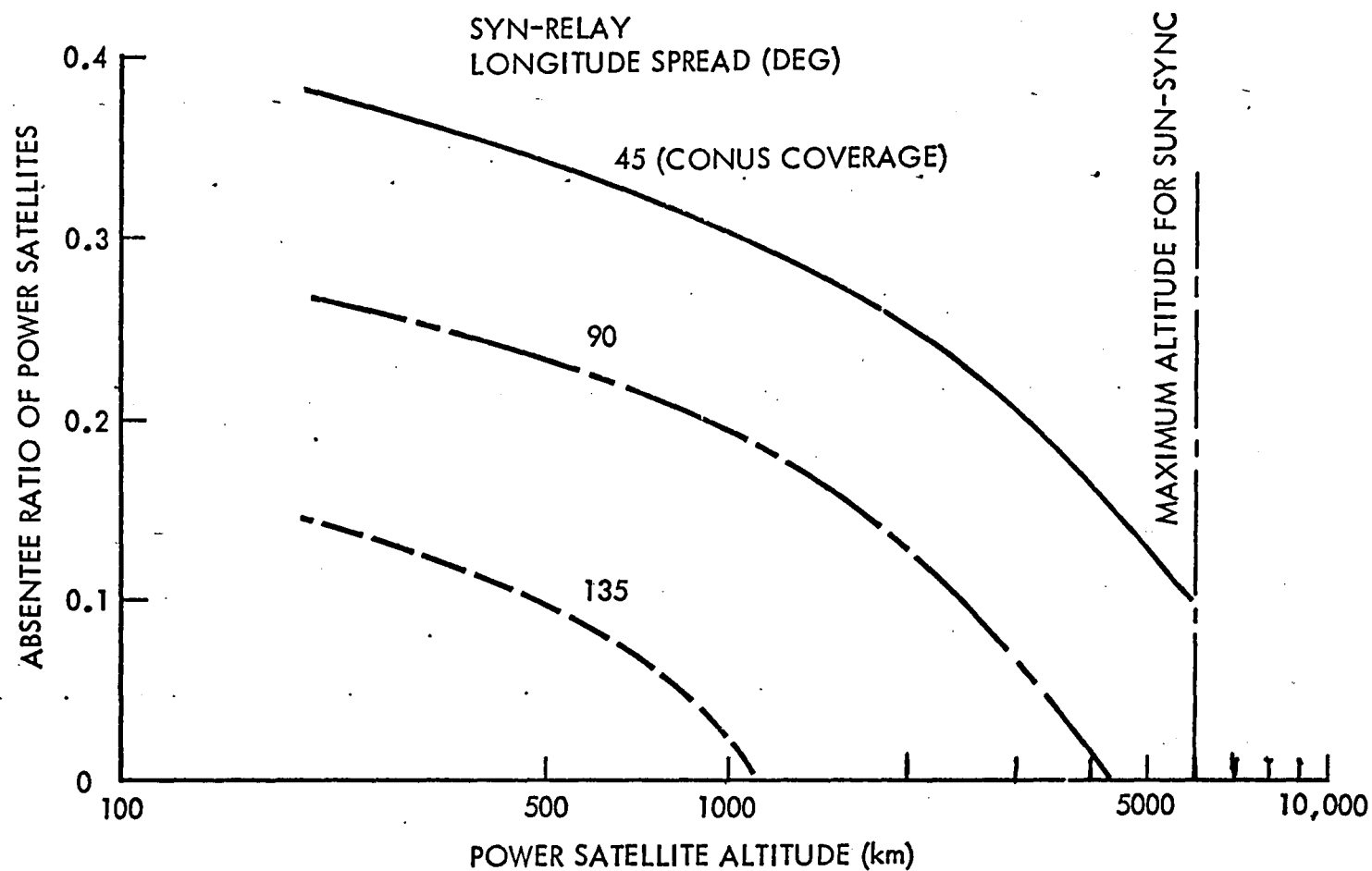


Figure 31. Absentee ratio of laser power satellites from earth occultations of relay units

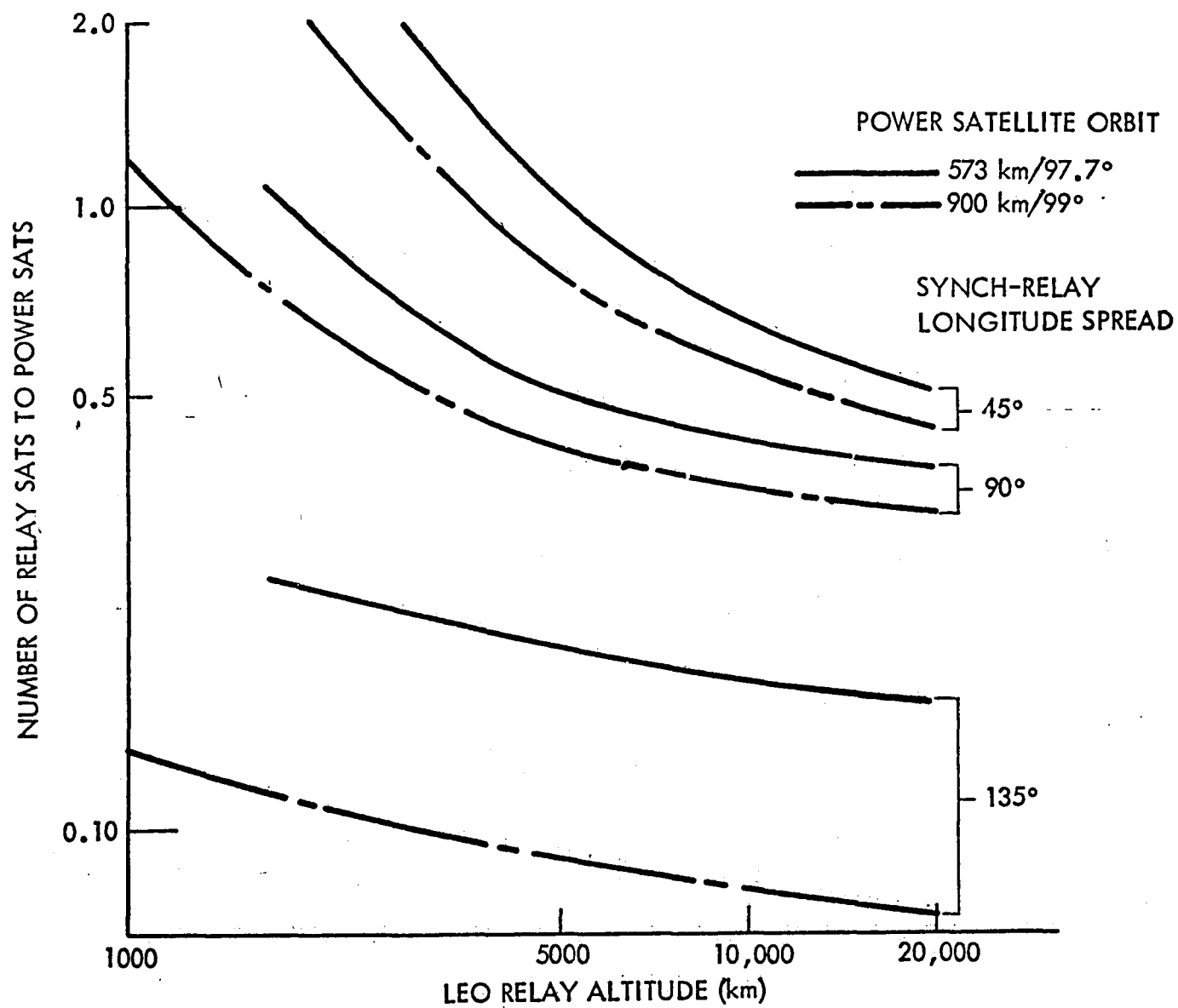


Figure 32. LEO relay requirements, 0° inclined circular orbits



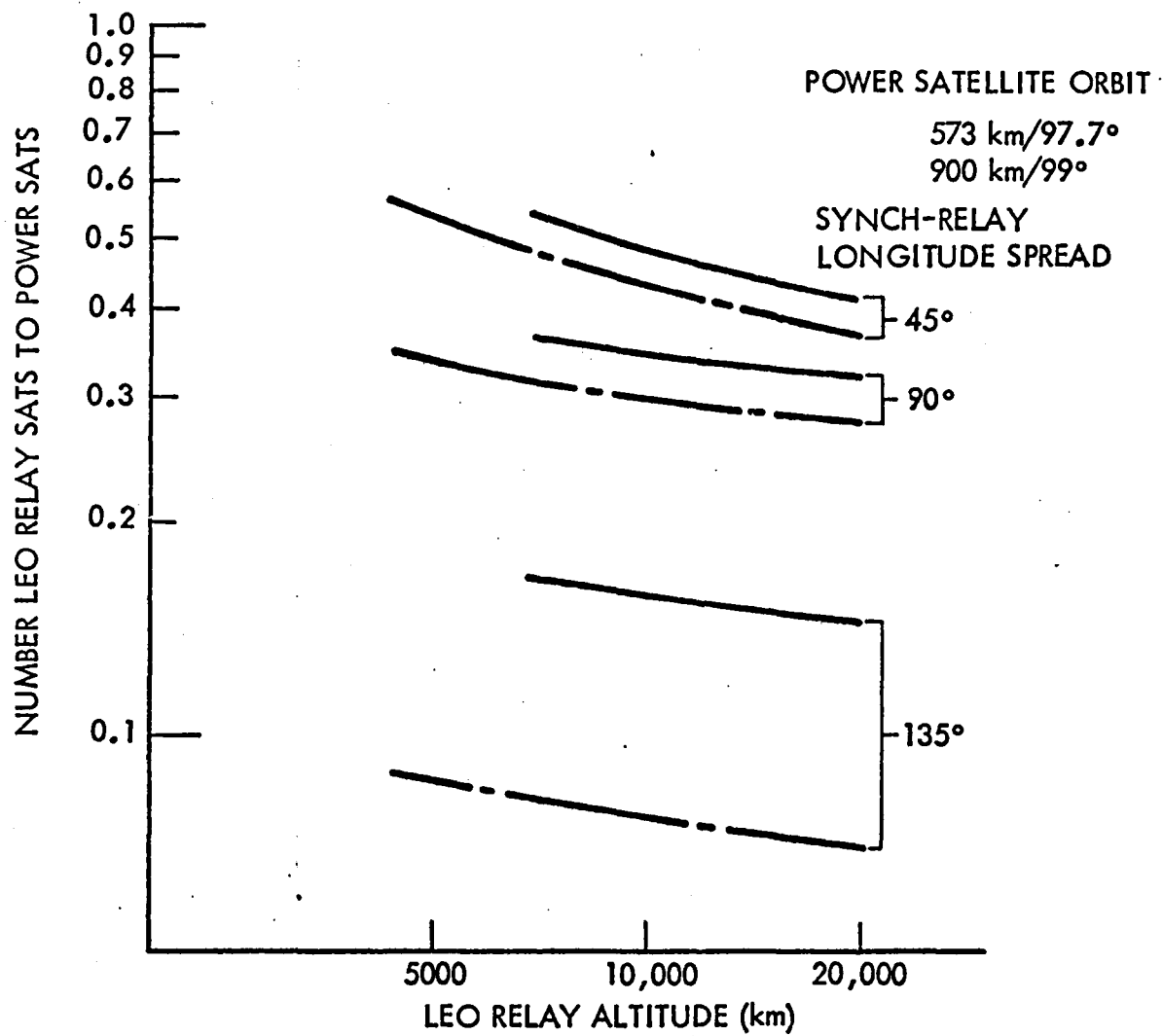


Figure 33. LEO relay requirements, 30° inclined circular orbits

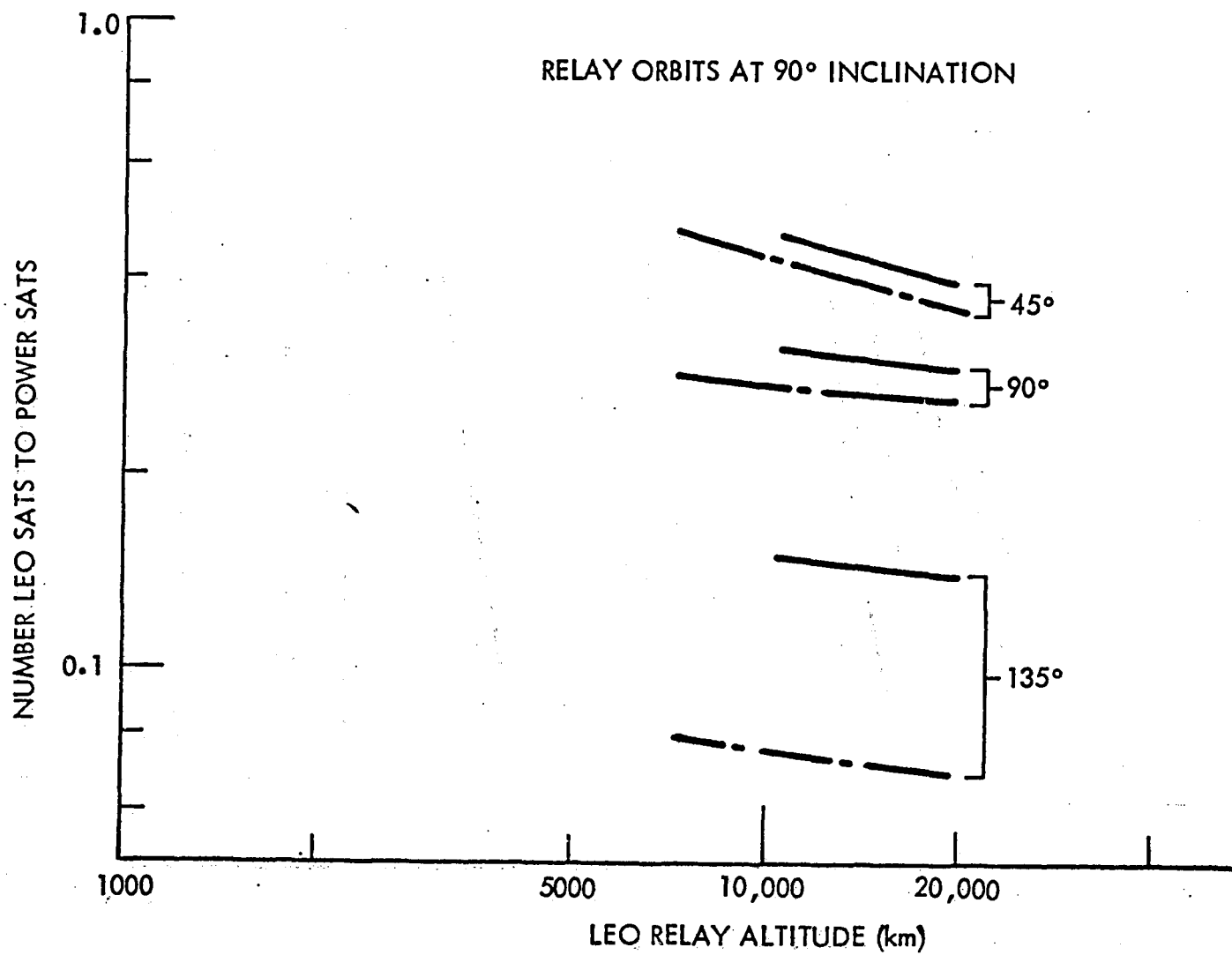


Figure 34. LEO relay requirements, 90° inclined circular orbits

POWER SATELLITE ORBITS 900 km/99°

LEO RELAY SATELLITE ALTITUDE = 7500 km

LONGITUDE SPREAD OF SYNCHRONOUS RELAYS = 45°

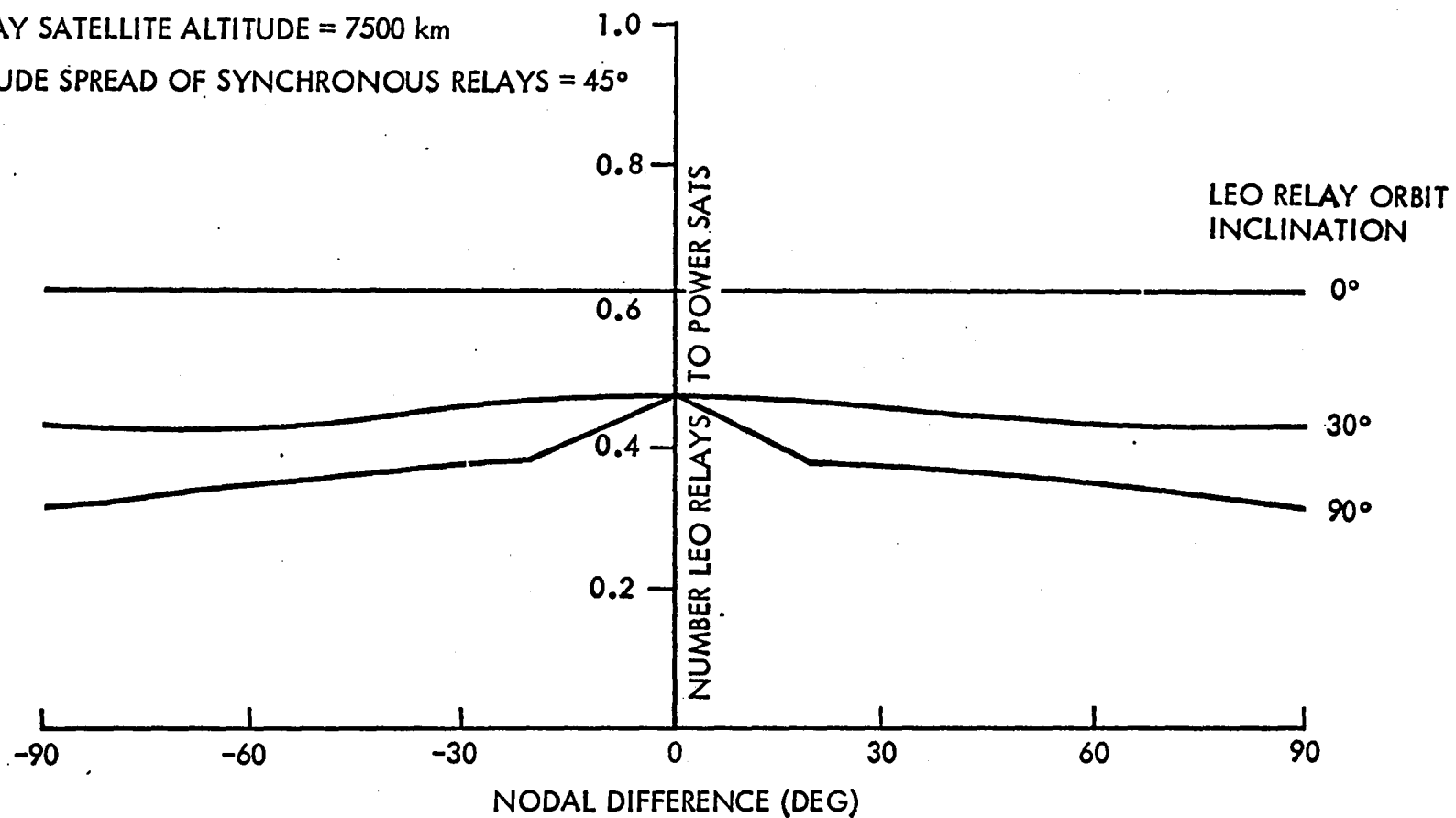


Figure 35. Effect of nodal location and inclination on LEO relay requirements

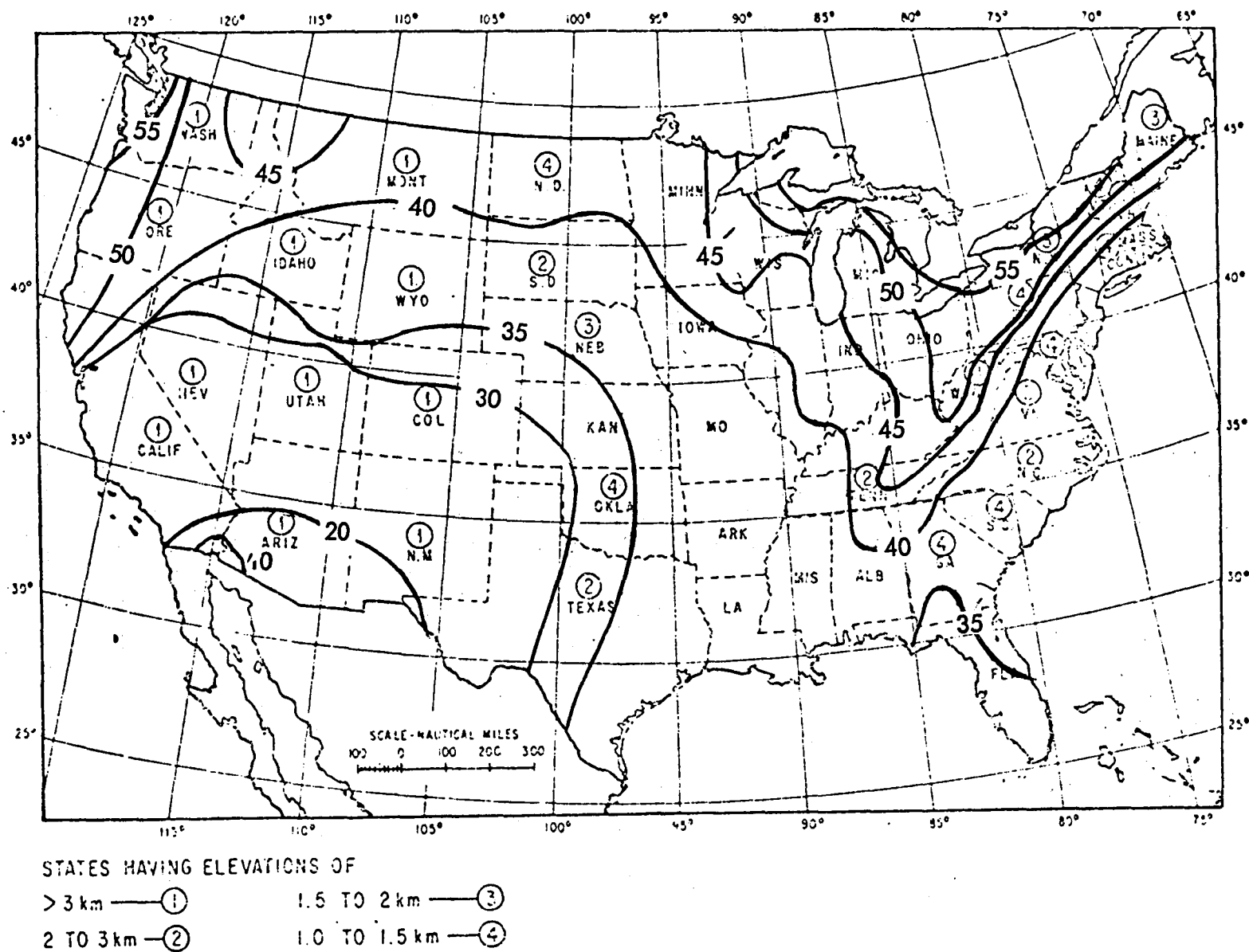


Figure 36. Ground elevations and normal percentage of cloudiness in the United States

from a cloudy site to one that is clear. The second scenario is that without additional ground stations, more than 50% of the energy needs of the United States could be supplied which would reduce the consumption of fossil fuels by an equal percentage. In fact, existing power-plants operating from thermal energy (coal, oil, gas) could be supplied the thermal energy via the laser beam.

### 3.5.3 System Concepts

Based on the subsystem analysis (section 3.4) and the deployment of the system (sections 3.5.1 and 3.5.2), five system concepts (Table XVI) were synthesized and evaluated.

TABLE XVI. SYSTEMS CONCEPTS EVALUATED

System	Solar Energy Collector	Electrical Power Conversion	Laser Subsystem	Ground Power Conversion
I	Reflector/Cavity	Energy exchanger and binary cycle	CO <sub>2</sub> EDL	Energy exchanger and binary cycle
II	Reflector/Cavity	Energy exchanger and binary cycle	CO EDL	
III	Reflector/Cavity	Energy exchanger and binary cycle	Solar pumped laser	
	Reflector/Solar Laser Cavity			
IV	Reflector/Solar Cell Array	Solar Cells	CO <sub>2</sub> EDL	
V	Reflector/Solar Cell Array	Solar Cells	CO EDL	

#### 3.5.3.1 Solar Energy Collection

A solar energy collector/concentrator is required for all five systems. Systems I and II require that the solar energy be concentrated as much as possible to minimize the size and weight of the thermal cavity. The apparent angle (0.53°) of the sun limits the concentration from the primary collector/concentrator and a secondary concentrator is used to reduce the spot size an additional 29%.

System III has the same requirements as systems I and II for a thermal cavity providing energy to the energy exchanger, but the requirement for pumping the laser provides

an option. A second collector/concentrator could be used to supply the energy to heat a blackbody for pumping the laser or the laser pumping could be accomplished by circulating potassium heating a blackbody from a single collector/concentrator supplying a single thermal cavity. The blackbody radiation spectra as directed to the laser which absorbs a certain wavelength to pump the laser. The blackbody temperature requirement is approximately 1500 K, and could be constructed from a number of materials including carbon. Since multiple lasers will be used, multiple blackbody radiation units will be required which makes circulation of potassium gas to provide the laser energy very attractive. This plus the complications of multiple collector/concentrator resulted in the selection of the single collector/concentrator and thermal cavity which supply energy for both electrical conversion and laser pumping.

Systems IV and V use silicon solar cell arrays to convert solar energy to electrical energy and the array itself is the solar collector. No solar concentration is used. Design concepts for these arrays were extracted from Refs. 5 and 6. An end-of-life efficiency of 10.6% was used based on extrapolations from the postulated 18% at the beginning of life.

### 3.5.3.2 Electric Power Conversion

The energy exchanger with binary cycle was selected for systems I, II, and III because of the high potential efficiency of energy conversion. Multiple units per system were selected to provide reasonable sizes and weights for transportation, installation, maintenance, and to reduce the probability of total power failure. As evaluations would be made for systems with 100, 500, and 1000 MW<sub>e</sub> outputs on the ground, the number of conversion units selected were 2, 10, and 20, respectively. Each energy exchanger/binary cycle would have two generator units — one for the topping cycle and one for the bottoming cycle. The electrical power generators are based on production of alternating current which will require power conditioning to convert the high voltage alternating current to direct current sustainer power, to direct current electron gun power and alternating power suitable for compressor motors. The approximate voltages and power type for CO<sub>2</sub> EDL systems are:

<u>Application</u>	<u>Type</u>	<u>Voltage</u>
Sustainer	dc	7000 to 8000
E-Gun	dc	150,000
Equipment	ac	400

For CO EDL lasers the E-gun voltage requirement will be about 600,000 Vdc. The solar pumped laser electrical power requirements is basically for equipment rather than to stimulate the laser.

The silicon solar cell array electrical power conversion for the CO<sub>2</sub> EDL and CO EDL, systems IV and V, were extrapolated from data in Refs. 5 and 6.

### 3.5.3.3 Laser Subsystems

The lasers selected for the systems evaluation were the CO<sub>2</sub> EDL for systems I and IV, the solar pumped laser for system III, and the CO EDL for systems II and V. Laser power requirements are a function of the efficiencies attainable between the laser and the electrical output on the ground, which differs only with wavelength. The CO<sub>2</sub> EDL and the solar-pumped lasers have wavelength of 10.6  $\mu\text{m}$  and would require about 98-MW output each to meet the ground electrical output requirement. The CO EDL lasers would have output about 106 MW. Multiples of these laser power outputs will provide the 100, 500, and 1000 MW<sub>e</sub> systems to be evaluated.

### 3.5.3.4 Laser Energy Conversion

An energy exchanger with binary cycle was selected for conversion of laser energy to electrical energy on the ground for all five systems. This conversion technique provides the highest conversion efficiency of all laser to electrical conversion techniques evaluated.

### 3.5.4 Parametric Evaluations

The five systems previously described and shown in Table XVI were evaluated by:

- Determining the subsystem efficiencies
- Establishing output power requirements
- Estimating subsystem weights
- Determining total system orbital weights and overall efficiencies

#### 3.5.4.1 System Efficiencies

The efficiencies of each subsystem of the laser power satellite was determined and are shown in Table XVII.

The solar collector/concentrator used in systems I, II, and III are aluminized membrane reflectors which can be maintained above 95% reflective. Initial reflectivity will be somewhat higher and some degradation is accepted. Should reflectivity drop below 95%, the surface can be recoated by vapor deposition. All of the capabilities required for vapor deposition can be easily provided. The necessary vacuum is present as well as the thermal requirements. A coating several angstroms thick over the collector surface can be provided with about two liters of aluminum. The stray light losses are estimated to be about 10% due to the reflector figure control and the size of the cavity window. The efficiency of the solar cells is estimated to be about 10.6% which is near the current beginning of life capability of silicon cells. Better cell efficiency is postulated, but degradation will effect the end-of-life efficiency which is the design criteria.

The 83% efficiency of the solar cavity is based on the losses due to reflection at the cavity window and unrecoverable losses of energy in the cavity and ducting walls.

TABLE XVII. LASER POWER SATELLITES EFFICIENCIES

Sys No.	Type	Solar Reflector (or Array) (%)	Solar Cavity (%)	Solar Laser Cavity (%)	E. Exch. & Binary Cycle (%)	Power Gen (%)	Power Cond (%)	Laser S/5 (%)	Phasing Array (%)	Transmitter Aperture (%)	Space Overall
I	CO <sub>2</sub> EDL/ E.E. Binary	85	83	—	73	98	95	20.2	99.7	99.7	9.62
II	CO EDL/ E.E. Binary	85	83		73	98	95	24.8	99.7	99.7	11.82
III	Solar Pumped CO <sub>2</sub>	85	83	95	(73)	(98)	(95)	(19.9)	99.7	99.7	12.34
IV	CO <sub>2</sub> EDL/ Solar Cells	10.6					95	20.2	99.7	99.7	2.02
V	CO EDL/ Solar Cells	10.6					95	24.8	99.7	99.7	2.48



The energy exchanger and binary cycle efficiencies were calculated based on data presented in Ref. 10. The unit operates at very high temperatures where Carnot efficiencies in excess of 90% are possible. The energy exchanger increase the efficiencies of the Brayton cycle by replacing the relatively inefficient compressor and starting with very high temperatures. The temperature exiting the heat exchanger is sufficient to supply a Rankine cycle.

The power generation and power conditioning efficiencies are estimated based on current state-of-the-art. The laser efficiency not only considers the laser cavity output to input, but includes the total electrical power including compressor motors, pumps, and refrigeration. The phasing array and transmitter aperture efficiencies are calculated based on the number and reflectivity of mirrors used. Reflectivities of better than 99.85% have been accomplished at 10.6- $\mu$ m wavelength.

The efficiencies from the laser power satellite to the busbar on the ground are shown in Table XVIII. The space relay efficiency considers losses from diffraction in two transmissions plus the absorption losses in the relay mirror train. Atmospheric losses are due to absorption during the transfer through the atmosphere which is governed by wavelength as maybe noted by the differences between systems I and II (CO<sub>2</sub> and CO EDLs). The efficiency of the ground receiver accounts for diffraction losses as well as the higher absorption losses in the mirrors in the atmosphere. The rest of the efficiencies are similar to the efficiencies calculated for space power conversion.

TABLE XVIII. SPACE/GROUND SYSTEM EFFICIENCIES

Sys No.	Type	Space Relay	ATM Trans.	Ground Receiver	Ground Cavity	E. Exch and Binary Cycle	Ground Power Gen.	Overall Space/Ground	System Overall
I	CO <sub>2</sub> EDL/ E.E. Binary	90	85	96	98	73	98	51.5	4.96
II	CO EDL/ E.E. Binary	90	78	96	98	73	98	47.2	5.58
III	Solar Pumped CO <sub>2</sub>	90	85	96	98	73	98	51.5	6.32
IV	CO <sub>2</sub> EDL/ Solar Cells	90	85	96	98	73	98	51.5	1.04
V	CO EDL/ Solar Cells	90	78	96	98	73	98	47.2	1.17

#### 3.5.4.2 System Weights

The weights of each of the subsystems of the five laser power satellites were determined basically through analyses with scaling laws used for some of the lesser components. A major portion of the weight of the orbital systems is in the radiators. Radiators are required to reject heat from the energy exchangers with binary cycles, power generators, power conditioning, laser subsystem, optical train, and transmitter aperture.

The most effective radiators for the systems were determined to be heat pipe radiators, with water selected as the heat pipe fluid. An advantage of this approach is that if a heat pipe is penetrated by a meteorite, only a small portion of the effective area will be lost. It was estimated that at least one heat pipe per 100 m<sup>2</sup> will be penetrated every year.

A radiator model was constructed and parametric analyses conducted by computer to optimize the weights as a function of the average temperature of the system being cooled and the temperature of the radiator midway between heat pipes. The relationship of heat output per unit weight and the source temperature is shown in Figure 37.

The orbital system weight breakdown for the five systems at a delivered ground power of 1000 MW is presented in Table XIX. As may be seen, the major weight subsystems are the solar cavity, energy exchanger/binary cycle, and the laser subsystems.

The dimensions of the major components in the systems are presented in Table XX. The numbers in parentheses are the number of subsystems or components of the indicated dimensions. The solar reflector and the radiators dominate the dimensions. The differences in the distribution of the radiator areas between the EDLs and the solar-pumped lasers are very appreciable.

The system weights and efficiencies for all the ground delivered power levels are summarized in Table XXI. The weights and efficiencies between similar systems are probably within the statistical errors that might result from the assumptions and the range of performance parameters.

### 3.6 SYSTEM SAFETY

System safety is of major importance. High-energy lasers have already been stigmatized with the misnomer "death ray." A thorough search of laser safety standards and conversations with personnel responsible for laser safety in the United States indicate that laser systems, if properly used, can be equally as safe or more safe than any other system handling a like amount of power. In fact, not one person has been killed by a laser to date; however, two persons have been electrocuted in laser facilities from inadvertently contacting electrical power sources.

The most sensitive area of humans to laser irradiation is the eye. Current safety standards are based on corneal exposure and wavelengths. The eye is most sensitive

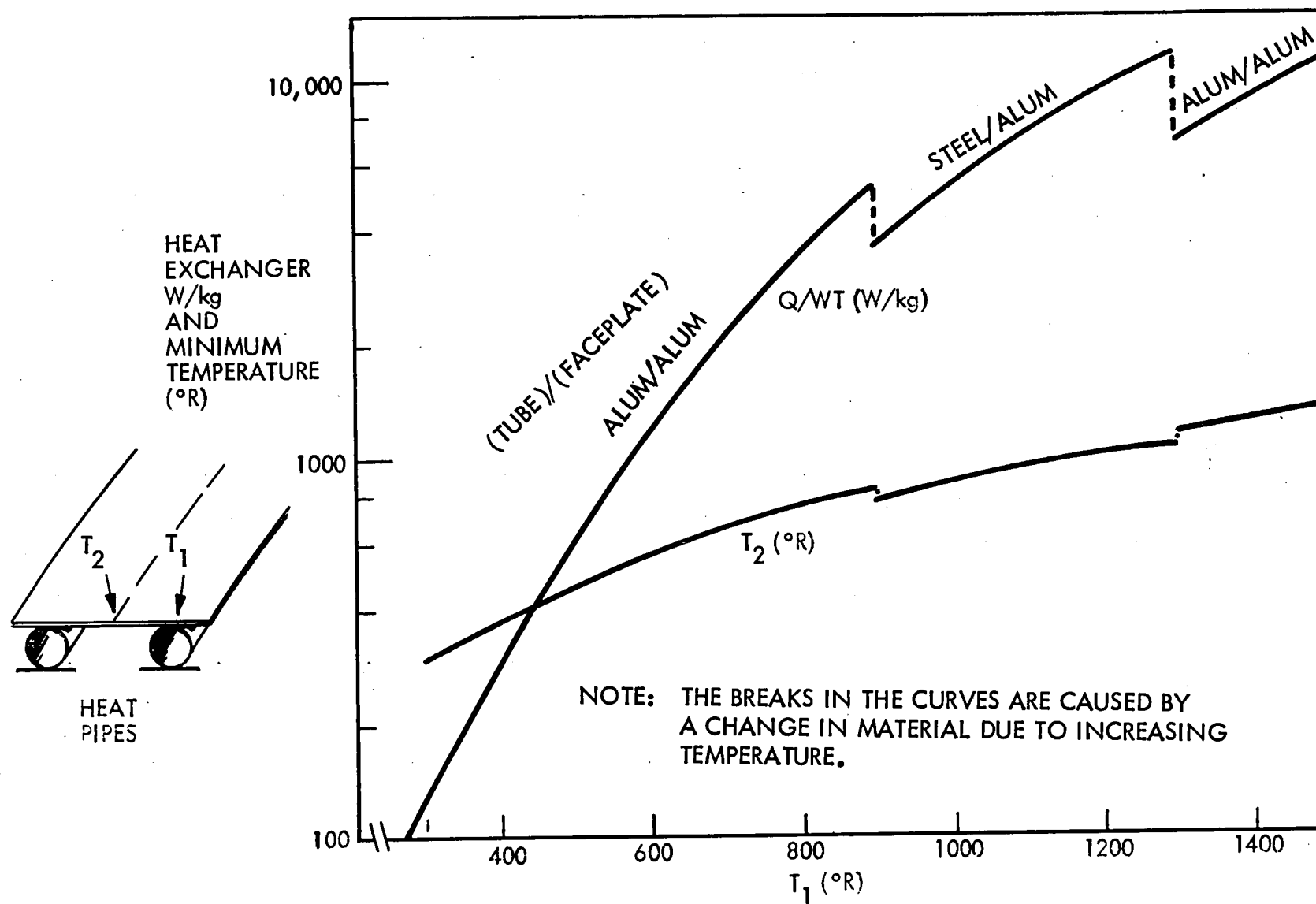


Figure 37. Radiator evaluations

TABLE XIX. ORBITAL SYSTEM WEIGHT BREAKDOWN: 1000 MW

System Subsystem	I CO <sub>2</sub> EDL/ E.E. Binary (10 <sup>6</sup> kg)	II CO EDL/ E.E. Binary (10 <sup>6</sup> kg)	III CO <sub>2</sub> Solar Pumped (10 <sup>6</sup> kg)	IV CO <sub>2</sub> EDL/ Solar Cells (10 <sup>6</sup> kg)	V CO EDL/ Solar Cells (10 <sup>6</sup> kg)
Solar Reflector	0.609	0.5677	0.467	—	—
Solar Cell Array	—	—	—	16.78	15.70
Solar Cavity	3.34	2.37	0.955	—	—
Solar Laser Cavity	—	—	0.440	—	—
Energy Exchanger/ Binary Cycle	4.461	4.192	2.045	—	—
Power Generation	1.039	0.9734	0.454	—	—
Power Conditioning	0.6109	0.572	0.267	0.6109	0.572
Laser Subsystem	4.46	5.387	9.476	4.46	5.387
Optical Train	0.017	0.019	0.017	0.017	0.019
Space Aperture	0.231	0.163	0.231	0.231	0.163
Total	14.773	14.241	14.353	22.099	21.84
Space Relays (Each)	0.262	0.198	0.262	0.262	0.198

TABLE XX. COMPONENT DIMENSIONS

Basis - 1000 MW Ground Power

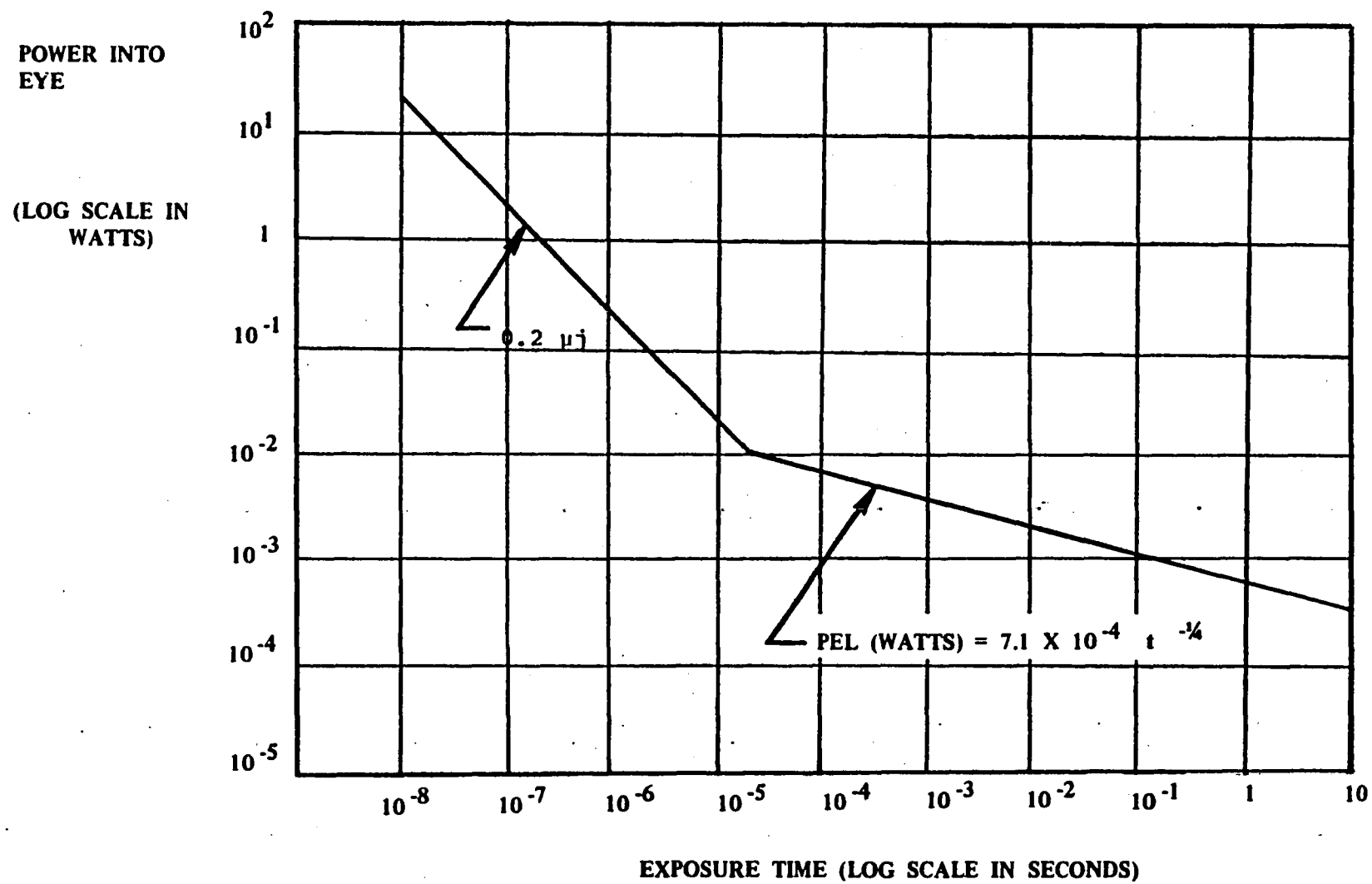
System Component	I CO <sub>2</sub> EDL/ E.E. Binary (m)	II CO EDL/ E.E. Binary (m)	III Solar Pumped CO <sub>2</sub> (m)	IV CO <sub>2</sub> EDL/ Solar Array (m)	V CO EDL/ Solar Array (m)
Solar Reflector	4,224	4,185	3,822		
Solar Cell Array				9,407	9,107
Solar Cavity	32	28.4	19.9		
Solar Laser Cavity			5 × 10 × 10		
Solar Array Radiator				8.7 × 10 <sup>6</sup> m <sup>2</sup>	8.2 × 10 <sup>6</sup> m <sup>2</sup>
E.E./Binary					
● Energy Exchanger	D-3, L-6 (20)	D-3, L-6 (20)	D-2, L-4 (20)		
● Radiator	157,200 m <sup>2</sup> (20)	147,300 m <sup>2</sup> (20)	68,700 m <sup>2</sup> (20)		
Laser Subsystem					
● Equipment	15 × 25 (20)	15 × 25 (20)	25 × 25 (20)	15 × 25 (20)	15 × 25 (20)
● Radiator	39,150 m <sup>2</sup> (20)	51,200 m <sup>2</sup> (20)	225,000 m <sup>2</sup> (20)	39,150 m <sup>2</sup> (20)	51,200 m <sup>2</sup> (20)
Space Aperture	40 (2)	30 (2)	40 (2)	40 (2)	30 (2)
Relay Aperture	50 (2+)	35 (2+)	50 (2+)	50 (2+)	35 (2+)
Ground Aperture	30	15	30	30	15

TABLE XXI. SYSTEM SUMMARY RESULTS

System No.	Type	Power on Ground (MW)	Solar Power Received (MW)	Overall Efficiency (%)	System Weight (kg)
I	CO <sub>2</sub> EDL/ E.E. Binary	100	2,017.3	4.96	1,469,200
		500	10,086.6		6,926,000
		1,000	20,173.2		14,773,600
II	CO EDL/ E.E. Binary	100	1,890.2	5.58	1,468,100
		500	9,450.9		7,125,500
		1,000	18,901.9		14,240,600
III	Solar Pumped CO <sub>2</sub>	100	1,573	6.32	1,925,900
		500	7,865.9		7,107,300
		1,000	15,732		14,353,300
IV	CO <sub>2</sub> EDL/ Solar Cells	1,000	95,524	1.04	22 099
V	CO EDL/ Solar Cells	1,000	89,500	1.17	21.84

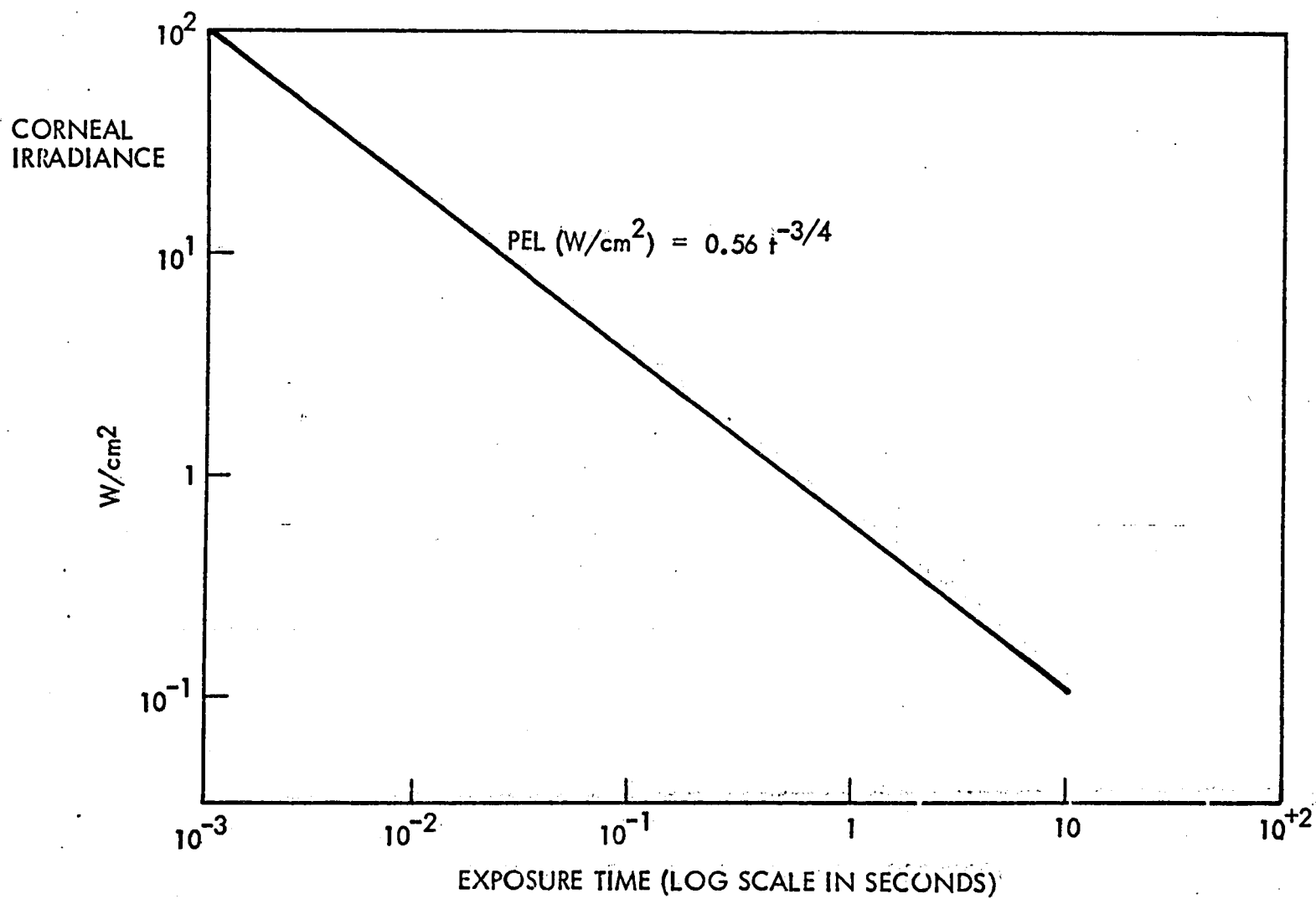
at visible wavelengths and current standards for permissible exposure levels is shown in Figure 38. As a point of reference,  $1.6 \times 10^{-4}$  W/cm<sup>2</sup> at 0.55- $\mu$ m wavelength is equivalent to a bright, overcast day, which on the figure is beyond the 10-s exposure time. At 10.6- $\mu$ m wavelength, the eye is far less sensitive as illustrated in Figure 39 where 0.1 W/cm is permissible for a 10-s exposure. This indicates that at 10.6- $\mu$ m wavelengths an intensity of  $1.6 \times 10^{-4}$  W/cm<sup>2</sup> is more than safe for continuous corneal exposure. Figure 40 shows the results of a parametric analysis to determine the size of a protected area around the receiver that would be required to eliminate the possibility of hazardous amounts of radiation impinging on eyes. The 40-m-diameter, diffraction-limited, 10.6- $\mu$ m, 10,000-MW case shows that a 1-km radius would provide a protected area with  $1 \times 10^{-4}$  W/cm<sup>2</sup> flux density at the outer boundary. Analysis of the beam for the selected configuration shows a beam profile as shown in Figure 41. With a boundary radius of 200 m, the flux density at the perimeter would be  $1 \times 10^{-4}$  W/cm<sup>2</sup>. Doubling the radius in one direction to account for a 60° zenith angle would encompass a total of 62 acres of land to provide the protection.

With a protected area to keep personnel away from hazardous laser radiation, other safeguards must be initiated to guard against other factors which might be a hazard. It would be necessary to have a fail-safe system in conjunction with the cooperative



\*AF MANUAL 161-32, LASER HEALTH HAZARDS CONTROL

Figure 38. Permissible exposure level (0.4 – 1.4 μm)



\*AF MANUAL 161-32, LASER HEALTH HAZARDS CONTROL

Figure 39. Permissible exposure level (10.6 μm)



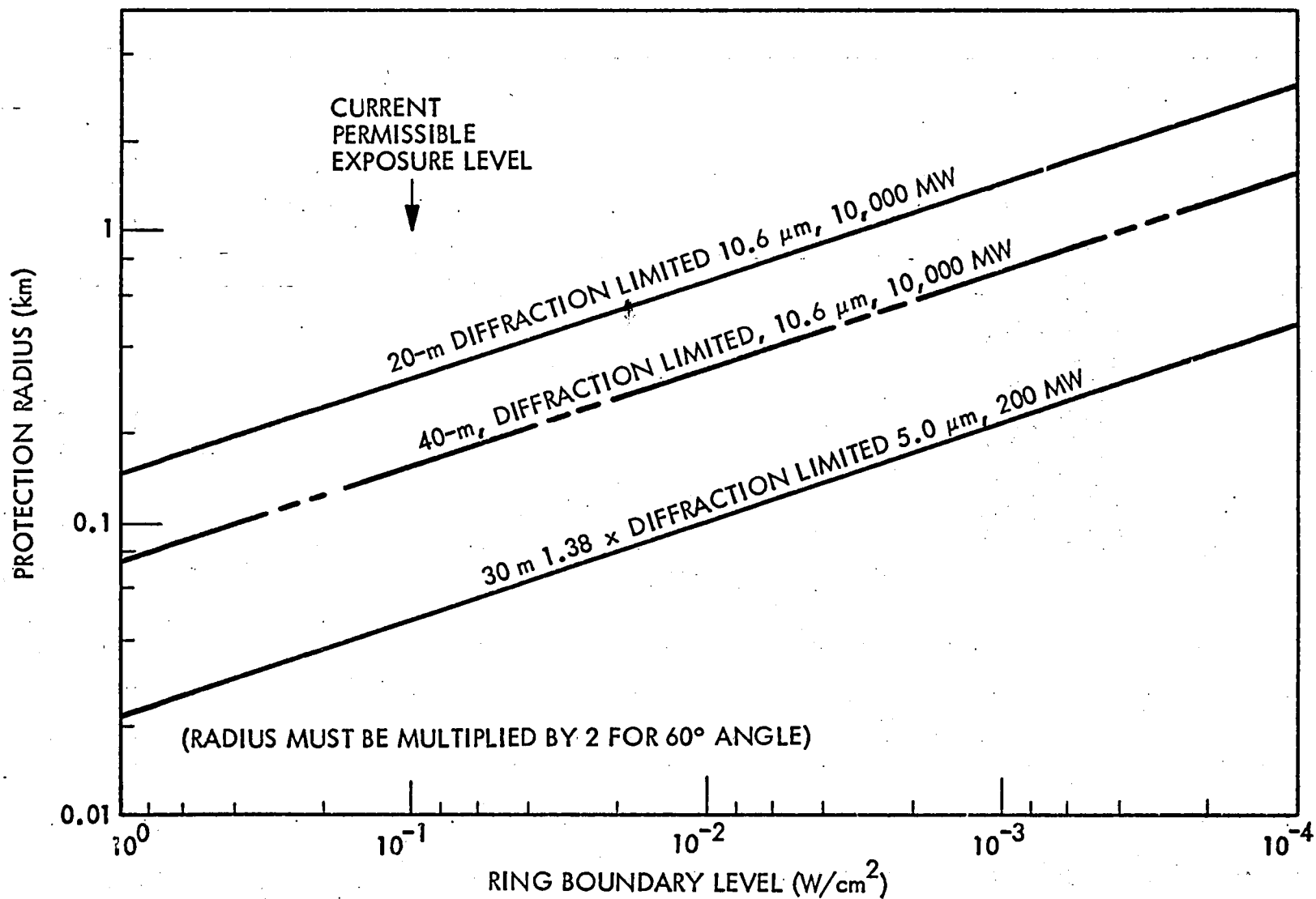


Figure 40. Protection radius extremes

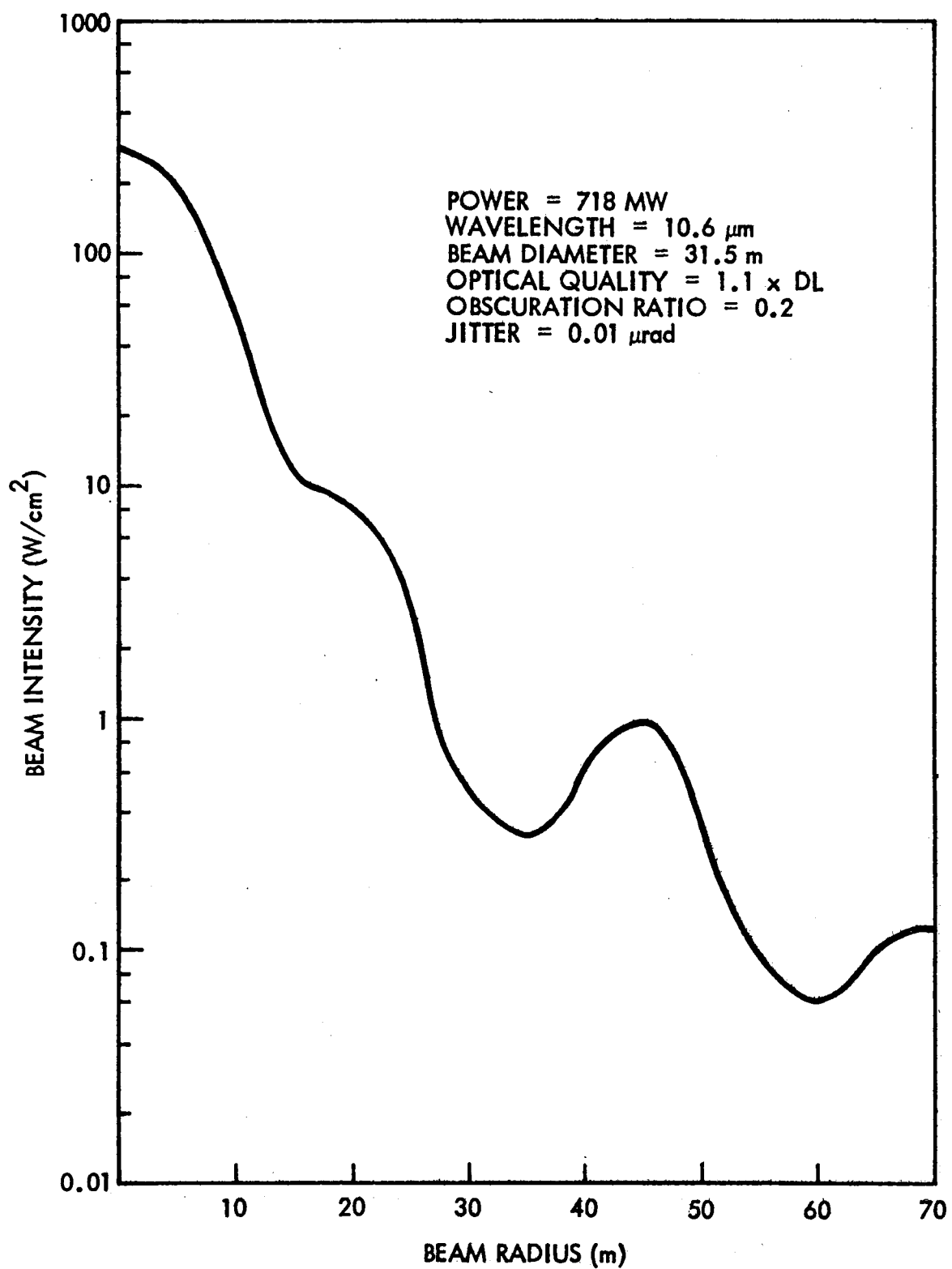


Figure 41. Beam profile for selected configuration

pointing and tracking system to assure that the beam's energy stayed within acceptable limits and, should it exceed those limits, to switch off the beam. Shutting down the laser may take several seconds, but switching of the beam at the director optics could be accomplished in fractions of a second. Then the laser could be shut down. Sensors to detect aircraft flying through the beam would also probably be a requirement even though the area was off limits for airplane flights and a radar site on the ground could monitor planes and warn them when necessary. However, let us examine how much energy would be deposited on a jet airliner flying directly through the center of the beam. Figure 41 shows that intensities greater than the sun extends less than 30 m from the center.

There is a total of about 700 MW of power being deposited over this area for an average flux density of about  $25 \text{ W/cm}^2$ . A jet airliner flying at 600 miles/hr is traveling 268 m/s which would take 0.22 s for a point on the plane to pass through the 60-m diameter. During this period,  $5.6 \text{ J/cm}^2$  would be deposited on the surface of the plane and if unpainted probably 70% reflected away for a total absorbed energy of  $1.7 \text{ J/cm}^2$ . The temperature change of the airplane can be calculated with

$$\Delta T = \frac{E}{c \rho \ell}$$

where

$\Delta T$  = temperature change ( $^{\circ}\text{C}$ )

$E$  = absorbed energy ( $\text{J/cm}^2$ )

$c$  = specific heat (aluminum =  $1 \text{ J/gm } ^{\circ}\text{C}$ )

$\rho$  = density (aluminum =  $2.78 \text{ gm/cm}^3$ )

$\ell$  = material thickness (assume 0.020 in. or 0.051 cm)

$$\Delta T = \frac{1.7}{(1)(2.78)(0.05)} = 12.2^{\circ}\text{C} (22^{\circ}\text{F})$$

This temperature rise would not affect the structural capability of the airframe and would be dissipated rather quickly by the flow of cold air passing the surface. This conservative analysis shows no damage to the airplane. The window material and metal exterior of aircraft are opaque to  $10.6\text{-}\mu\text{m}$  radiation and the personnel inside the airplane would have had zero exposure. While a jet airliner could fly through the beam with only slightly detrimental effects, smaller light aircraft flying slower may possibly be damaged.

### 3.7 BEAM PROPAGATION AND ENVIRONMENTAL EFFECTS

After a thorough search, studies on the environmental effects of laser beams revealed reams of data on what the atmosphere will do to laser beams, but not one study on what

the laser beam does to the atmosphere. As a result, an effort was initiated to investigate the general atmospheric propagation and to try to determine at least top-level environmental effects.

### 3.7.1 Diffraction and Turbulence

The diameter of the spot at the receiver with a range  $R$  and a focus at  $F$  (Ref. 18) is given in Equation 1.

$$d(R) \approx \frac{4R}{k} \left\{ \underbrace{\frac{1}{D^2}}_{\text{diffraction}} + \underbrace{\frac{1}{\rho_o^2}}_{\text{turbulence}} + \underbrace{\left(\frac{kD}{R}\right)^2 \left(1 - \frac{R}{F}\right)}_{\text{defocus}} \right\}^{1/2} \quad (1)$$

The atmosphere coherence diameter  $\rho_o$  is related to the profile of the structure constant,  $C_n^2(h)$ :

$$\rho_o = \left\{ 1.46 k^2 \int_{s=0}^R (s/R)^{5/3} C_n^2(s) ds \right\}^{-3/5} \quad (2)$$

where the path integral is from the receiver to the transmitter (Ref. 19). The resulting minimum diameter to which the beam can be focused is then given by

$$d_T = \frac{4R}{k\rho_o} \quad (3)$$

which, for a given line-of-sight through the atmosphere, is independent of transmitter diameter.

Values of  $\rho_o$  have been calculated using Eq. (2) and a profile of  $C_n^2$  shown in Figure 42. At the ground  $C_n^2$  is equal to  $10^{-13} \text{ m}^{-2/3}$ , corresponding to moderate turbulence. Above  $h = 0$ ,  $C_n^2$  decreases with altitude according to  $h^{-1.08}$  to about  $h = 1.6 \text{ km}$ . Above this altitude  $C_n^2$  is given by Hufnagel's model:

$$C_n^2 = 10^{-16} \exp(-h/1.5) + 2.2 \times 10^{-13} [(h/10) \exp(-h/10)]^{10} \quad (4)$$

The corresponding spot sizes, using Eq. (3), are shown in Figure 43. For small zenith angles  $d_T \sim 2 \text{ cm}$  for  $\lambda \approx 1 \mu\text{m}$ ; this may be compared with the diffraction spot size  $4R/kD$  for a large, low-altitude transmitter at  $R = 300 \text{ km}$  and width  $D = 50 \text{ m}$  for which the diffraction spot is about  $0.3 \text{ cm}$ . This is a lower limit for the ranges of altitudes and diameters of interest here. It should be noted that the wavelength

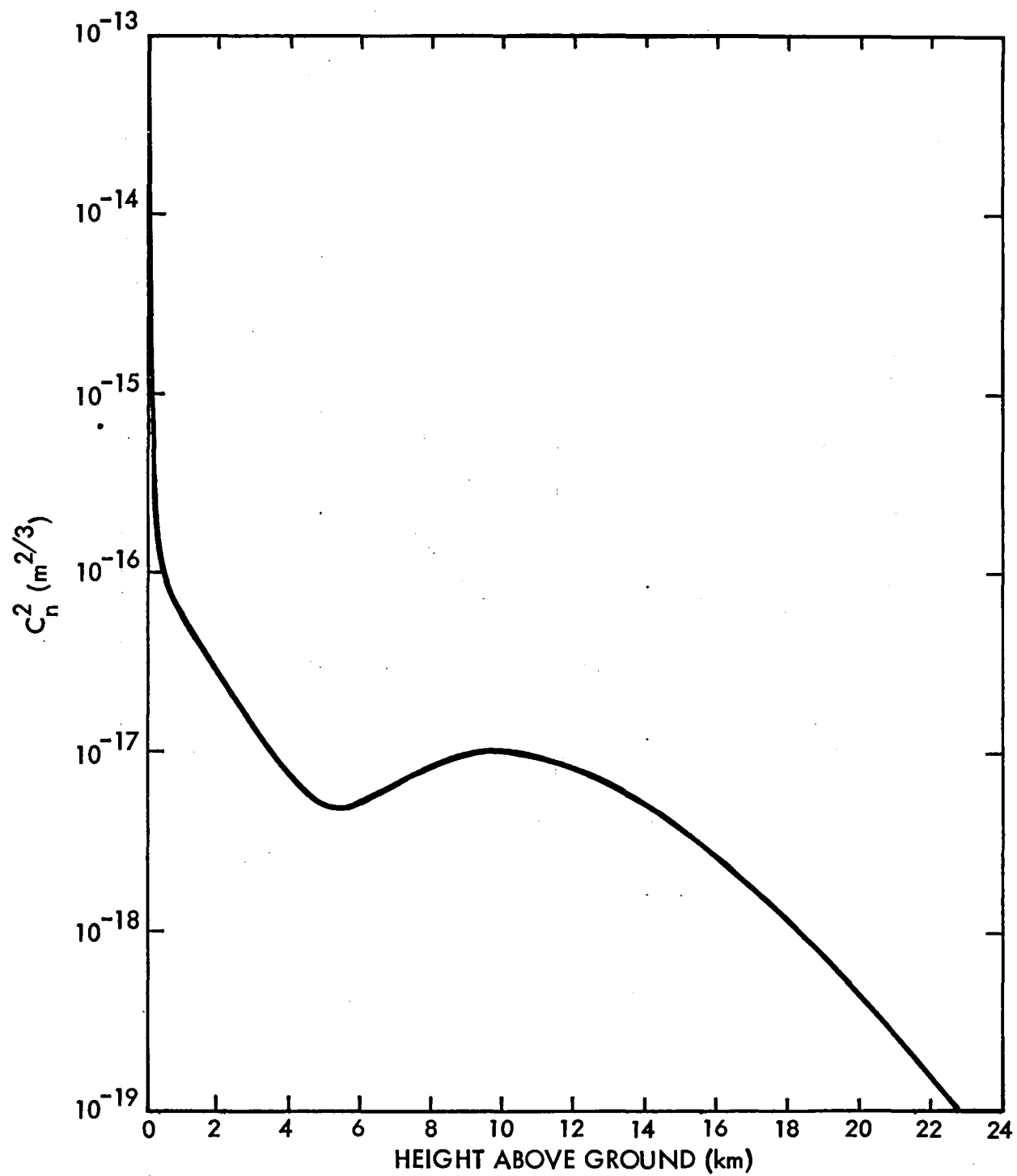


Figure 42. Hufnagel model for the altitude dependence of  $C_n^2$ , modified below 1.6 km to represent moderate low-altitude turbulence ( $10^{-13} \text{ m}^2/3$  at  $h = 0$ )

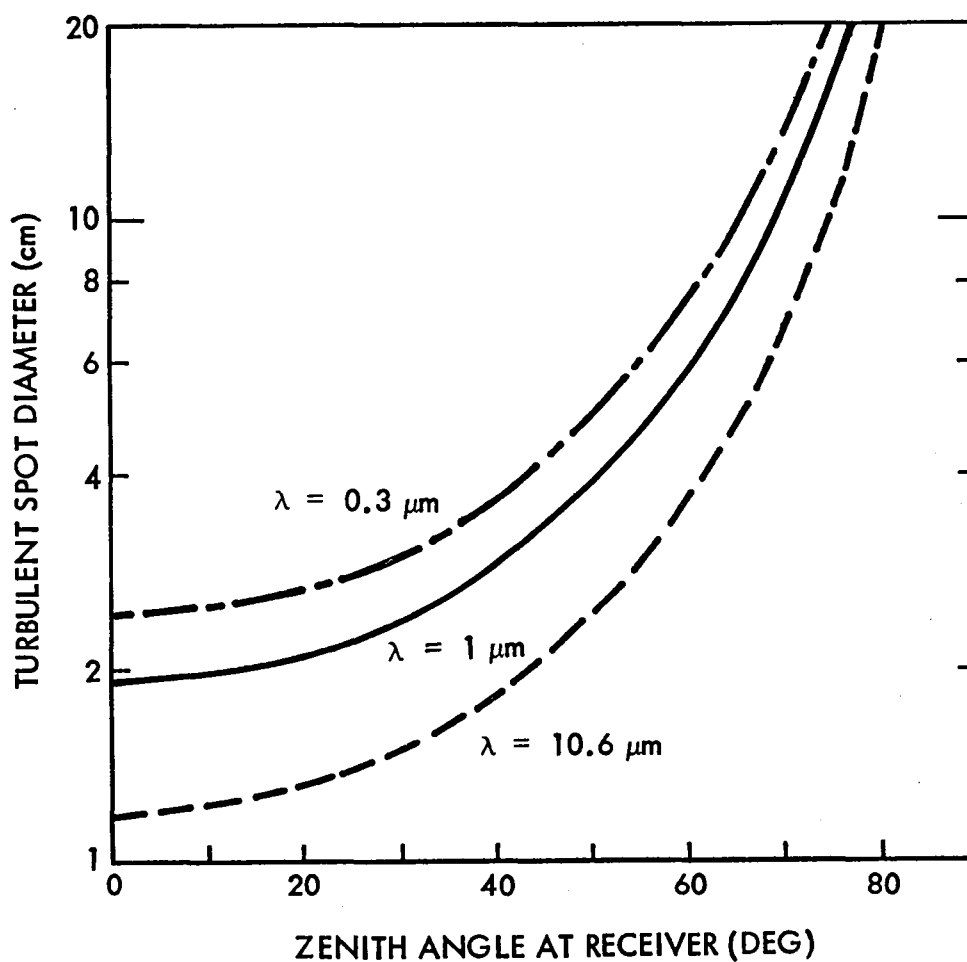


Figure 43. Time-average turbulent beam spread for a beam propagating from space to ground level, based on Hufnagel's turbulence model at high altitudes plus moderate low-altitude turbulence

dependence is different for turbulent and diffraction spreading. The turbulent spot size varies as  $\lambda^{-0.2}$ , while diffraction varies as  $\lambda^{+1}$ .

The general conclusion is that for receiver apertures on the order of 10 m in diameter, turbulent beam spreading is not a problem for reasonable zenith angles.

### 3.7.2 Attenuation

At short wavelengths ( $\lesssim 1 \mu\text{m}$ ), the beam is attenuated by aerosols, Rayleigh scattering and ozone absorption (Figure 44); at longer wavelengths the latter two processes are negligible (Figure 45), but molecular vibration-rotation lines and absorption continua are highly dependent on the exact laser wavelength. The aerosols primarily scatter the radiation, while the molecular absorption leads to heating of air within the beam and produces thermal blooming.

From Figures 44 and 45 it might appear that wavelengths shorter than about  $2 \mu\text{m}$  should be avoided because the severe aerosol attenuation implies very high transmitter power if 1 to 5 GW are to be delivered to the receiver. This may indeed be the appropriate conclusion, unless receivers can be located where the horizontal visibility is greater than 23 km ("clear" atmosphere).

For many laser lines with  $\lambda > 2 \mu\text{m}$  the molecular attenuation is minor, favoring these wavelengths as far as transmittance is concerned. The limiting factor, however, is thermal blooming.

### 3.7.3 Thermal Blooming

In the steady-state, a CW laser beam produces a density perturbation across the beam due to heating:

$$\frac{\Delta p}{p}(x, y) = \frac{(\gamma - 1)\alpha}{\gamma p v} \int_{-\infty}^x I(x, y) dx \quad (5)$$

$\gamma$  = ratio of specific heats = 1.4,  $p$  = ambient pressure,  $\alpha$  = absorption coefficient,  $I(x, y)$  = intensity profile at a particular range along the beam, and  $v$  = transverse flow speed (due to wind and slew), Ref. 21. The variation of the index of refraction across the beam is given by  $(n_0 - 1) \Delta p/p$ , and this leads to a variation in the phase of the wave as it propagates through the heated region. To date, the literature on thermal blooming has been restricted to investigations in which the unperturbed medium is uniform:  $\alpha$  is assumed to be independent of distance along the beam. A distortion number  $N_D$  is then defined (Ref. 22), which is proportional to  $kR(n_0 - 1) \Delta p/p$  and for  $N_D \gtrsim 1$  there is significant thermal blooming.

To estimate the relative importance of thermal blooming for the present purpose we use the phase distortion calculated for an unbloomed collimated beam. For a uniform medium this phase is equivalent to the distortion number. We have

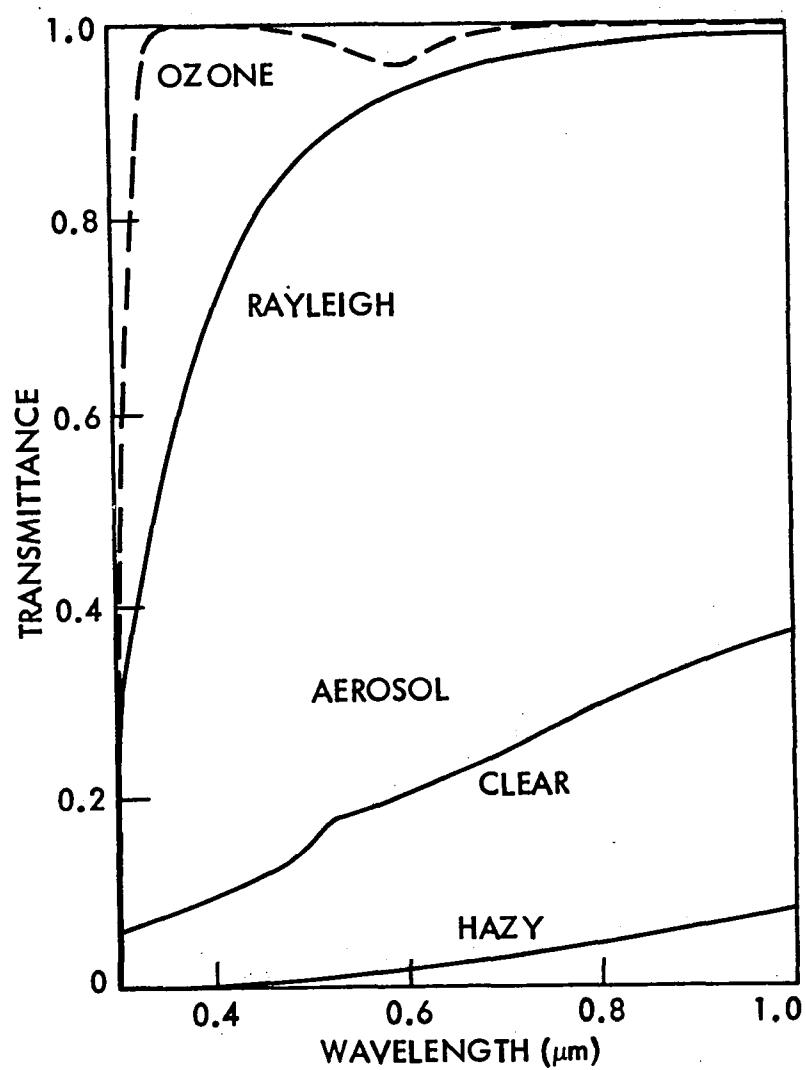


Figure 44. Vertical atmosphere transmittance as a function of wavelength, due to ozone, Rayleigh scattering, and aerosol attenuation. The aerosol models are from Ref. 20: "clear" and "hazy" correspond to ground level horizontal visibilities of 23 km and 5 km, respectively



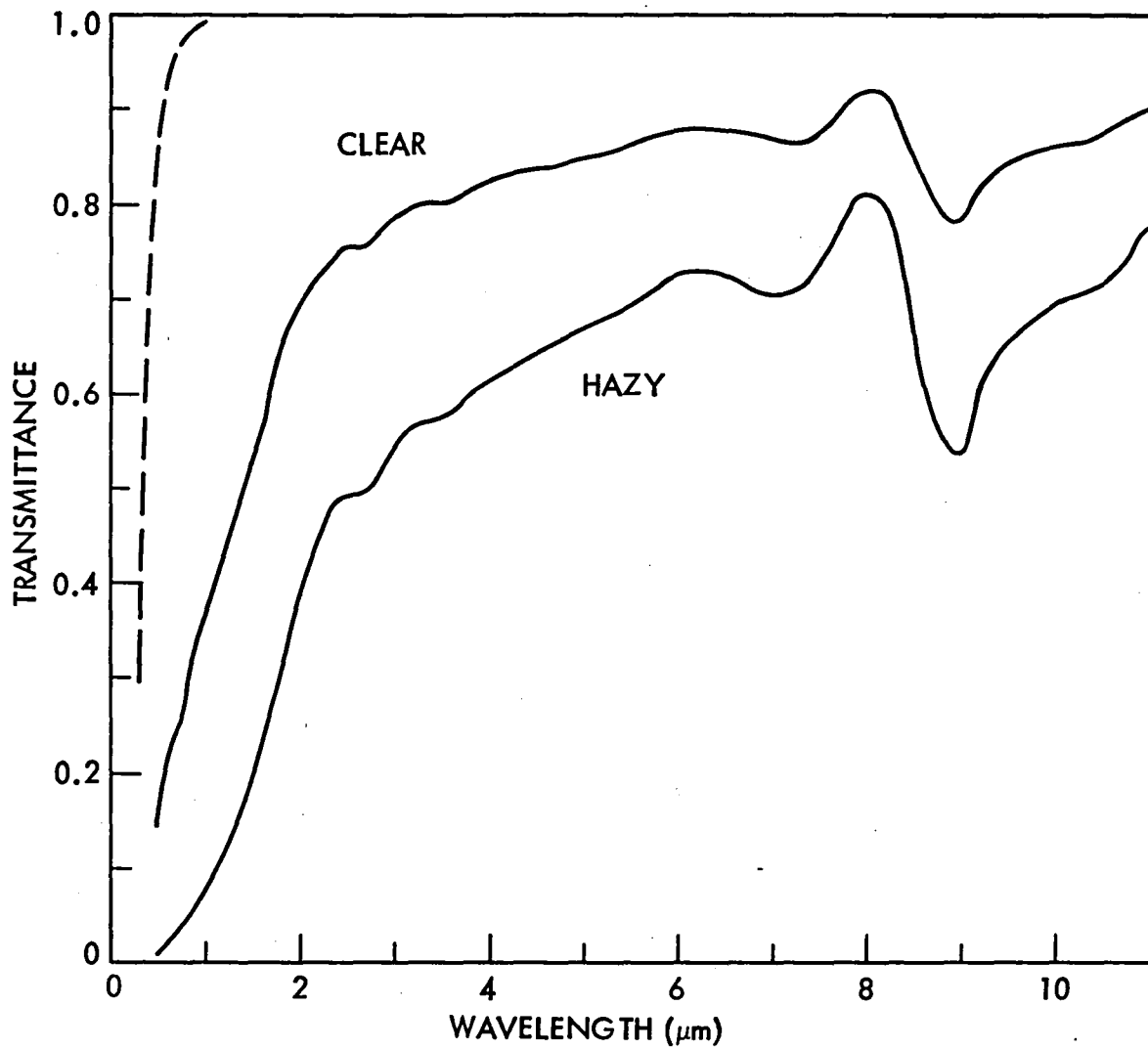


Figure 45. Transmittance for a vertical line-of-sight through the entire atmosphere; dashed curve: Rayleigh scattering; solid curves, aerosol

$$\phi_{TB} = k \int_0^R (n - 1) \frac{\Delta \rho}{\rho} dZ \quad (6)$$

By the time the beam propagates into the atmosphere the intensity profile near beam center can be approximated by a Gaussian, and

$$\int_{-\infty}^{\infty} I(x, y) d_x \approx 4.51 \times 10^9 P'/D \quad \text{Wm}^{-1} \quad (6a)$$

where  $P'$  is the beam power in GW and the diameter  $D$  is in meters. Then with  $(n - 1)/\rho \approx 2.67 \times 10^{-9} \text{ Pa}^{-1}$ , assuming the absorption coefficient decreases exponentially

$$\alpha \approx \alpha_0 \exp(-h/H) \quad (7)$$

and the wind increases linearly with altitude

$$v \approx v_0 + v' h, \quad (8)$$

it is possible to show that

$$\phi_{TB} \approx \frac{2.16 \times 10^7}{\lambda} \frac{P' \alpha_0 H}{V_{av} D} \quad \text{radians} \quad (9)$$

where  $\lambda$  is the wavelength in microns. The average transverse wind speed,  $v_{av}$  is related to  $v_0$ ,  $v'$  and  $H$  as shown in Figure 46. Typical values for natural wind (Ref. 23) are  $v_0 \sim 10 \text{ m/s}$ ,  $v' \sim 3 \text{ to } 4 \text{ m/s/km}$ , so with  $H \sim 2 \text{ to } 4 \text{ km}$  the parameter  $v_0/v'H \sim 0.5 \text{ to } 2$ . Figure 46 then gives  $v_{av} \lesssim 2 v_0$ . The actual velocity gradient  $v'$  will include a contribution from the slew rate due to transmitter orbital motion, as shown in Figure 47. For transmitters above 5000 km, this contribution is less than 1 m/s/km.

Using Eq. (9) we can put limits on the average wind speed and the molecular absorption for which the thermal blooming will not be severe, i.e., so that  $\phi_{TB} < 1$  radian:

$$\frac{v_{av}}{\alpha_0 H} > 4.32 \times 10^5 P'/\lambda \quad (10)$$

this is shown graphically in Figure 48.

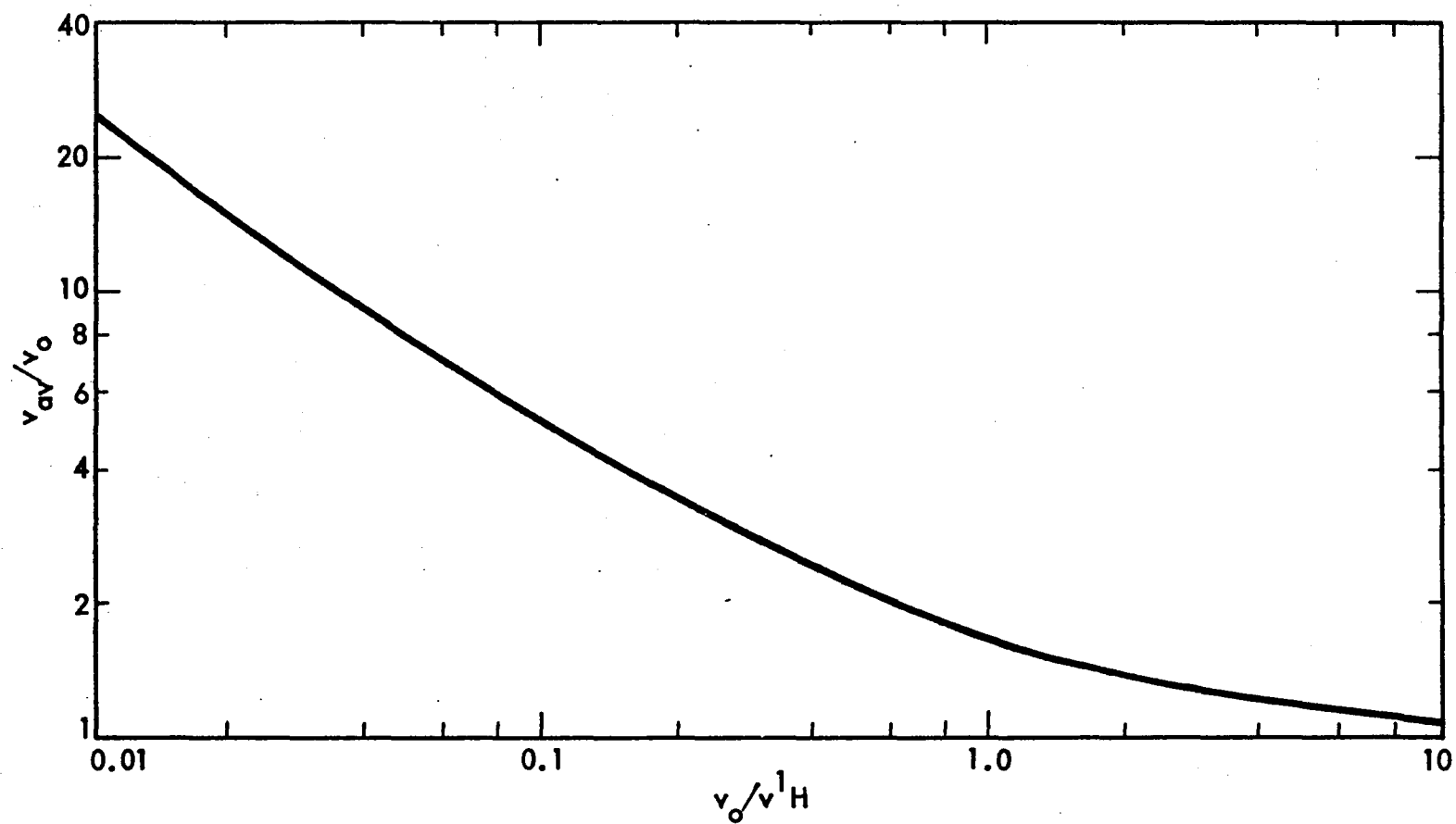


Figure 46. Effective transverse wind-speed,  $v_{av}$ , as a function of ground-level wind,  $v_o$ , vertical gradient,  $v'$ , and absorption scale height,  $H$

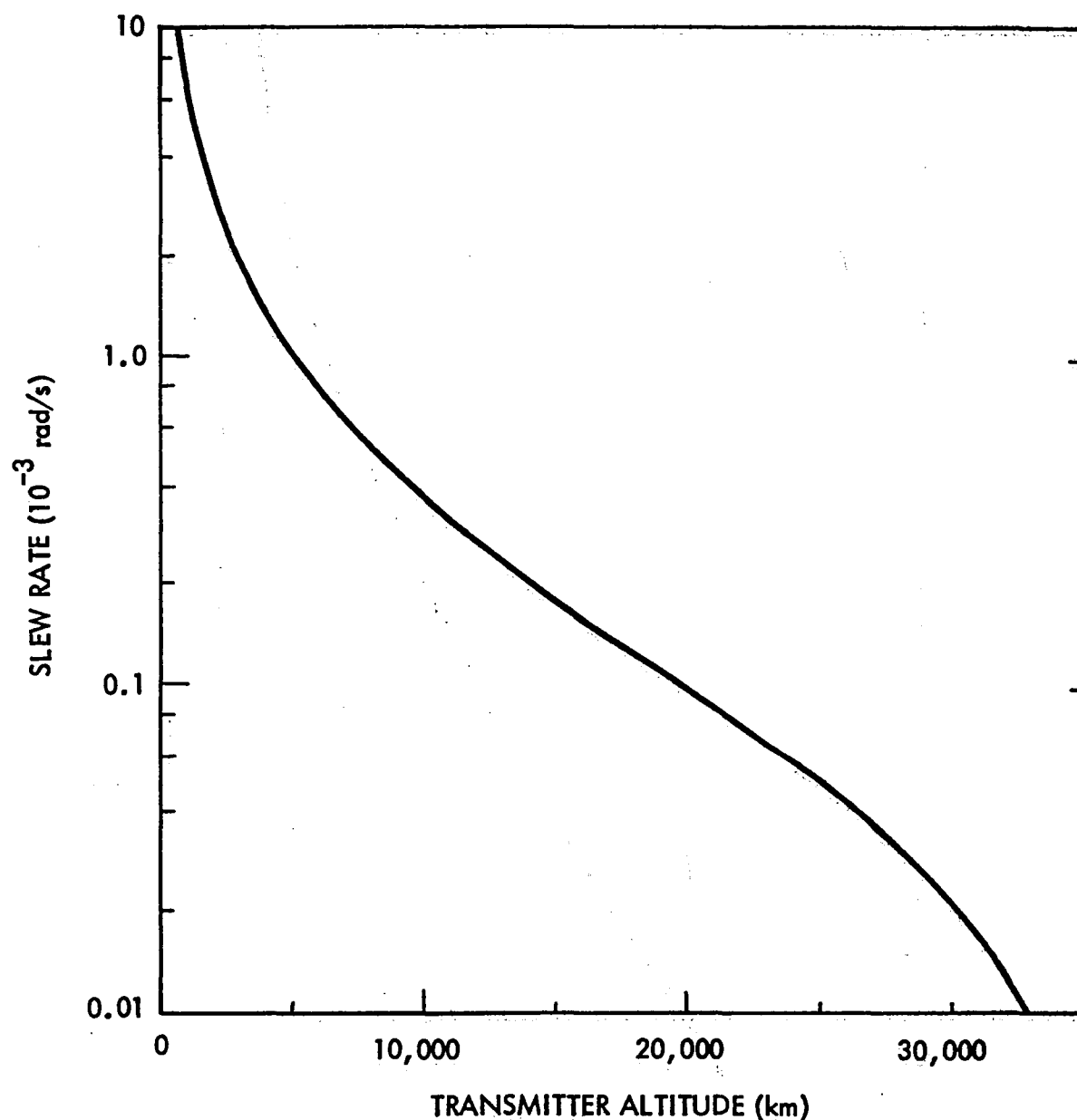


Figure 47. Slew rate at the receiver as the transmitter passes the local zenith. In these units ( $10^{-3}$  rad/s), the slew rate is numerically equal to the resulting vertical gradient of a transverse velocity,  $v'$ , in m/s/km

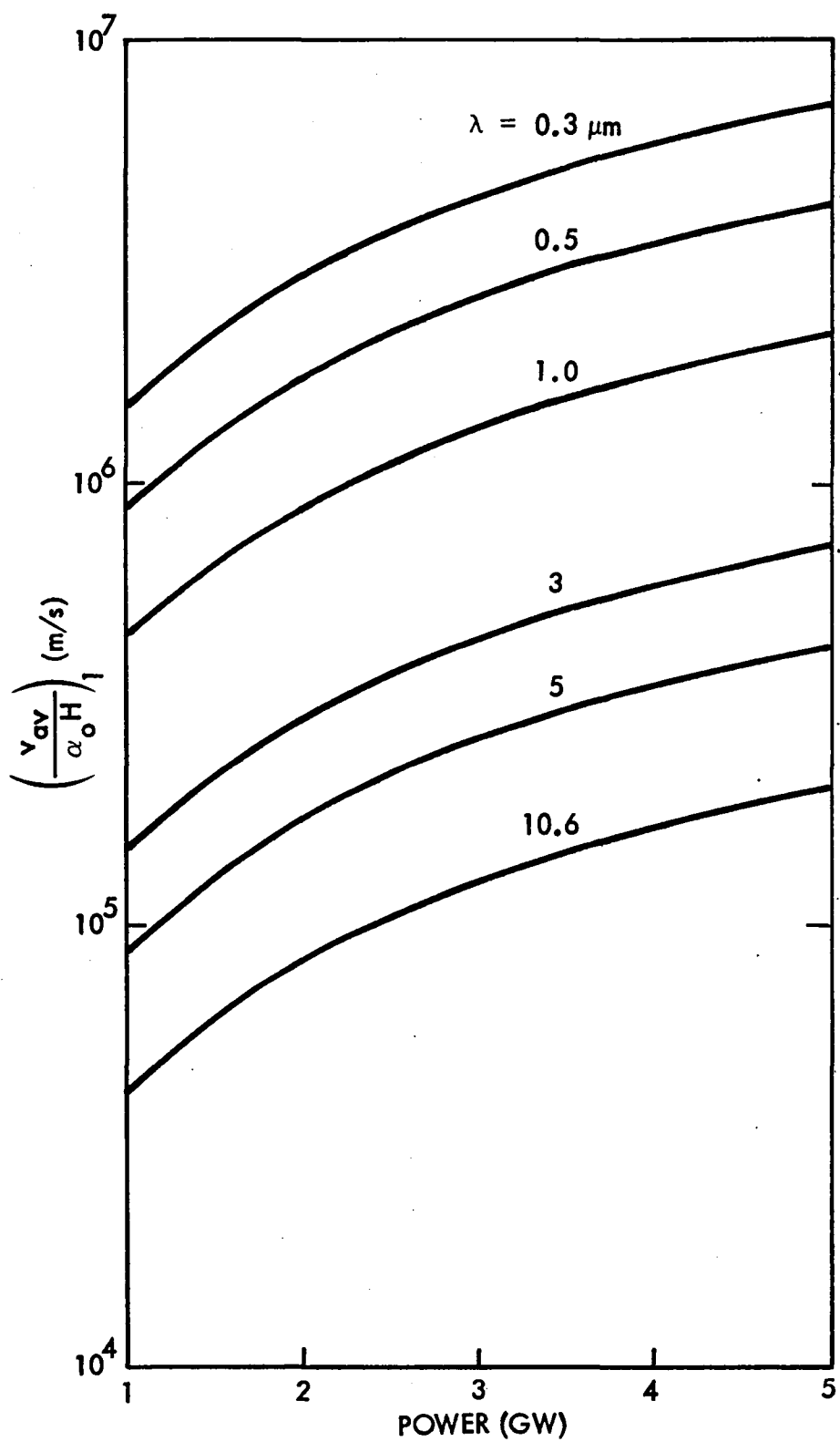


Figure 48. Limiting values of windspeed  $v_{av}$  and low-altitude absorption  $\alpha_0 H$ : for  $(v_{av}/\alpha_0 H) < (v_{av}/\alpha_0 H)_1$ , thermal blooming is significant. Beam diameter = 50 m

The wind speed  $v_{av}$  is governed primarily by the low-altitude natural wind  $v_0$  and is insensitive to the gradient  $v'$ , unless  $v'$  is large (as for a low-altitude transmitter). It should be noted that the satellite slew rate and the natural wind gradients in general will not be in opposite directions as has been assumed here — their sum is a vector quantity. The net transverse flow speed will therefore vary in direction as well as magnitude as a function of distance along the beam. Should the net flow speed be zero at some point in the beam, very serious blooming would result.

The molecular absorption  $\alpha_0 H$  [the transmittance is approximately  $\exp(-\alpha_0 H)$ ] depends strongly on the particular laser line, but also may exhibit variation with meteorological conditions. In general, high temperature and high humidity increase absorption. The ground level absorption coefficient  $\alpha_0$  is seldom less than  $0.01 \text{ km}^{-1}$  for any laser line with  $\lambda > 1 \mu\text{m}$  (Ref. 20). The scale height  $H \sim 2$  to  $4 \text{ km}$ . An important exception is ozone absorption for  $\lambda < 1 \mu\text{m}$ .

As an optimistic estimate of atmospheric conditions, we assume  $v_{av} = 40 \text{ m/s}$ ,  $\alpha_0 = 0.01 \text{ km}^{-1}$  and  $H = 1 \text{ km}$ . This gives

$$\left( v_{av} / \alpha_0 H \right)_{\text{atm}} \approx 4 \times 10^3 \text{ m/s} , \quad (11)$$

which implies that thermal blooming may be a problem at the power levels being considered.

Quantitative evaluation of the beam spreading due to blooming requires detailed wave optics computations including the appropriate altitude dependence of propagation conditions. All existing propagation scaling laws are for a homogeneous propagation path. The detailed computations can be done at LMSC, but they require more time than is available for this preliminary analysis. The blooming occurs in the lower few kilometers of the propagation path, so its effect is less than if it were more evenly distributed.

A separate analysis is indicated for laser wavelengths less than  $1 \mu\text{m}$  because the absorbing molecule, ozone, is dissociated when it absorbs a photon. Since this is related to environmental impact of the system, the discussion is given in a separate section.

### 3.7.4 Propagation at $\lambda < 1 \mu\text{m}$ : Ozone Destruction

As the transverse wind carries a given parcel of air through the beam, the ozone is depleted at a rate

$$\frac{dn}{dt} = - \frac{\lambda n \sigma}{hc} I(x, y, z, t) \quad (12)$$

The symbols are defined by

- $n(x, y, z, t)$  = number density of ozone  
 $\sigma(\lambda)$  = ozone absorption cross section per molecule  
 $I(x, y, z, t)$  = beam irradiance seen by a given mass of air

Assuming a steady-state, the time dependence of  $I$  is related to the spatial variation of the beam intensity, and we may write

$$\frac{dn(x, y)}{n} = - \frac{\lambda \sigma I(x, y)}{hc v} dx \quad (13)$$

Now  $I(x, y)$  represents the intensity profile across the beam at a particular range,  $z$ , and  $v$  is the transverse flow speed.

Assuming for simplicity that the beam intensity is Gaussian with  $e^{-1}$  intensity radius  $a$ , Eq. (13) can be integrated to give

$$n(x, y) = n_o \exp \left\{ - \frac{\lambda \sigma}{hc} \cdot \frac{P}{a} \frac{\exp(-y^2/a^2)}{2\sqrt{\pi}} \left[ \operatorname{erf}(x/a) + 1 \right] \right\} \quad (14)$$

$n_o$  represents the ambient ozone density. After a given sample of air has passed entirely through the beam ( $x \gg a$ ) the ozone has been depleted to

$$n(\infty, y) = n_o \exp \left\{ - \frac{\lambda \sigma P \exp(-y^2/a^2)}{\sqrt{\pi} hc v a} \right\} \quad (15)$$

To evaluate this expression we assume

- $P = 10^9 \text{ W}$   
 $\lambda = 0.6 \mu\text{m}$  (maximum ozone absorption)  
 $\sigma = 4.89 \times 10^{-21} \text{ cm}^2/\text{molecule}$  (Ref. 24)  
 $a = 10 \text{ m}$

and

$$\frac{\lambda \sigma P}{\sqrt{\pi} hc a} = 8.3 \times 10^3 \text{ m/s} \quad (16)$$

Therefore the air passing through the center of the beam is depleted of ozone by the factor  $\exp(-8300/v)$ , and for any plausible values of  $v$ , the ozone is essentially

completely destroyed. The width of the depleted region is governed by the  $y$ -dependence of Eq. (15), and the ozone depletion factor is  $e^{-1}$  within a zone of total width  $2 y_c$ , where

$$y_c = a \left\{ \ln \left( \frac{\lambda \sigma P}{\sqrt{\pi} h c a v} \right) \right\} \quad (17)$$

Using Eq. (16), for  $1 \leq v \leq 100$  m/s Eq. (17) gives  $3.0 a \geq y_c \geq 2.09 a$ . So within wide ranges of conditions, the entire beam is essentially free of ozone. There are two implications of this result:

- (1) Thermal blooming will be due to aerosol absorption because the ozone is depleted within the beam. Aerosol blooming may be important, except in very clear atmospheres.
- (2) The atmospheric ozone depletion rate for the entire beam is given by

$$\int_0^{\infty} n(z) v(z) D(z) dz \quad (18)$$

This integral depends primarily on the wind near the ozone density maximum ( $\sim 20$ - to  $30$ -km altitude).

### 3.8 DISCUSSION OF RESULTS

The results of the study are based on relatively conservative approaches to establish the system. System optimization was not performed nor were laser devices projected for the time frame of use. Under these conditions, the Space Laser Power System still showed to be feasible technically with only moderate technology advancements and to be economically competitive with the Solar Power Satellite. The Space Laser Power System has clearly been shown to be an alternate method of transferring energy from space to the earth. Also, the funding level required for a pilot program to demonstrate proof-of-concept is reasonable in respect to the system costs and expected benefits. The results obtained in this study were derived from basic analyses designed to provide realistic, conservative answers. These results deserve to be verified by more and broader in-depth studies. Many areas still need to be investigated.



Section 4  
REFERENCES

1. A. R. Kantrowitz, "Propulsion to Orbit by Ground-Based Lasers," Aeronautics and Astronautics, May 1972
2. W. S. Jones, Laser Rocket System Analysis Study, Contract NAS 3-20372, LMSC-D564671A, Aug 1978
3. W. S. Jones, "Laser Powered Aircraft and Rocket Systems With Laser Energy Relay Units," Progress in Astronautics and Aeronautics, Vol. 61, Jan 1978
4. R. R. Berggren and G. E. Lenertz, Feasibility of a 30-Meter Space-Based Laser Transmitter, NASA CR-134903, NASA Lewis Research Center, Oct 1975
5. R. O. Piland, Initial Technical, Environmental, and Economic Evaluations of Space Solar Power Concepts, " Vols. 1 and 2, NASA Johnson Space Center, JSC 11568, Aug 1976
6. G. R. Woodcock et al., Solar Power Satellites - System Definition Study, Parts I and II, Vols. 1-8, Boeing Aerospace Co., Dec 1977
7. R. J. Stirn, "Overview of Novel Photovoltaic Conversion Techniques at High Intensity Levels," Radiation Energy Conversion In Space, AIAA Progress in Astronautics and Aeronautics, Vol. 61, Jan 1978
8. Rockwell International, Satellite Power System Feasibility Study, SD 76-SA-02392, 1976
9. A. Hertzberg et al., "High Temperature Solar Photon Engines," AIAA Fluid and Plasma Dynamics Conference, Paper 78-1177, Jul 1978
10. A. Hertzberg and C. Lau, "A High Temperature Binary Cycle for Ground and Space Solar Engine Application," AIAA Progress In Astronautics and Aeronautics, Vol. 61, Jan 1978
11. R. T. Taussig et al., "Energy Exchanger Technology, Applied to Laser Heated Engines," AIAA Progress In Astronautics and Aeronautics, Vol. 61, Jan 1978
12. -----, "Study, Optimization, and Design of a Laser Heat Engine," AIAA Progress In Astronautics and Aeronautics, Vol. 61, Jan 1978
13. R. C. Weatherston and A. Hertzberg, "The Energy Exchanger, A New Concept for High Efficiency Gas Turbine Cycles," Trans. ASME, Journal of Engineering for Power, Vol. 89, Apr 1967, p. 217
14. P. K. Bailey and R. C. Smith, Closed Cycle Electric Discharge Laser Design Investigation, Hughes Aircraft, NASA CR-135408, Mar 1978

15. W. H. Christiansen, University of Washington, personal communication
16. A. S. Gilmour et al., High Power Study -- Power Conditioning, New York State University, AF APL-TR-76-101, Air Force Aero-Propulsion Laboratory
17. A. T. Mattick, "Absorption of Solar Radiation by Alkali Vapors," AIAA Progress in Astronautics and Aeronautics, Vol. 61, Jan 1978
18. R. L. Fante, Proc. IEEE, Vol. 63, 1975, p. 1669
19. D. L. Fried and G. E. Mevers, Appl. Opt., Vol. 13, 1974, p. 2620; corrections on: Vol. 14, 1975, p. 2567; Vol. 16, 1977, p. 549
20. R. A. McClatchey and J. E. A. Selby, Atmospheric Attenuation of Laser Radiation From 0.76 to 31.25  $\mu$ m, AFCRL-TR-74-0003, 3 Jan 1974
21. F. G. Gebhardt, Appl. Opt., Vol. 15, 1976, p. 1479
22. L. C. Bradley and J. Herrmann, Appl. Opt., Vol. 13, 1974, p. 331
23. M. W. Munn, Propagation Modeling for Ground to Space Laser Scenarios, LMSC-D558929, Feb 1977
24. M. Ackerman, "Ultraviolet Solar Radiation Related to Mesospheric Processes," in Mesospheric Models and Related Experiments, Fiocco (ed.), D. Reidel Publishing Co., Dordrecht-Holland, 1971

DISTRIBUTION LIST  
LASER POWER CONVERSION SYSTEM ANALYSIS

1. National Aeronautics & Space Administration  
Lewis Research Center  
21000 Brookpark Road  
Cleveland, OH 44135

Attn: Contracting Officer, MS 500-312	1
Technical Utilization Office, MS 3-16	1
Technical Report Control Office, MS 5-5	1
AFSC Liaison Office, MS 501-3	2
Library, MS 60-3	2
Office of R&QA, MS 500-211	1
N. T. Musial, Patent Counsel, MS 500-113	1
John W. Dunning, Jr., Project Manager, MS 500-202	10
Lester D. Nichols, MS 500-202	1
Wolfgang E. Moeckel, MS 3-12	1

2. National Aeronautics & Space Administration  
Headquarters  
Washington, D.C. 20546

Attn: Office of Aeronautics and Space Technology Director, Space Power and Propulsion/RTS-3	1
Attn: F. C. Schwenk/RT-3	1
Attn: Office of Space Transportation Systems Director, Advanced Programs/MT-3	1
Attn: James Lazar/RP-6	1
Attn: Jerome P. Mullin/RP-6	1
Attn: Stanley R. Sadin/RX-4	1

3. National Aeronautics & Space Administration  
Ames Research Center  
Moffett Field, CA 94035

Attn: Library	1
Dr. Kenneth W. Billman	1

4. National Aeronautics & Space Administration  
Flight Research Center  
P. O. Box 273  
Edwards, California 93523

Attn: Library 1

5. National Aeronautics & Space Administration  
George C. Marshall Space Flight Center  
Huntsville, Alabama 35812

Attn: Library 1  
Lott W. Brantley 1  
Jimmy L. Miller 1

6. National Aeronautics & Space Administration  
Goddard Space Flight Center  
Greenbelt, Maryland 20771

Attn: Library 1

7. National Aeronautics & Space Administration  
John F. Kennedy Space Center  
Cocoa Beach, Florida 32931

Attn: Library 1

8. National Aeronautics & Space Administration  
Lyndon B. Johnson Space Center  
Houston, Texas 77058

Attn: Library 1  
Douglas Lilly 1  
Richard F. Baillie 1  
Robert Piland 1  
Richard B. Ferguson 1  
Tony E. Redding 1

9. National Aeronautics & Space Administration  
Langley Research Center  
Langley Station  
Hampton, Virginia 23365

Attn: Library 1  
R. Hless 1  
L. Bernard Garrett 1

10. NASA Scientific & Technical Information Facility  
P. O. Box 8757  
Balt/Wash International Airport  
Maryland 21240  
  
Attn: Accessioning Department 10
11. Jet Propulsion Laboratory  
4800 Oak Grove Drive  
Pasadena, California 91103  
  
Attn: Library 1  
G. R. Russell 1
12. Defense Documentation Center  
Cameron Station  
Building 5  
5010 Duke Street  
Alexandria, Virginia 22314  
  
Attn: TISLA 1
13. Defense Advanced Research Projects Agency  
1400 Wilson Bl.  
Arlington, Virginia 22209  
  
Attn: Director, Laser Division 1
14. ODDR&E  
Pentagon  
Washington, D.C. 20301  
  
Attn: Asst. Dir. (Space and Advanced Systems) 1
15. AF Materials Lab.  
Wright Patterson AFB, OH 45433  
  
Attn: Major Paul Elder (LPJ) 1
16. Air University  
Institute for Professional Development  
Maxwell AFB, Alabama 36112  
  
Attn: ACSC/EDCS 1
17. National Security Agency 1  
Ft. George G. Meade, MD 20755  
  
Attn: Mr. Richard C. Foss, A42, FANX III

18. Department of the Army 2  
Office of the Deputy Chief of Staff for Research,  
Development, and Acquisition  
Washington, D.C. 20310  
  
Attn: DAMA-WS (1 cy)  
DAMA-WSM-A (LTC F. Holmes)
19. Department of the Army 1  
Office of the Deputy Chief of Staff for Operations and Plans  
Washington, D.C. 20310  
  
Attn: DAMO-RQA (Major Garner)
20. Commander 1  
U.S. Army Intelligence Agency  
Ft. George G. Meade, MD 20755  
  
Attn: MILA-OSS, Mr. Sherman Delmage
21. Ballistic Missile Defense Program Office 1  
5001 Eisenhower Avenue  
Alexandria, VA 22333  
  
Attn: Albert J. Bast, Jr.
22. U.S. Army Missile Research and Development Command 5  
Redstone Arsenal, AL 35809  
  
Attn: DRCPM-HEL (V. P. De Fatta)  
DRCPM-HEL-P  
DRCPM-HEL-S  
DRCPM-HEL-T (Dr. W. H. Evers)  
DRDMI-HAL (Dr. R. Rose)
23. Commander 1  
U.S. Army Missile Research and Development Command  
Redstone Arsenal, AL 35809  
  
Attn: DRDMI-NS
24. Commander 1  
U.S. Army Materiel Systems Analysis Agency  
Aberdeen Proving Ground, MD 21005  
  
Attn: DRXSY-AAF (Doug Smith)

25. Director 1  
Ballistic Missile Defense Advanced Technology Center  
P.O. Box 1500  
Huntsville, AL 35807  
Attn: ATC-O, Mr. W. O. Davies
26. Director 3  
U.S. Army Ballistic Research Laboratory  
Aberdeen Proving Ground, MD 21005  
Attn: Dr. Robert Eichelberger  
Mr. Frank Allen  
Dr. E. C. Alcaarez
27. Commandant 1  
U.S. Army Air Defense School  
Ft. Bliss, TX 79916  
Attn: ATSA-CD-MS
28. Commander 1  
U.S. Army Training & Doctrine Command  
Ft. Monroe, VA 23651  
Attn: ATCD-CF
29. Commander 1  
USA Frankford Arsenal  
Bridge & Tacony Streets, Bldg. 201.3  
Philadelphia, PA 19137  
Attn: Mr. M. Elnick (SARFA-FCD)
30. Commander 1  
U.S. Army Electronics Command  
Ft. Monmouth, NJ 07703  
Attn: DRSEL-CT-L (Dr. R. G. Buser)
31. Department of the Navy 2  
Office of the Chief of Naval Operations  
Washington, D.C. 20350  
Attn: Cdr. L. E. Pellock (OP-982F3)  
Mr. L. E. Triggs (OP-35E)

32. Office of Naval Research 1  
495 Summer Street  
Boston, MA 02110  
  
Attn: Dr. Fred Quelle
33. Office of Naval Research 1  
800 N. Quincy Street  
Arlington, VA 22217  
  
Attn: Dr. W. J. Condell (421)
34. Department of the Navy 1  
Deputy Chief of Naval Materiel (Dev)  
Washington, D.C. 20360  
  
Attn: Mr. R. Gayload (MAT 032B)
35. Commander, Naval Sea Systems Command 1  
Department of the Navy  
Washington, D. C. 20362  
  
Attn: Capt. J. G. Wilson, PMS-405
36. Superintendent 1  
Naval Postgraduate School  
Monterey, CA 93940  
  
Attn: Prof. John Neighbours
37. U.S. Naval Weapons Center 1  
China Lake, CA 93555  
  
Attn: Mr. E. B. Niccum (Code 3173)
38. Naval Research Laboratory 8  
Washington, D. C. 20375  
  
Attn: Dr. J. M. MacCallum (Code 4109) EOTPO  
Dr. H. W. Gandy (Code 7905)  
Dr. J. L. Walsh (Code 4109)  
Dr. J. T. Schriempf (Code 6410)  
Dr. R. F. Wenzel (Code 6415)  
Mr. R. W. Rice (Code 6360)  
Dr. L. R. Hettche (Code 6310)  
Dr. F. W. Patten (Code 6440)



39. Commander 2  
Naval Surface Weapons Center  
White Oak  
Silver Spring, MD 20910  
  
Attn: M. T. Madden, WA-23  
Dr. Leroy Harris
40. Hq, AFSC/XRLW 1  
Andrews AFB, Washington, D.C. 20334  
  
Attn: Capt. Larry Curtis
41. Hq, USAF (RDPS) 1  
Washington, D.C. 20330  
  
Attn: Lt. Col. A. J. Chiota
42. Hq, AFSC (DLCAW) 1  
Andrews AFB, Washington, D.C. 20334  
  
Attn: Capt. Pulley
43. Air Force Weapons Lab 5  
Kirtland AFB, NM 87117  
  
Attn: Col. Donald L. Lamberson (AR)  
Col. C. E. Brunson (PO)  
Col. L. Bernasconi (PG)  
Col. Demos Kyrazis (LR)  
Lt. Col. A. D. Maio (AL)
44. Hq, SAMSO 1  
P.O. Box 92960, Worldway Postal Center  
Los Angeles, CA 90009  
  
Attn: Lt. Col. J. R. Doughty (DYV)
45. Hq, Aeronautical Systems Division 2  
Wright Patterson AFB, OH 45433  
  
Attn: Lt. Col. J. R. Doughty (YAD)  
Major Art Smith (INH)
46. AF Avionics Laboratory (DHIO) 1  
Wright Patterson AFB, OH 45433  
  
Attn: Mr. K. Hutchinson

47. Hq, Foreign Technology Division 1  
Wright Patterson AFB, OH 45433  
Attn: Mr. R. W. Buxton (ETEO)
48. AF Aero Propulsion Lab 1  
Wright Patterson AFB, OH 45356  
Attn: Lt. Col. Bobbie L. Jones
49. RADC (OCSE/Mr. R. Urtz) 1  
Griffiss AFB, NY 13441
50. Hq., Electronics Systems Division/XRE/SIO 1  
Hanscom AFB, MA 01731
51. AF Rocket Propulsion Lab 1  
Edwards AFB, CA 93523  
Attn: B. R. Bornhorst (LKCB)
52. USAF/INAKA 1  
Washington, D.C. 20330  
Attn: LTC Fredric C. Dunlap
53. Defense Intelligence Agency 1  
Washington, D.C. 20301  
Attn: Mr. Seymour Berler (DTLA)
54. Central Intelligence Agency 3  
Washington, D.C. 20505  
Attn: Mr. Julian C. Nall (OSI/PSTD)  
Dr. John E. Ashman (OWI/DSD)  
Dr. Bernard Lubarsky
55. Dr. Fred A. Koomanoff 1  
U.S. Department of Energy  
Room 509  
400 First Street, N.W.  
Washington, D.C. 20545
56. Aerodyne Research Inc. 1  
Bedford Research Park  
Bedford, Massachusetts 01730  
Attn: Charles E. Kolb

57. Analytic Services, Inc. 1  
5613 Leesburg Pike  
Falls Church, VA 22041  
  
Attn: Dr. A. Deshmukh
58. Aerospace Corp. 3  
P.O. Box 92957  
Los Angeles, CA 90009  
  
Attn: Dr. G. P. Millburn  
Dr. Walter R. Warren, Jr.  
Dr. M. A. Clark
59. Aeronutronic Ford Corp. 3  
Fort Road, P.O. Box A  
Newport Beach, CA 92663  
  
Attn: R. R. Auelmann, Systems Engineering
60. Mr. A. Colin Stancliffe 1  
AiResearch Manufacturing Co.  
2525 West 190th Street  
Torrance, CA 90503  
  
Attn: Dept. 93-6
61. Atlantic Research Corporation 1  
Shirley Highway at Edsall Road  
Alexandria, VA 22314  
  
Attn: Mr. Robert Naismith
62. AVCO - Everett Research Laboratory 2  
2385 Revere Beach Parkway  
Everett, MA 02149  
  
Attn: Dr. George Sutton  
Dr. Jack Dougherty
63. Battelle Columbus Labs 1  
505 King Avenue  
Columbus, OH 43201  
  
Attn: Mr. Fred Tietzel

64. Battelle Memorial Institute 1  
2030 M Street, N.W.  
Washington, D.C. 20036  
  
Attn: Mr. Alan Bow
65. Dr. John Rather 1  
BDM Corporation  
McLean, VA
66. Bell Aerospace Co. 1  
Buffalo, NY 14240  
  
Attn: Dr. Wayne C. Solomon
67. Boeing Aerospace Co. 2  
P.O. Box 3999  
Seattle, WA 98124  
  
Attn: Mr. M. I. Gamble  
Orgn 2-2883, M.S. 13-85
68. Gerald L. Borrowman 1  
P. O. Box 1032  
Weyburn, Saskatchewan, Canada  
S4H2L3
69. Eastman Kodak Company 1  
901 Elmgrave Road  
Rochester, NY 14650  
  
Attn: R. E. Keim, Dept 394
70. Environmental Research Institute of Michigan 2  
P.O. Box 618  
Ann Arbor, MI 48107  
  
Attn: IRIA (Laser Library)
71. Sidney W. Silverman 1  
Electrical Power Systems  
Boeing Aerospace Co.  
Box 3707/Mail Stop 8C-62  
Seattle, WA 98124
72. Electro-Optical Systems 1  
300 North Halstead  
Pasadena, CA 91107  
  
Attn: Dr. Andrew Jensen

73. ESL Inc. 1  
495 Java Dr.  
Sunnyvale, CA 94086  
  
Attn: Arthur Einhorn
74. General Electric Co.  
P.O. Box 8555  
Philadelphia, PA 19101  
  
Attn: Mr. W. J. East 1  
Dr. C. E. Anderson 1  
Dr. R. R. Sigismonti 1  
Dr. Thomas W. Karras 1
75. General Electric Co. 1  
100 Plastics Avenue  
Pittsfield, MA 01201  
  
Attn: Mr. D. G. Harrington (Rm 1044)
76. General Research Corporation 1  
307 Wynn Drive  
Huntsville, AL 35806  
  
Attn: Dr. K. Warmbrod
77. General Research Corporation 3  
7655 Old Springhouse Road  
McLean, VA 22101  
  
Attn: Gary F. Gurski  
Thomas F. Zakrzewski  
Dr. R. Holbrook
78. Sima Miluschewa 1  
Grumman Aerospace  
NASA Space Programs  
M.S. A09  
Bethpage, NY 11714
79. Hercules, Inc. 1  
Industrial Systems Department  
910 Market Street  
Wilmington, DE 19899  
  
Attn: Dr. R. S. Fey  
Mr. W. H. Fuller

80. Hercules, Inc. 1  
P.O. Box 210  
Cumberland, MD 21502  
  
Attn: Dr. R. Musso
81. Hughes Research Labs 4  
3011 Malibu Canyon Road  
Malibu, CA 90265  
  
Attn: Dr. Arthur N. Chester  
Dr. Richard L. Abrams  
Dr. Viktor Evtuhov  
Dr. Gerald S. Picus
82. Hughes Aircraft Co. 4  
Centinela and Teale Streets  
Culver City, CA 90230  
  
Attn: Dr. Eugene Peressini (Bldg. 6, MS/E-125)  
Dr. John Fitts (MS 5B-138)  
Dr. J. A. Alcalay (Bldg. 6, MS E182)  
Dr. M. M. Mann (MS D131)
83. Hughes Aircraft Co. 1  
P.O. Box 3310  
Fullerton, CA 90230  
  
Attn: Dr. William Yates
84. Itek Corp. 1  
Optical Systems Division  
10 Maguire Road  
Lexington, Mass. 02173  
  
Attn: R. J. Wollensak
85. Institute for Defense Analyses 1  
400 Army Navy Drive  
Arlington, VA 22202  
  
Attn: Dr. Alvin Schnitzler
86. Johns Hopkins University 2  
Applied Physics Lab  
Johns Hopkins Road  
Laurel, MD 20810  
  
Attn: Dr. Albert M. Stone  
Dr. R. E. Gorozdos

87. Lawrence Livermore Lab. 5  
P.O. Box 808  
Livermore, CA 94550  
  
Attn: Dr. R. E. Kidder  
Dr. Joe Fleck  
Dr. E. Teller  
Dr. John Emmett  
Dr. William F. Krupke
88. Los Alamos Scientific Lab 2  
P.O. Box 1663  
Los Alamos, NM 87544  
  
Attn: Dr. Keith Boyer (MS 530)  
Dr. O. P. Judd
89. Lulejian and Associates, Inc. 1  
Fifth Floor, Skyline Center  
5205 Leesburg Pike  
Falls Church, VA 22041
90. Lockheed Palo Alto Research Laboratory 1  
3251 Hanover Street  
Palo Alto, CA 94304  
  
Attn: L. R. Lunsford  
Org. 52-03, 201
91. Lockheed Missiles & Space Company, Inc. 2  
P.O. Box 504  
Sunnyvale, CA 94088  
  
Attn: Dr. M. Bina, O/55-40, Bldg. 572  
Mr. L. D. Montague, O/55-01, Bldg. 572
92. Martin Marietta Aerospace 1  
P. O. Box 179  
Denver, COL 80201  
  
Attn: Mr. Stewart Chapin (Mail No. 0485)

93. Massachusetts Institute of Technology 5  
Lincoln Lab  
P.O. Box 73  
Lexington, MA 02173  
  
Attn: Dr. S. Edelberg  
Dr. J. Freedman  
Dr. R. H. Rediker  
Dr. L. C. Marquet  
Mr. W. E. Morrow
94. Mathematical Sciences Northwest, Inc. 1  
P.O. Box 1887  
Bellevue, WA 98009  
  
Attn: Mr. Peter H. Rose  
Mr. Abraham Hertzberg
95. McDonnell Douglas Astronautics Co. 1  
5301 Bolsa Avenue  
Huntington Beach, CA 92647  
  
Attn: Mr. P. L. Klevatt  
Dept A3-360-B3G, M/S 14-1
96. McDonnell Douglas Research Labs 1  
Department 220, Box 516  
St. Louis, MO 63166  
  
Attn: Dr. D. P. Ames
97. University of Missouri - Rolla 1  
103 Physics Building  
Rolla, MO 65401  
  
Attn: Kaare J. Nygaard
98. MITRE Corporation 1  
P.O. Box 207  
Bedford, MA 01730  
  
Attn: Norman F. Harmon



99. Northrop Corporation 3  
Research & Technology Center  
3401 West Broadway  
Hawthorne, CA 90250  
  
Attn: Dr. G. Hasserjian  
Dr. B. B. O'Brien  
Dr. M. L. Bhaumik
100. Phaser Telepropulsion Inc. 1  
1888 Century Park East  
Suite 1606  
Los Angeles, CA 90067  
  
Attn: Dr. M. A. Mirovitch
101. Dr. Anthony N. Pirri 1  
Physical Sciences Inc.  
30 Commerce Way  
Woburn, MA 01801
102. Pacific Missile 1  
Point Mugu, CA 93042  
  
Attn: Robert Dichl, Code 0141
103. Pacific Sierra Research Corp. 1  
1456 Cloverfield Blvd.  
Santa Monica, CA 90404  
  
Attn: Dr. R. Lutomirski
104. Perkin-Elmer Corporation 1  
Central Library,  
Main Avenue  
Norwalk, CT 06856  
  
Attn: M. D. Wood
105. Claud N. Bain 1  
PRC/Energy Analysis Co.  
7600 Old Springhouse Road  
McLean, VA 22101
106. Gerard K. O'Neill 1  
Princeton University  
Box 708  
Princeton, NJ 08540

107. RAND Corporation 1  
1700 Main Street  
Santa Monica, CA 90406  
  
Attn: Dr. Claude R. Culp
108. Rasor Associates 1  
420 Persian Drive  
Sunnyvale, CA 94086  
  
Attn: Dr. Ned S. Rasor
109. Raytheon Company 1  
Bedford Labs  
Bedford, MA 01730  
  
Attn: Dr. H. A. Mehlhorn (Opt. Sys. Dept)  
MS S4-55
110. Raytheon Company 1  
28 Seyon Street  
Waltham, MA 02164  
  
Attn: Dr. Hermann Statz
111. William C. Brown 1  
Raytheon Company  
New Products Center, Bldg. 12  
Waltham, MA 02154
112. Radio Corporation of America 2  
Missile and Surface Radar Division  
Morrestown, NJ 08057  
  
Attn: Mr. J. A. Colligan  
Information Control
113. Riverside Research Institute 1  
80 West End Street  
New York, NY 10023  
  
Attn: Dr. Marvin King
114. Riverside Research Institute 1  
1701 N. Fort Myer Drive, Suite 711  
Arlington, VA 22209

115. R&D Associates, Inc. 2  
P.O. Box 9695  
Marina del Rey, CA 90291  
  
Attn: Dr. R. E. LeLevier  
Dr. R. Hundley
116. Rockwell International Corporation 3  
3370 Miraloma Avenue  
Anaheim, CA 92803  
  
Attn: R. E. Hovda (DB29)  
Dr. J. SooHoo (D/528/HA14)  
Dr. Cecil Hayes
117. Rockwell International Corporation 2  
3636 Menaul Blvd., NE, Suite 211  
Albuquerque, NM 87110  
  
Attn: Mr. C. K. Kraus, Manager
118. Rockwell International Corporation  
Rocketdyne Division  
6633 Canoga Avenue  
Canoga Park, CA 91804  
  
Attn: Mr. Mare T. Constantine 1  
Dr. Stan V. Gann 1
119. SANDIA Labs 1  
P.O. Box 5800  
Albuquerque, NM 87115  
  
Attn: Dr. A. Narath, Org 5000
120. W. J. Schafer Associates, Inc. 1  
607 N. Avenue, Door 14  
Wakefield, MA 01880  
  
Attn: Francis W. French
121. W. J. Schafer Associates, Inc. 2  
1901 N. Fort Myer Drive, Suite 803  
Arlington, VA 22209  
  
Attn: Dr. Edward T. Gerry  
Mr. A. C. Cron

122. Science Applications, Inc. 1  
P.O. Box 2351  
La Jolla, CA 92037  
  
Attn: Dr. John Asmus
123. Mr. Lawrence N. Peckham 1  
Science Applications, Inc.  
2201 San Pedro NE, Suite 214  
Albuquerque, NM 87110
124. Science Applications, Inc. 1  
P.O. Box 328  
Ann Arbor, MI 48103  
  
Attn: Dr. R. E. Meredich
125. Dr. Frank A. Horrigan 1  
Science Applications, Inc.  
3 Preston Court  
Bedford, MA 01730
126. Mr. Dorian A. DeMaio 1  
Science Applications, Inc.  
101 Continental Bldg., Suite 310  
El Segundo, CA 90245
127. Harold A. Malliot 1  
Science Applications, Inc.  
2680 Hanover Street  
Palo Alto, CA 94304
128. Sperry Systems Management 1  
Mail Station H-4  
Great Neck, L.I., NY 11020  
  
Attn: Harold E. Whalen
129. Stanford Research Institute 4  
Menlo Park, CA 94025  
  
Attn: Dr. Don M. LeVine (JASON)
130. Systems Consultants, Inc. 1  
1050 31st Street, NW  
Washington, D.C. 20007  
  
Attn: Dr. Robert B. Keller

131. Systems, Science and Software 1  
P.O. Box 1620  
La Jolla, CA 92037  
  
Attn: Mr. Alan F. Klein
132. Thiokol Chemical Company 1  
WASATCH Division  
P.O. Box 524  
Brigham City, UT 84302  
  
Attn: Mr. James E. Hansen
133. TRW Systems Group 2  
One Space Park  
Redondo Beach, CA 90278  
  
Attn: Mr. Don M. Culler (Bldg. R3, Rm 2036)  
Mr. Norman F. Campbell (Bldg. 01, Rm 1050)
134. United Technologies Research Center 4  
400 Main Street  
East Hartford, CT 06108  
  
Attn: Mr. A. W. Angelbeck  
Mr. R. M. Grose
135. United Technologies Corporation 3  
Pratt & Whitney Aircraft Group  
P.O. Box 2691  
West Palm Beach, FL 33402  
  
Attn: Dr. R. A. Schmidtke (1)  
Mr. E. A. Pinsley (2)
136. VARIAN Associates 1  
EIMAX Division  
301 Industrial Way  
San Carlos, CA 94070  
  
Attn: Mr. Jack Quinn
137. Vought Systems Division 1  
LTV Aerospace Corporation  
P.O. Box 5907  
Dallas, TX 75222  
  
Attn: Mr. F. G. Simpson (MS-2-54142)

138. Westinghouse Electric Corporation  
Defense and Space Center  
Friendship International Airport, Box 746  
Baltimore, MD 21203

1

Attn: Mr. W. F. List

139. Westinghouse Research Laboratory  
Beulah Road, Churchill Boro.  
Pittsburgh, PA 15235

2

Attn: Dr. E. P. Riedel  
Mr. R. L. Hundstad



